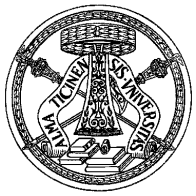

Università
degli Studi
di Pavia

Dipartimento
di Fisica
"A. Volta"

DOTTORATO DI RICERCA IN FISICA – XXI CICLO

Phase fluctuations of the order parameter in high-T_c Sm-based superconducting cuprates

dissertation submitted by

Ettore Bernardi

to obtain the degree of

DOTTORE DI RICERCA IN FISICA

Supervisor: Prof. Alessandro Lascialfari

Referee: Prof. ssa Laura Romanò
(Dept. of Physics, University of Parma)

Cover: Experimental isothermal magnetization curves in $SmBa_2Cu_{2.85}Al_{0.15}O_{6+\delta,}$ for different representatives temperatures above the superconducting transition.

Phase fluctuations of the order parameter in High-T_c Sm-based superconducting cuprates

Ettore Bernardi

PhD thesis – University of Pavia
Printed in Pavia, Italy, November 2008
ISBN 978-88-95767-14-7

Ai miei amici e alla mia famiglia,
per quando non è stato facile.

Contents

Chapter 1

Introduction and overview of the thesis

The superconducting transition can be described, in the framework of Ginzburg-Landau (GL) theory, in terms of the complex superconducting order parameter $\Psi(\mathbf{r})$. The mean value , $\langle\Psi(\mathbf{r})\rangle$, is zero in the normal state and is different from zero in the superconducting state, below the transition temperature T_c, where $|\Psi(\mathbf{r})|^2$ is related to the density of Cooper pairs. On approaching T_c from above the superconducting order parameter undergoes superconducting fluctuations(SF): the mean square value of the amplitude $\sqrt{\langle|\Psi(\mathbf{r})|^2\rangle}$ is different from zero, causing local concentration of fluctuating, i.e. metastable, Cooper pairs. The fluctuating pairs above T_c are accompanied by the appearance of a diamagnetic contribution $-M_{fl}(H,T)$ to the magnetization. This phenomenon is usually called fluctuating diamagnetism (FD).

The fluctuating diamagnetism was studied since the early 70's. Tinkam and coworkers carried out [1] susceptibility measurements at constant fields in different BCS superconductors (In, Pb, Nb, and In-Tl and Pb-Tl alloys). The experimental data at low fields were found in agreement with the predictions of the standard GL theory, namely with $-M_{fl}(H, T =\text{const})$ going linearly with H for $T \gg T_c$ and $-M_{fl}(H, T =\text{const}) \propto H^{1/2}$ for $T = T_c$. However on increasing the magnetic field above a characteristic value, H_{up}, $|M_{fl}|$ was found to decrease on increasing field. To describe the fluctuating diamagnetism for non-evanescent field, where short wave-length fluctuations and non locality effects becomes important, it is necessary to take to account the microscopic Gor'kov theory [2].

The presence of un upturn field H_{up} in the isothermal magnetization curves was experimentally studied in detail in a more recent work on lead nanoparticles [3] with diameter d shorter than the coherence length. In these particles the SF are enhanced and one can express M_{fl} analytically assuming the zero dimensional condition in the framework of GL functional fluctuation theories. The investigation of zero-dimensional systems allowed us to describe quantitatively the field dependence of M_{fl} at constant T, and the inverse proportion-

ality of H_{up} with the size of the particle [3].

The study of fluctuating diamagnetism has turn on new interest in recent years with the discovery of high-temperature superconductors (HTSC). In these systems the small coherence length, the high transition temperature, the reduced carrier density and the marked anisotropy cause strong enhancement of SF and extend the range of temperatures in which SF can be detected. On the other hand, the reduced coherence length increases the value H_{up} above which the SF are suppressed by the field, thus, at least for optimally doped compounds at the maximum in T_c, extending the validity of the GL theory to higher magnetic fields.

Experiments on $YBa_2Cu_3O_7$ (YBCO) optimally doped [4, 5, 6, 7] showed that the fluctuating contribution to the magnetization can be ascribed to conventional fluctuations in the framework of the GL theory using the Lawrence-Doniach Hamiltonian[8], which is the generalization of GL functional for layered superconductors. No upturn in the magnetization curves was detected up to 7 T. Furthermore, the laws derived from scaling arguments for 3-D anisotropic systems were found to be well obeyed.

On the contrary in underdoped YBCO [9] a strong enhancement of the reduced magnetization $m = M_{fl}(T_c)/H^{1/2}T_c$, irreversibility effects, and upturn in $M_{fl}(H)$ around $H_{up} \approx 200$ Oe were observed. Similar behaviors were also detected in underdoped $La_{1.9}Sr_{0.1}CuO_4$[10]. In order to explain the experimental findings the observed enhanced FD was ascribed to vortices created by the external field where phase fluctuations of the order parameter are present, under the assumption of charge inhomogeneities inducing local stable superconducting regions with T_c^{loc} higher than the bulk transition temperature T_c[9, 11, 12]. This description is also in agreement with the dependence of H_{up} on temperature.

The research work carried out in the cuprates had left open questions, such as the role of the oxygen chains modified in controlling the doping amount and also the interplay between diffuse superconducting transition with local T_c^{loc} and phase fluctuations among the non-percolating superconducting regions. It should be observed that a crucial issue is the temperature dependence of H_{up}. For diffuse transition, with little role, if any, of SF the upturn field in practice coincide with H_{c1} and thus decrease on increasing temperature. At variance, for phase fluctuations of the order parameter and lack of long-range coherence, H_{up} increases on increasing temperature [13].

In recent times a new family of HTSC has been synthetized by M. Scavini and C. Oliva and coworkers [14, 15], the Sm-based $SmBa_2Cu_{3-x}Al_xO_{6+\delta}$. Besides the novelty of the SC family, these compounds have the great advantage to allow the control of the holes by means of Al for the in-chains Cu substitutions, without any role of the oxygen. Thus the study of the underdoped regime in regards of the SF can be carried out in ideal condition and the interplay of the phenomena of diffuse transition and phase fluctuations of the order parameter can be better investigated.

The present thesis deals with the study of fluctuating diamagnetism in the Sm-based HTSC.

Both the pure system $SmBa_2Cu_3O_{6+\delta}$ ($\delta \simeq 1$) and the Al-doped one $SmBa_2Cu_{2.85}Al_{0.15}O_{6+\delta}$ ($\delta \simeq 1$) are considered. In the Al-doped compound, Al substitutes Cu just along the Cu chains (without substituting Cu in the plain). Moreover it was observed [14, 16] that crystals of $SmBa_2Cu_{3-x}Al_xO_{6+\delta}$ annealed in reducing atmospheres at high temperatures and then reoxidized at low temperatures, exhibits an increased Cu-O chain fragments length. This offers also the opportunity of studying the fluctuating diamagnetism in samples with different average length of Cu-O chain fragments but having the same aluminium and oxygen concentration. From magnetization curves we have shown that fluctuating diamagnetism in $SmBa_2Cu_3O_7$ can be described on the basis of an anisotropic Ginzburg-Landau functional similarly to what observed in YBCO optimally doped. On the contrary, fluctuating diamagnetism in $SmBa_2Cu_{2.85}Al_{0.15}O_{6+\delta}$ has to be ascribed to the formation of vortex-antivortex pairs and the related phase fluctuations of the order parameter in a system where the regions at non-zero order parameter lack of long range coherence.

The thesis is organized as follows. Chapt.2 deals with the description of the diamagnetism due to superconducting fluctuations, in the framework of fluctuation theories based on Ginzburg-Landau functional. Both the contribution to the magnetization due to fluctuations of the order parameter and the one related to fluctuation of the phase of the order parameter are described for a layered superconductor.

In Chapter 3 the structural characterization of $SmBa_2Cu_3O_{6+\delta}$ and of the two samples of $SmBa_2Cu_{2.85}Al_{0.15}O_{6+\delta}$ with different thermal treatment is illustrated. The effects of thermal treatment on clustering of Al-defects and on Cu-O chain fragments length is briefly discussed.

Chapter 4 is devoted to the presentation of experimental results. Isothermal and isofield magnetization curves, collected by means of a high resolution superconducting quantum interference device, for $SmBa_2Cu_3O_{6+\delta}$ and the two samples of $SmBa_2Cu_{2.85}Al_{0.15}O_{6+\delta}$ with different thermal treatment are reported. The experimental measurements were performed under both zero-field-cooling and field-cooling condition to reveal irreversibility effects.

In Chapter 5 experimental data are discussed in the framework of GL theory and of the theory dealing with phase fluctuations of the order parameter.

Chapter 2

Diamagnetic response due to thermal fluctuations in superconductors

In this Chapter, after a brief presentation of the main properties derived from Ginzburg-Landau (GL) theory of superconductivity (§1), main theoretical results on fluctuating diamagnetism in framework of fluctuation theory based on Ginzburg-Landau functional (GL) are showed (the results will be compared with experimental data in Chapter 5. In particular, in (§2) the contribution of fluctuations of the order parameter modulus, causing local concentration of fluctuating Cooper pairs, to the diamagnetic response in a superconductor above the transition temperature is presented. In (§2) the contribution to the diamagnetism related to the presence of vortices due to fluctuations of the phase of the order parameter in superconducting islands below the transition temperature is pesented.

2.1 Generalities of the Ginzburg-Landau theory

2.1.1 GL Functional

The Ginzburg-Landau theory describes the superconducting transition by introducing a complex order parameter

$$\Psi(\mathbf{r}) = |\Psi(\mathbf{r})|e^{i\theta(\mathbf{r})}, \tag{2.1}$$

and a free energy functional, that in presence of an external magnetic field takes the form:

$$\mathcal{F}[\Psi(\mathbf{r}),\mathbf{A}(\mathbf{r})] = F_N + \int dV \Bigg\{ a\,|\Psi(\mathbf{r})|^2 + \frac{b}{2}\,|\Psi(\mathbf{r})|^4 + \frac{1}{4m}\left|\left(-i\hbar\nabla - \frac{2e}{c}\mathbf{A}(\mathbf{r})\right)\Psi(\mathbf{r})\right|^2 + \frac{[\nabla\times\mathbf{A}(\mathbf{r})]^2}{8\pi} - \frac{\nabla\times\mathbf{A}(\mathbf{r})\cdot\mathbf{H}}{4\pi}\Bigg\}. \tag{2.2}$$

with:

$$a = \alpha(T - T_c) = \alpha T_c \epsilon, \tag{2.3}$$

and

$$b \geq 0, \tag{2.4}$$

where T_c is the transition temperature and $\epsilon = \frac{T-T_c}{T_c}$ is the reduced temperature. The values of $\Psi(\mathbf{r})$ and $\mathbf{A}(\mathbf{r})$ that characterize a superconductor in equilibrium in an external field $\mathbf{H}$ at a temperature T are the ones that minimize the functional in Eq. 2.2. In particular it can be proved that $\Psi(\mathbf{r})$ and $\mathbf{A}(\mathbf{r})$ obey to the two GL equations:

$$a\,\Psi(\mathbf{r}) + b\,\Psi(\mathbf{r})|\Psi(\mathbf{r})|^2 + \frac{1}{4m}\left(-i\hbar\nabla - \frac{2e}{c}\mathbf{A}(\mathbf{r})\right)^2\Psi(\mathbf{r}) = 0 \tag{2.5}$$

and

$$\mathbf{J}_s = \frac{c}{4\pi}\,\nabla\times\nabla\times\mathbf{A} = -\frac{-ie\hbar}{2m}\left(\Psi\nabla\Psi^* - \Psi^*\nabla\Psi\right) - \frac{2e^2}{mc}\,|\Psi|^2\mathbf{A}, \tag{2.6}$$

where $\mathbf{J}_s$ in Eq.2.6 is the supercurrent density. In the homogeneous case the order parameter takes the value

$$|\widetilde{\Psi}|^2 = \begin{cases} -\alpha T_c\epsilon/b & \text{, when } \epsilon < 0, \\ 0 & \text{, when } \epsilon > 0. \end{cases}$$

and Eq.2.6 is reduced to

$$\mathbf{J}_s = -\frac{2e^2}{mc}\,|\widetilde{\Psi}|^2\mathbf{A}. \tag{2.7}$$

Comparing this equation to the one derived in the microscopic theory of superconductivity

$$\mathbf{J}_s = -n_s\frac{2e^2}{2mc}\mathbf{A}, \tag{2.8}$$

the amplitude of the order parameter $|\Psi(\mathbf{r})|$ can be related to the local density of Cooper pairs n_s. Finally, if the normalized value of the order parameter, $\psi = \frac{|\Psi(\mathbf{r})|}{|\widetilde{\Psi}|}$ is introduced, GL equations take a simpler form

$$\xi^2(T)\left(-i\nabla - \frac{2\pi}{\Phi_0}\right)^2\psi - \psi + \psi|\psi|^2 = 0 \tag{2.9}$$

$$\nabla \times \nabla \times \mathbf{A} = -\frac{\Phi_0}{4\pi\lambda^2}\left(\psi\nabla\psi^* - \psi^*\nabla\psi\right) - \frac{|\psi|^2}{\lambda^2}\mathbf{A}, \tag{2.10}$$

where λ is the penetration length

$$\lambda = \left(\frac{mc^2 b}{4\pi e^2 \alpha(T_c - T)}\right)^{1/2}, \tag{2.11}$$

ξ is the coherence length

$$\xi(T) = \left(\frac{\hbar^2}{4ma(T)}\right)^{1/2} = \xi_0 \epsilon^{-1/2} \qquad \xi_0 = \left(\frac{\hbar^2}{4m\alpha T_c}\right)^{1/2} \tag{2.12}$$

and $\Phi_0 = \frac{hc}{2e}$ is the quantum flux. The physical quantities ξ and λ are characteristic lengths in which the order parameter $|\Psi(\mathbf{r})|$ and the magnetic field varies [17]. These quantities defines also the limits of validity of GL theory; in fact both $\xi(T)$ and $\lambda(T)$ have to be larger than the Cooper pair size

$$\xi_P = \frac{\hbar v_F}{\pi\Delta(0)} \tag{2.13}$$

derived in the microscopic theory, where $\Delta(0)$ is the value of superconducting gap at zero temperature and v_F is the Fermi velocity [17]. In this way all quantities change spatially in a sufficient smooth way as assumed in the GL theory.

2.1.2 Thermal Fluctuations

The physical properties presented till this point are derived under the hypothesis that the system is always in the equilibrium state characterized by the value $\widetilde{\Psi}$ that minimize the free energy functional $\mathcal{F}[\widetilde{\Psi}]$. But, from thermodynamical theory we know that for a system in thermal contact with a reservoir, the state that minimizes the free energy is only the one with the greater probability to be obtained, and the system has a non-zero probability to be in a state different from that[18]. So, in our case, for a superconductor placed in a external field $\mathbf{H}$ and at a temperature T, $\widetilde{\Psi}$ is not the only possible value of the order parameter, but $|\Psi(\mathbf{r})|$ has to be considered a statistical variable subjected to fluctuations that take the name of superconducting fluctuations (SF), around the mean value $\widetilde{\Psi}$.

Formally the partition function Z is obtained carrying out the functional integration over all possible value of the order parameter, everyone weighted with the thermodynamic probability $e^{-\frac{\mathcal{F}[\Psi(\mathbf{r}),\mathbf{A}(\mathbf{r})]}{k_B T}}$:

$$Z = \int D^2\Psi(\mathbf{r}) \exp\left(-\frac{\mathcal{F}[\Psi(\mathbf{r}),\mathbf{A}(\mathbf{r})]}{k_B T}\right). \tag{2.14}$$

From Eq.2.14, the fluctuation part of the free energy is obtained by the relation

$$F(\epsilon > 0) = -k_B T \ln Z, \tag{2.15}$$

and from the free energy the other thermodynamical quantities can be derived by standard thermodynamical relations.

Let us illustrate this method for the zero-dimensional condition, i.e for a superconducting sample of size $d \ll \xi(T)$, in absence of the field and omitting the term in $|\Psi(\mathbf{r})|^4$, the last approximation corresponding to the so-called "gaussian approximation". In this case the order parameter is considered position independent and takes the form

$$\Psi_0 = \Psi\sqrt{V}. \tag{2.16}$$

So the functional in Eq.2.2 results

$$\mathcal{F}_0[\Psi_0] = a|\Psi_0|^2. \tag{2.17}$$

The functional integral in Eq.2.14 can be resolved exactly and results

$$\begin{aligned} Z_{(0)} &= \int d^2\Psi_0 \exp\left(-\frac{\mathcal{F}_0[\Psi_0]}{k_B T}\right) = \pi \int d|\Psi_0|^2 \exp -\frac{a|\Psi_0|^2}{k_B T} \\ &= \pi \frac{k_B T}{a} = \pi \frac{k_B T}{\alpha\epsilon T_c} = \pi \frac{k_B}{\alpha\epsilon} \end{aligned} \tag{2.18}$$

giving for the fluctuation part of the free energy

$$F_{(0)} = -k_B T \ln \pi \frac{k_B}{\alpha\epsilon}.. \tag{2.19}$$

2.2 Diamagnetism induced by fluctuations of the order parameter modulus

The physical origin of a negative diamagnetic contribution $M_{fl}(H,T)$ in the magnetic response of a superconductor approaching T_c from above is the presence of metastable fluctuating Cooper pairs also for $T \geq T_c$. In fact, we have seen that the order parameter $\Psi(\mathbf{r})$ is a statistical variable subjected to fluctuations; this means that approaching T_c from above the mean square value of the order parameter $\sqrt{\langle|\Psi(\mathbf{r})|^2\rangle}$ is different from zero and this is related to local concentration of fluctuating Cooper pairs.

Formally, to derive $M_{fl}(H,T)$ we will utilize the relation:

$$M_{fl} = -\frac{1}{V}\frac{\partial F}{\partial H} \tag{2.20}$$

where F is the fluctuation part of the free energy derived from the G-L functional $\mathcal{F}[\Psi(\mathbf{r}), \mathbf{A}(\mathbf{r})]$ using the method described in the previous paragraph.

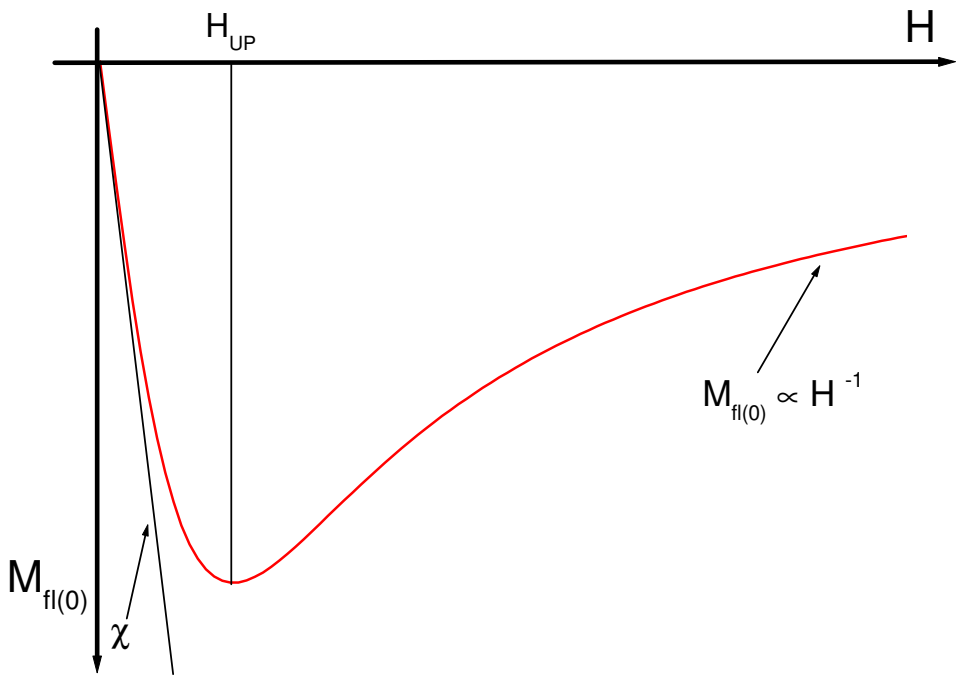

Figure 2.1: Sketchy behaviour of the fluctuating magnetization $M_{fl(0)}$ in function of the field, for $T > T_c$, for zero-dimensional condition and in gaussian approximation.

2.2.1 Zero-dimensional diamagnetic susceptibility

Let us consider a superconducting grain of diameter $d \ll \xi(T)$ for which we assume the zero-dimensional condition and the gaussian approximation. Introducing the homogeneous order parameter Ψ_0 (see Eq.2.16), the G-L functional takes the form

$$\mathcal{F}_0[\Psi(\mathbf{r}), \mathbf{A}(\mathbf{r})] = a|\Psi_0|^2 + \frac{e^2}{mc^2}\langle \mathbf{A^2} \rangle |\Psi_0|^2. \tag{2.21}$$

where $\langle \cdots \rangle$ means averaging over the sample volume. The last two terms in Eq.2.2 have been omitted because, being $d \ll \lambda$, the equivalence between the external magnetic field H and the average magnetic field in metal $\mathbf{B} = \frac{1}{V}\int dV \nabla \times \mathbf{A}(\mathbf{r})$ it is assumed [19]. We can see that this functional have the same form of the one obtained in absence of field, see Eq.2.17, but with the renormalized parameter:

$$a'(H) = a + \frac{e^2}{mc^2}\langle \mathbf{A}^2 \rangle = \alpha T_c \epsilon(H) \tag{2.22}$$

where the reduced temperature is field-dependent and takes the form

$$\epsilon(H) = \epsilon + \frac{4\pi^2 \epsilon_0^2}{\Phi_0^2}. \tag{2.23}$$

So we can use the results obtained in absence of the field, and write, from Eq.2.19,

$$F_{(0)}(\epsilon, H) = -k_B T \ln \pi \frac{k_B}{\alpha(\epsilon + \frac{4\pi^2 \xi_0}{\Phi_0^2}\langle \mathbf{A}^2 \rangle)} \tag{2.24}$$

for the fluctuation part of the free-energy. Finally, from this equation, considering that for a spherical particle $\langle \mathbf{A}^2 \rangle = \frac{1}{10} H^2 d^2$ and using Eq.2.20, it can be found:

$$M_{fl(0)}(\epsilon, H) = -\frac{1}{V}\frac{\partial F_0(\epsilon, H)}{\partial H} = -\frac{24\pi k_B T \xi_0^2}{5\Phi_0^2 d}\frac{H}{(\epsilon + \frac{2\pi^2 \xi_0^2}{5\Phi_0^2} H^2 d^2)}. \tag{2.25}$$

It can be seen that the fluctuating magnetization is negative and linear in the field for weak field; then increasing the field, an upturn in the field dependence occurs for the value $H_{up}(\epsilon) \sim \frac{\Phi_0}{d\xi(\epsilon)}$ and $|M_{fl(0)}|$ decreases, while for higher fields $M_{fl(0)}(\epsilon, H) \propto -\frac{1}{H}$. In the weak field region the diamagnetic susceptibility is:

$$\chi_{fl(0)}(\epsilon, H) = \frac{\partial M_{fl(0)}(\epsilon, H)}{\partial H} = -\frac{24\pi k_B T \xi_0^2}{5\Phi_0^2 d}\frac{1}{\epsilon}. \tag{2.26}$$

In Fig.2.1 the behavior of the fluctuating magnetization, according to Eq.2.25, is sketched.

2.2.2 Layered Superconductors in magnetic field

Let us consider the calculation of the fluctuation magnetization in a layered superconductor. This is of primary interest for us because the theoretical results presented below will be compared to experimental magnetization curves in $SmBa_2Cu_3O_7$ in chapter five of this thesis.

The generalization of GL functional for a layered superconductor is the Lawrence-Doniach (LD) functional [8]:

$$\begin{aligned}\mathcal{F}_{LD}[\Psi] = \sum_l \int d^2\mathbf{r} \Bigg\{ & a\,|\Psi_l|^2 + \frac{b}{2}\,|\Psi_l|^4 + \frac{1}{4m}\left|\left(-i\hbar\nabla_\parallel - \frac{2e}{c}\mathbf{A}_\parallel\right)\Psi_l\right|^2 \\ & + \mathcal{J}\,|\Psi_{l+1} - \Psi_l|^2 \Bigg\}.\end{aligned} \tag{2.27}$$

In this equation the gauge with $A_z = 0$ is chosen, $\Psi_l(\mathbf{r})$ is the order parameter in the l-th layer and $\mathcal{J}$ is proportional to the Josephson coupling between adiacent layers. If the variation along $\mathbf{z}$ is so smooth that $\frac{|\Psi_{l+1} - \Psi_l|}{s}$, where s is the interlayer distance, can be replaced by $\frac{\partial \Psi}{\partial z}$, the LD functional is reduced to an anisotropic GL functional, where

$$M = \frac{\hbar^2}{4\mathcal{J}s^2} \tag{2.28}$$

is the effective mass along c-direction, and, from the relation Eq.2.12 a coherence length along the z-direction

$$\xi_{0\perp} = \frac{\mathcal{J}s^2}{2\alpha T_c}. \tag{2.29}$$

can be defined.

Expanding the order parameter in terms of Landau state eigenfunction $\phi_n(\mathbf{r})$:

$$\Psi_l(\mathbf{r}) = \sum_{n,k_z} \Psi_{n,k_z}\phi_n(\mathbf{r})\exp(ik_z l), \tag{2.30}$$

where n is the quantum number related to the degenerate Landau state and k_z is the momentum component along the direction of the magnetic field, the LD-functional can be expressed in terms of the Ψ_{n,k_z} coefficients

$$\mathcal{F}_{LD}[\Psi_{n,k_z}] = \sum_{n,k_z}\{\alpha T_c\epsilon + \hbar\omega_c(n+1/2) + \mathcal{J}(1-\cos(k_z s))\}|\Psi_{n,k_z}|^2. \tag{2.31}$$

In this way the functional integral for the partition function (2.14) can be factored out to a product of Gaussian type integrals over this coefficient:

$$Z = \prod_{n,k_z}\int d^2\Psi_{n,k_z}\exp\frac{\{\alpha T_c\epsilon + \hbar\omega_c(n+1/2) + \mathcal{J}(1-\cos(k_z s))\}|\Psi_{n,k_z}|^2}{k_B T}. \tag{2.32}$$

Carrying out these integral, one gets for the fluctuation contribution to the free energy:

$$F_{LD}(\epsilon, H) = -\frac{HS}{\Phi_0}k_B T\sum_{n,k_z}\ln\frac{\pi k_B T}{\alpha T_c\epsilon + \hbar\omega_c(n+\frac{1}{2}) + \mathcal{J}(1-\cos(k_z s)}. \tag{2.33}$$

where the factor $\frac{HS}{\Phi_0}$ takes account of the degeneracy of each Landau level. Averaging over the Cooper pair motion ortogonal to layers Eq.2.33 takes the form:

$$F_{LD}(\epsilon, h) = -\frac{hk_B TS}{2\pi\xi_{\parallel}^2}\int_{-\frac{\pi}{s}}^{\frac{\pi}{s}}\frac{\mathcal{N}sdk_z}{2\pi}\sum_{n=0}^{n_c-1}\ln\frac{\pi k_B/\alpha}{\epsilon + 2h(n+\frac{1}{2}) + \frac{r}{2}[1-\cos(k_z s)]} \tag{2.34}$$

where we have introduced the anisotropy factor

$$r = \frac{2\mathcal{J}}{\alpha T_c} = \frac{4\xi_{0\perp}^2}{s^2} \tag{2.35}$$

and the reduced field

$$h = \frac{\hbar\omega_c}{2\alpha T_c} = \frac{\hbar eH}{2m\alpha T_c} = \frac{H}{H_{c2}(0)} \tag{2.36}$$

where

$$H_{c2}(0) = \Phi_0/2\pi\xi_{0\|}^2 \tag{2.37}$$

is the lower critical field at zero temperature. The expression 2.34, using the Euler gamma function [20], can be reduced to

$$F_{LD}(\epsilon,h) = -\frac{k_BTV}{2\pi s\xi_{\|}^2}\left\{h\int_0^{2\pi}\frac{d\theta}{2\pi}\ln\frac{\Gamma[1/2+\frac{\epsilon+\frac{r}{2}(1-\cos(k_zs)}{2h}]}{\sqrt{2\pi}}+\frac{\epsilon}{2}\ln h+const\right\}. \tag{2.38}$$

Finally, from this equation, using the relation (2.20) a general expression for magnetization can be derived

$$M_{fl(LD)}(\epsilon,h;r) = -\frac{k_BT}{\Phi_0 s}\int_0^{\pi/2}\frac{d\phi}{\pi/2}\left\{\frac{\epsilon+r\sin^2\phi}{2h}\left[\psi\left(\frac{\epsilon+r\sin^2\phi}{2h}+\frac{1}{2}\right)-1\right]\right. \\ \left. -\ln\Gamma\left(\frac{\epsilon+r\sin^2\phi}{2h}+\frac{1}{2}\right)+\frac{1}{2}\ln(2\pi)\right\}, \tag{2.39}$$

where $\phi(z)$ is the logarithmic derivative of the Euler gamma function. Let us discuss now the different crossovers described by equation 2.39.

Near the transition, $\epsilon \leq r$, handling with Hurvitz zeta function the expression (2.39) takes the form [20, 21, 22]:

$$M_{fl(3)}(\epsilon \ll r,h) = 3\frac{k_BT}{\Phi_0 s}\left(\frac{2}{r}\right)^{1/2}\sqrt{h} \\ \times\left[\zeta\left(-\frac{1}{2},\frac{1}{2}+\frac{\epsilon}{2h}\right)-\zeta\left(\frac{1}{2},\frac{1}{2}+\frac{\epsilon}{2h}\right)\frac{\epsilon}{6h}\right]. \tag{2.40}$$

From this equation it can be seen that, fixed the reduced temperature ϵ, for weak fields the magnetization grows linearly with magnetic field

$$M_{fl(3)}(\epsilon \ll r, h\to 0) = -\frac{e^2k_BTH}{\hbar^2 3\pi c^2}\xi_{\|}(\epsilon) \tag{2.41}$$

but for fields of the order $of H_{c2}(\epsilon)$ $M_{fl} \propto \sqrt{H}$ and the magnetization enter in 3D non linear regime. If the magnetic field is increased further there is another crossover to 2D nonlinear regime.

On the other hand, for high temperatures,($\epsilon > r$), expression 2.39 is reduced to the 2D result:

$$M_{fl(2)}(\epsilon,H) = -\frac{1}{H_{c2}(0)S}\frac{\partial}{\partial h}[\delta F_{(2)}(\epsilon,h)] \\ = \frac{k_BT}{\Phi_0}\left\{h\ln\frac{\Gamma(1/2+\epsilon/2h)}{\sqrt{2\pi}}-\frac{\epsilon}{2h}[\psi(1/2+\epsilon/2h)-1]\right\} \tag{2.42}$$

which implies a linear dependence for weak fields

$$M_{fl(2)}(h \ll \epsilon) = -\frac{1}{d}\frac{e^2 k_B T}{3\pi c^2 \hbar^2}\frac{\xi_{0\|}^2}{\epsilon}, \tag{2.43}$$

and the saturation of magnetization for high fields

$$M_{fl(2)}(h \gg \epsilon) \to M_\infty = -0.346\left(-\frac{k_B T}{\Phi_0}\right). \tag{2.44}$$

Finally at T_c the result obtained by Prange [23] is reproduced, with an anysotropy correction multiplier $\frac{\xi_{0\|}}{\xi_{0\perp}}$

$$M_{fl(3)}(0,h) = -\frac{0.32 k_B T}{\Phi_0^{3/2}}\frac{\xi_{0\|}}{\xi_{0\perp}}\sqrt{H}. \tag{2.45}$$

The different regimes for fluctuating magnetization are sketched in Fig.2.2

2.2.3 Scaling arguments

To take in account the $|\Psi(\mathbf{r})|^4$ omitted in LD-functional (2.27), we can rely on scaling arguments [24]. In this approach it is assumed that the singular part of free energy depends only on the number of flux quanta per coherence area, so that the free energy per unit volume, in the isotropic case, takes the form:

$$F = -k_B T \xi^{-D}\varphi(x) \tag{2.46}$$

and

$$x \equiv \frac{H\xi^2}{\Phi_0}, \tag{2.47}$$

where $\xi(T) = \xi_0|\epsilon|^\nu$ (ν is a critical exponent), D the dimension of the system and φ an unknown dimensionless function. The fluctuating magnetization results:

$$M_{fl} = -\frac{dF}{dH} = \frac{k_B T}{\Phi_0^{D/2}} H^{(D/2)-1} m_D(x) \tag{2.48}$$

where

$$m_D(x) \equiv x^{1-(D/2)}\frac{d\varphi(x)}{dx}. \tag{2.49}$$

These imply for the magnetization at T_c

$$M_{fl}(T_c) = \frac{k_B T}{\Phi_0^{D/2}} H^{(D/2)-1} m_D(\infty). \tag{2.50}$$

For 3D system these equation takes the form:

$$\frac{M_{fl}(T_c)}{H^{1/2}} = \frac{k_B T_c}{\Phi_0^{3/2}} m_3(\infty), \tag{2.51}$$

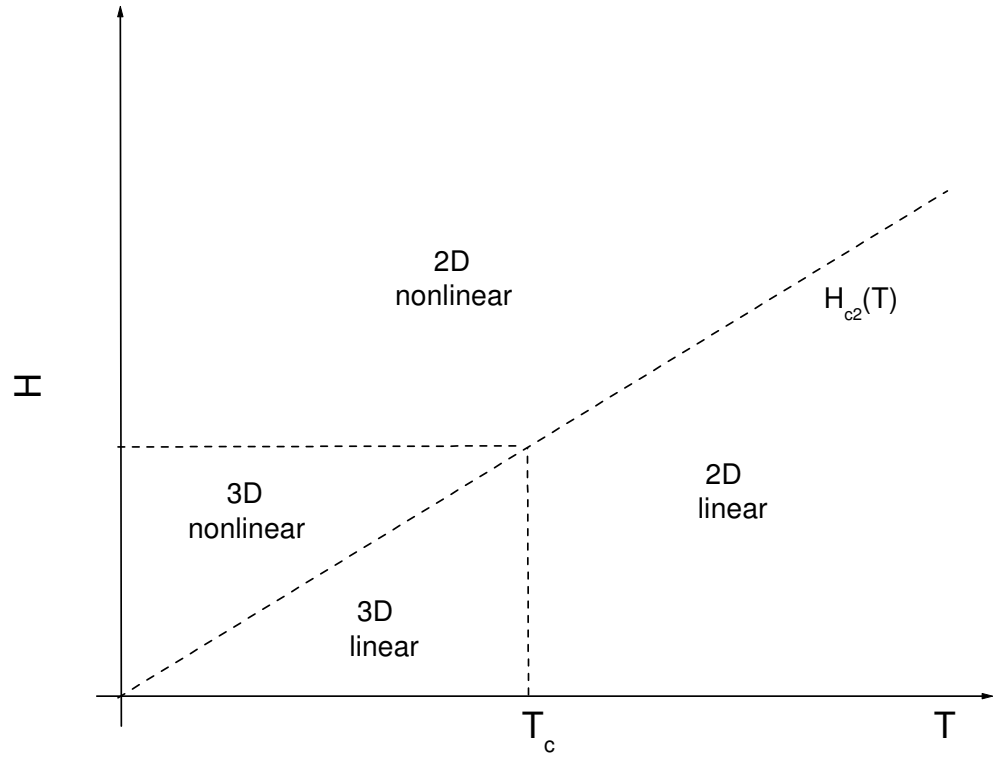

Figure 2.2: Sketch of the different regimes for fluctuating magnetization in the (H, T) diagram.

and T_c is a crossing point for the scaled magnetization $m = M_{fl}/H^{1/2}T_c$.

For 3D anisotropic system, for an applied field $H_\perp$ perpendicular to the layer, the number of flux quanta per coherence area is

$$x \equiv \frac{H_\perp \xi_\parallel^2}{\Phi_0} \tag{2.52}$$

so that the free energy per unit volume can be expressed as

$$F = -k_B T \xi_\parallel^{-2} \xi_\perp^{-1} \varphi(x) \tag{2.53}$$

and the magnetization normal to the planes at T_c results:

$$\frac{M_{fl\perp}(T_c)}{H_\perp^{1/2}} = \gamma \frac{k_B T_c}{\Phi_0^{3/2}} m_3(\infty) \tag{2.54}$$

where γ is the anysotropy correction multiplier

$$\gamma = \frac{\xi_{0\parallel}}{\xi_{0\perp}}, \tag{2.55}$$

and Eq.2.54 is in agreement with GL results (2.45).

Finally, we consider 2D system. In this case, the field dependence in Eq.2.50 cancels out and M_{fl} is field independent:

$$\frac{M_{fl}(T_c)}{H_{\perp}^{1/2}} = \gamma \frac{k_B T}{\Phi_0 s} m_2(\infty); \tag{2.56}$$

in agreement with what predicted in GL theory, see Eq.2.44.

2.3 Diamagnetism induced by phase fluctuations of the order parameter

In the previous section we have considered a superconducting system above the transition temperature, i.e. with a zero average order parameter amplitude $\langle|\Psi(\mathbf{r})|\rangle$. In this case the diamagnetism is related to the existence of metastable superconducting zones with fluctuations of the order parameter modulus, $\langle|\Psi(\mathbf{r})|^2\rangle \neq 0$.

Let us now consider superconducting islands below the transition temperature and the diamagnetism related to vortices due to the external field and to fluctuations of the phase of order parameter. In this case the order parameter amplitude $|\Psi(\mathbf{r})|$ is frozen to a non zero average value but the phase θ of the order parameter can fluctuate [11].

Fluctuations of θ gives

$$\oint \nabla\theta dt = 2\pi n, \tag{2.57}$$

being θ a periodic variable. Taking in account the relation between the phase θ and the current

$$\mathbf{j_s} = \frac{2en_h\hbar}{2m}\nabla\theta, \tag{2.58}$$

it can be seen that fluctuations of θ produce produce current vortices. In the 2-D case the vortex system can be studied using a two dimensional Coulomb gas model: at each vortex is associated an effective charge

$$q_v = \sqrt{2\pi J_{\|}} \tag{2.59}$$

where the sign of q_v is positive for a vortex and negative for an antivortex, i.e a vortex of negative helicity. The interaction energy of a vortex-antivortex pair at a distance r is

$$E_0 = q_v^2 \ln(r/\xi_{\|}). \tag{2.60}$$

where $\xi_{\|}$ is the coherence length in the plane. At T=0 and in zero field there will be no vortices, with temperature increase tightly bounded pairs of antiparallel vortices will be generated, with a density given by:

$$n_{th} = n_o \exp\left(-\frac{E_0}{k_B T}\right). \tag{2.61}$$

The quantity $2\pi J_{\parallel}$ is linear with temperature, but for

$$\pi J_{\parallel} = k_B T_{KT} \tag{2.62}$$

the vortex-antivortex pairs start to unbind and a Berezinski-Kosterlitzt-Thouless (BKT) transition occours, as a consequence $2\pi J_{\parallel}$ is zero and thermally excited free vortices are created.

We are interested in 3D cases in presence of a finite magnetic field: this led us to consider 3D thermal excited vortex loops (corresponding to 2D vortex-antivortex pairs) and field induced vortex lines, so that total density of vortices is

$$n_v = n_{th} + n_F = n_o \exp\left(-\frac{E_0}{k_B T(1+\delta\left(\frac{H}{H^*}\right)^2)}\right) + \frac{H}{\Phi_0}, \tag{2.63}$$

where n_F is the term due to the external field, and the effective vortex charge q_v, from which depends the interaction energy, is renormalized, as will be shown below in the calculation of the susceptibility χ. Moreover, we are interested in layered systems, described by discrete value of the variable z, and so vortex lines (and vertical element of vortex loops) are formed by stacks of pancake vortices correlated along c-axis for a length $n's$, where s is the interlayer distance. Finally in quasi 2-D superconductor $2\pi J_{\parallel}$ does not have a discontinuity for $T = T_{BKT}$ as takes a small but finite value above T_{BKT} [25]. We will study the system both in the glassy phase, where the system is ordered and irreversibility effect occurs, and in the liquid phase, where the system is disordered and vortices are random distributed. The vortex lattice melting temperature, or irreversibility temperature T_{irr}, coincides with T_{BKT}.

In order to calculate the susceptibility, we start from the order-parameter phase contribution to the L-D functional 2.27 [9, 11, 12]

$$\mathcal{F}_{LD}[\theta, \mathbf{A}] = \frac{1}{s}\sum_l \int d^2\mathbf{r} \left\{ J_{\parallel}\left(\nabla_{\parallel}\theta - \frac{2ie}{c\hbar}\mathbf{A}_{\parallel}\right)^2 + J_{\perp}[1-\cos(\theta_{l+1}-\theta_l)] \right\}, \tag{2.64}$$

where $J_{\parallel} = \pi\hbar^2|\Psi|^2/4m_e$ and $J_{\perp} = 2\pi\mathcal{J}|\Psi|^2$ are the order parameter phase coupling constants, and we consider the partition function :

$$Z = \int d\theta \exp\left(\frac{\mathcal{F}_{LD}[\theta, \mathbf{A}]}{k_B T}\right), \tag{2.65}$$

where a functional integration over all possible configuration of the order-parameter phase $\theta(r)$ for a frozen amplitude of the order parameter $|\Psi| = n_h$ is carried out. Then we derived the orbital magnetic response

$$K(\mathbf{q}) = \frac{\delta^2 F}{\delta A^2} \tag{2.66}$$

as the second derivative of the free energy F with respect to the potential vector A in the Fourier space. Taking in account the relation $\mathbf{H}(\mathbf{q}) = i\mathbf{q} \times \mathbf{A}(\mathbf{q})$ the

homogeneous susceptibility is then given by

$$\chi(H) = \frac{\partial^2 F}{\partial H^2} = \lim_{q\to 0} \frac{K(\mathbf{q})}{q^2}. \tag{2.67}$$

$K(\mathbf{q})$ is obtained as the sum of three contributions:

$$K(\mathbf{q}) = \left\langle \frac{\delta^2 \mathcal{F}_{LD}}{\delta A^2} \right\rangle - \frac{1}{k_B T} \left\langle \left(\frac{\delta \mathcal{F}_{LD}}{\delta A} \right)^2 \right\rangle + \frac{1}{k_B T} \left(\left\langle \frac{\delta \mathcal{F}_{LD}}{\delta A} \right\rangle \right)^2 \tag{2.68}$$

where $\langle \ldots \rangle$ is the thermal average. The orbital magnetic response can be expressed as

$$K(\mathbf{q}) = \frac{J_\parallel}{s} \left(\frac{2\pi}{\Phi_0} \right)^2 \left[\frac{J_\parallel}{k_B T} [P(\mathbf{q}) - Q(\mathbf{q})] - 1 \right] \tag{2.69}$$

where $P(q)$ derives from the term $\left\langle \left(\frac{\delta \mathcal{F}_{LD}}{\delta A} \right)^2 \right\rangle$ in Eq. 2.68, $Q(q)$ from the term $\left(\left\langle \frac{\delta \mathcal{F}_{LD}}{\delta A} \right\rangle \right)^2$ and $\frac{J_\parallel}{s} \left(\frac{2\pi}{\Phi_0} \right)^2$ is the diamagnetic response due to the first term in Eq.2.68.

$P(q)$ is related to the current-current correlation function $\langle j_x(\mathbf{r}) j_x(\mathbf{r}') \rangle$, as quoted in ref. [12], and takes the form

$$\begin{aligned} P(\mathbf{q}) \; = & \frac{1}{NL^2} \sum_{l,l'} \int d^2\rho \int d^2\rho' \exp[i\mathbf{q}(\mathbf{r} - \mathbf{r}')] \\ & \left\langle \left(\nabla_x \theta_l(\rho) - \frac{2\pi}{\Phi_0} A_{\parallel,x}(\mathbf{r}) \right) \left(\nabla_x \theta'_l(\rho') - \frac{2\pi}{\Phi_0} A_{\parallel,x}(\mathbf{r}') \right) \right\rangle \end{aligned} \tag{2.70}$$

with

$$j_x(\mathbf{r}) = \nabla_x \theta_n(\rho) - \frac{2\pi}{\Phi_0} A_{\parallel,x}(\mathbf{r}) \tag{2.71}$$

where the coordinate $\mathbf{r}$ means (ρ, ns) and L is the island size in the plane normal to axis $\mathbf{c}$. The x component of the phase gradient is related to the position $\mathbf{R}(m_1, l_1)$ of each pancake m_1 on the layer l_1 by the equation

$$\nabla_x \theta_n(\rho) = s \sum_{s_1, l_1} \frac{y - R_y(m_1, l_1)}{|[\rho - \mathbf{R}(m_1, l_1)]^2 + d^2(l - l_1)^2|^{\frac{3}{2}}} \, t(m_1, l_1), \tag{2.72}$$

where $t(m_1, l_1)$ is 1 for a vortex and -1 for an antivortex.

$P(q)$ can be expressed as the sum of four contributions:

$$P(\mathbf{q}) = P_{\theta\theta}(\mathbf{q}) + P_{AA}(\mathbf{q}) + P_{A\theta}(\mathbf{q}) + P_{\theta A}(\mathbf{q}). \tag{2.73}$$

The first term, involving the positional correlation function of vortex line elements, was calculated by Sewer and Beck [12], and takes the form:

$$P_{\theta\theta}(\mathbf{q}) = \frac{4\pi^2}{q^2} n_v S_C(\mathbf{q}) [1 + 2X(\mathbf{q})] \tag{2.74}$$

where

$$S_C(\mathbf{q}) = \frac{q^2}{q^2 + 2\pi n_v q_v^2/k_B T} \tag{2.75}$$

is the Coulomb-2D gas structure factor, and the factor

$$X(\mathbf{q}) \approx \frac{1 - \exp(-k_B T n' s q^2/4\lambda)}{\exp(-k_B T s q^2/4\lambda) - 1} \tag{2.76}$$

takes in account of harmonic deviations of the vortex line along the z-direction; in the calculation an effective stiffness given by $\lambda \approx \frac{J_\perp}{s} \approx \frac{J_\parallel}{s\gamma^2}$ is assumed.

The term $P_{AA}(\mathbf{q})$ is due to the external field and one has

$$P_{AA}(\mathbf{q}) = \frac{\pi^2}{36}\left(\frac{HL^2}{\Phi_0}\right) L^2 q^2. \tag{2.77}$$

The last two terms in Eq. 2.73 involve the correlation between vortices and are equal to zero in the liquid phase above the irreversibility temperature T_{Irr}. This term is different from zero in the glassy phase below the irreversibility temperature, and is calculated in Ref. [9] assuming that the vortices are uniformely distributed in the planes, yielding

$$P_{\theta A} = -\frac{2\pi^2}{3}\left(\frac{HL^2}{\Phi_0}\right)^2 + \frac{2L^2}{45}\pi^2\left(\frac{HL^2}{\Phi_0}\right) q^2. \tag{2.78}$$

The term $Q((\mathbf{q}))$ is also related with the correlation between vortices and so is equal to zero for $T > T_{IRR}$, for $T < T_{IRR}$ it was calculated in Ref. [9] yielding:

$$Q = (2\pi)^2\left(\frac{HL^2}{\Phi_0}\right)^2\left[\frac{1}{q^2L^2} + \frac{1}{144\times 4}q^2L^2 + \frac{1}{12}\right]. \tag{2.79}$$

Then from Eqs. 2.68, 2.73, 2.74, 2.77, 2.78, 2.79 one obtains:

$$\begin{aligned} K(\mathbf{q}) = \frac{J_\parallel}{s}\left(\frac{2\pi}{\Phi_0}\right)^2 & \left[\frac{2\pi J_\parallel}{q_v^2}(1+2n') - \delta\left(\frac{H}{H^*}\right)^2 - 1\right] \\ & + \left\{-\frac{k_B T}{s\Phi_0^2}\frac{1}{1+2n'}\frac{\left[1+\delta\left(\frac{H}{H^*}\right)^2\right]^2}{n_v} - \frac{s^2\gamma^2(1+n')}{1+2n'}\cdot\left[1+\delta\left(\frac{H}{H^*}\right)^2\right]\right. \\ & \left. + \frac{47L^2}{540}\frac{J_\parallel}{s}\left(\frac{2\pi}{\phi_0}\right)^2\left(\frac{H}{H^*}^2\right)\right\}\mathbf{q}^2, \end{aligned} \tag{2.80}$$

where $H^* = \Phi_0/L^2$. Considering that the first term in Eq. 2.80 must go to zero, to avoid divergences in the susceptibility defined in Eq. 2.67, one have a renormalization of q_v related to to H and n':

$$q_v^2 = \frac{2\pi J_\parallel (1+2n')^2}{1+\delta\left(\frac{H}{H^*}\right)^2}, \tag{2.81}$$

and the susceptibility takes the form:

$$\begin{aligned}\chi(H) = &-\frac{k_B T}{s\Phi_0^2}\frac{1}{1+2n'}\frac{\left[1+\delta\left(\frac{H}{H^*}\right)^2\right]^2}{n_v} \\ &-\frac{s^2\gamma^2(1+n')}{1+2n'}\cdot\left[1+\delta\left(\frac{H}{H^*}\right)^2\right]+\frac{47L^2}{540}\frac{J_\parallel}{s}\left(\frac{2\pi}{\phi_0}\right)^2\left(\frac{H}{H^*}\right)^2,\end{aligned} \tag{2.82}$$

where

$$\delta = \begin{cases} \frac{\pi^2 J_\parallel}{3k_B T} & \text{, when } T > T_{irr}, \\ \frac{\pi^2 J_\parallel}{k_B T} & \text{, when T<T}_{irr}. \end{cases}$$

For $H \ll H^*$ the second and the third term in Eq. 2.80 can be negletected and there is only a negative contribution to susceptibility. Increasing the field this therm grows and χ can change the sign causing an upturn in magnetization curves. In 2D systems for $T > T_{irr}$ no upturn in the magnetization curves is expected, because in this systems $J_\parallel/k_B T$ is zero above the irreversibility temperature and so $\delta = 0$ in Eq. 2.82 and $\chi < 0$ for any field H. For 3D system (and for 2D system in the glassy phase) it can be proved that the equation $\chi = O$ has real solution (and so un upturn in magnetization curves is expected) only if the dimension of the island L is greater than a critical dimension L_c, depending on the temperature and from the other system parameters that appear in Eq. 2.82.

Chapter 3

Characterization data for $SmBa_2Cu_{2.85}Al_{0.15}O_{6+\delta}$

In this Chapter the crystal structure of two samples of $SmBa_2Cu_{2.85}Al_{0.15}O_{6+\delta}$ with the same oxygen content δ, derived from $SmBa_2Cu_3O_7$ but different thermally treated is described. The structural data result most from X-ray diffraction and Eletron Paramagnetic resonance (EPR), (§2). The dependence of crystal structure from thermal treatment is discussed in §3 in terms of clustering of Al-defects. The results reported in this Chapter originate from the group of M. Scavini and C. Oliva of the University of Milan.

3.1 Crystal structure of $SmBa_2Cu_3O_{6+\delta}$

In general, the crystal Structure of $SmBa_2Cu_3O_{6+\delta}$ can be described as the superposition of three perovskite cells: Sm is the central ion of central cell, Ba is the central ion of external cells.

The structure of $SmBa_2Cu_3O_{6+\delta}$ depends on the oxygen content δ (Fig. **??**)[26].

With $\delta = 0$ the O(4)and O(5) sites in the Cu(1) layer are vacant and the structure is tetragonal (space group $P4/mmm$), with lattice parameters a =b = 3.86 Å and c = 11.84 Å (see Table 3.1). O(4)and O(5) sites are equivalent and

	$SmBa_2Cu_3O_6$	$SmBa_2Cu_3O_7$
	Insulating	Superconducting
Space group	$P4/mmm$ Tetragonal	$Pmmm$ Orthorhombic
a(Å)	3.86	3.82
b(Å)	≡ a	3.89
c(Å)	11.84	11.68

Table 3.1: Crystal structure characteristics of $SmBa_2Cu_3O_6$ and $SmBa_2Cu_3O_7$

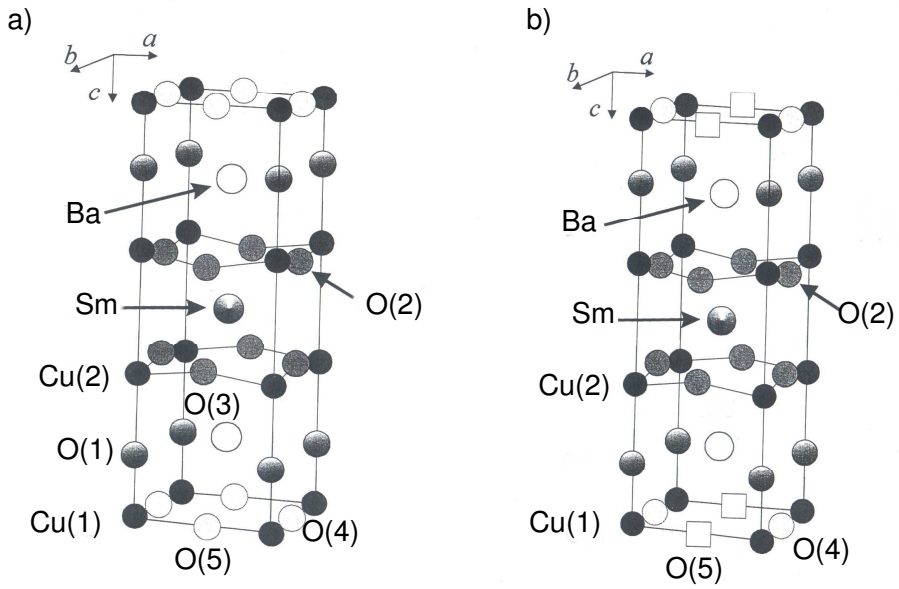

Figure 3.1: Sketches of the $SmBa_2Cu_3O_{6+\delta}$ unit cells, for the non superconducting tetragonal phase, $\delta < 0.5$ (a), and for the superconducting orthorhombic phase, $\delta > 0.5$ (b). Occupation factor of O(4) site is for tetragonal phase and for the orthorhombic phase.

also the O(2)and O(3) sites. The tetragonal phase of $SmBa_2Cu_3O_{6+\delta}$ ($\delta < 0.5$) is insulating and does not superconduct.

Increasing the oxygen content slightly causes more of O(4) and O(5) sites to become occupied, with occupational factor equal to $\frac{\delta}{2}$.

For $\delta > 0.5$ Cu-O chains along the b-axis of the crystal are formed, O(5) sites are vacant and O(4) sites are occupied with occupational factor equal to δ. Elongation of the b-axis changes the structure to orthorhombic (space group $Pmmm$), for $\delta = 1$ lattice parameters are a = 3.82, b = 3.89 and c = 11.68 Å (see Table 3.1). O(4)and O(5) sites are no longer equivalent and also the O(2)and O(3) sites are no equivalent. The orthorhombic phase of $SmBa_2Cu_3O_{6+\delta}$ is superconducting and the optimum superconducting properties occur when $\delta \sim 0.93$ and all of the O(4) sites are occupied with few vacancies. Charge transport is confined to the Cu(2)O planes while the Cu(1)O(4) chains act as charge reservoirs, which provide carriers to the CuO planes.

3.2 Crystal structure of oxidized and reoxidized $SmBa_2Cu_{2.85}Al_{0.15}O_{6+\delta}$

Polycrystalline $SmBa_2Cu_{2.85}Al_{0.15}O_{6+\delta}$ samples that we will study were synthesized by the solid-state reaction described in ref. [15]. Subsequently sample A

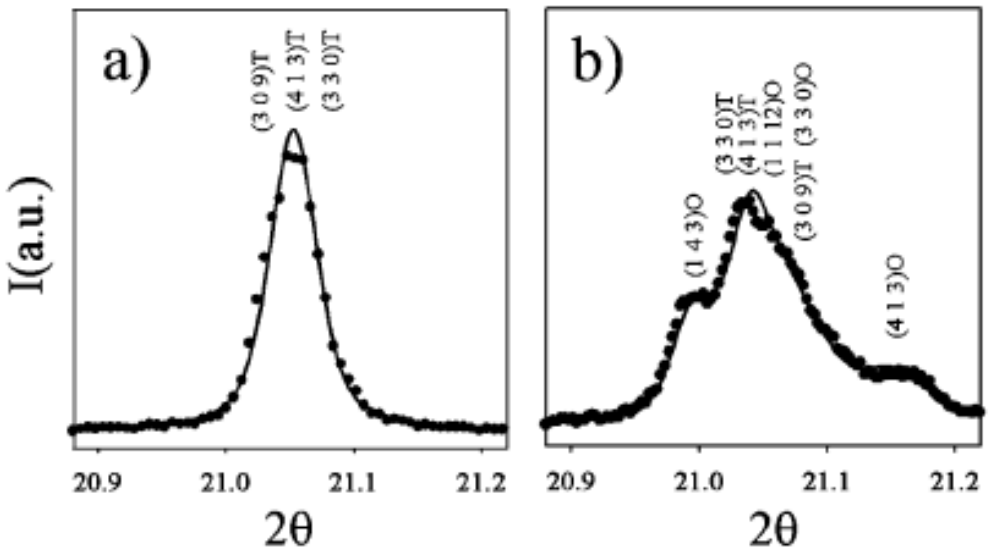

Figure 3.2: Details of the experimental (circles) and of the calculated(full lines) XRPD patterns relative a) to the A sample and b) to the B sample. O and T refer to the orthorombic and tetragonal phase respectively, from [14].

($\delta = 1$) was annealed for 96 hours at T = 673 K and $P(O_2) = 1$ atm to induce oxidation. An aliquot of sample A was annealed at T = 1073 K and $P(O_2) = 10^{-4}$ atm for 96 hours and then at T = 400 K and $P(O_2) = 1$ atm to give sample B, in order to obtain Al clustering (see [16] and §3 of this chapter).

The Al concentration is fixed by the preparation while Thermogravimetric measurements revealed that $\delta_A - \delta_B \sim 0.02$. This means that sample A (no Al clustering) and B (Al clustering) have approximately the same total holes concentration [14].

3.2.1 X-ray

X-ray powder diffraction (XRPD) patterns were collected at T = 80 K, covering a Q-range as large as $_{max} = 18.7$ Å^{-1} ($\lambda = 0.33483(1)$ Å) at the ID31 beamline of the ESRF, Grenoble, France [27]. Rietveld refinement has been performed using the GSAS software suite [28] and its graphical interface EXPGUI [29], while for real-space analysis the programs PDFGetX [30] and PDFFIT [31] were used.

Details of the XRPD patterns referring to the two samples are reported in Fig. 3.2. The numbers in brackets are the Miller indices, "O" and "T" standing for orthorhombic and tetragonal system, respectively. Some selected results of the refinements are reported in Table 3.2.

Different annealing procedures affect the sample structure. A single tetragonal phase matches well the XRPD pattern of sample A, while a biphasic

	Sample A	Sample B model 1		Sample B model 2	
		Phase 1	Phase 2	Phase 1	Phase 2
Space group	$P4/mmm$	$P4/mmm$	$Pmmm$	$P4/mmm$	$Pmmm$
Weight fraction	1	0.443	0.557	0.466	0.534
a(Å)	3.88	3.89	3.87	3.89	3.86
b(Å)	≡ a	≡ a	3.90	≡ a	3.90
c(Å)	11.67	11.64	11.67	11.64	11.67
o.f.(Cu(1))	0.85	0.85	0.85	0.808	0.892
o.f.(Al(1))	0.15	0.15	0.15	0.192	0.108
o.f.(O(4))	0.98	0.96	0.96	0.96	0.69
o.f.(O(5))	-	-	0.00	-	0.27

Table 3.2: Selected structural parameters and agreement values of sample A and B determinated by X-ray diffraction. Cu1 occupies the (0,0,0) site; Al1 occupies the (x,x,0) site, x$\sim \pm 0.06$ site; O4 occupies the (0,1/2,0) site (see Fig.??). The occupational factor (o.f.) are expressed as atoms per cells.

model is required to interpret the XRPD pattern of the reoxidized sample B: a tetragonal phase and an orthorhombic, ca. with the same weight.

The XRPD pattern of sample B has been best fitted using two structural models: in model 1, all the positional and thermal parameters are supposed to be identical for the two phases while in model 2 the positional coordinates and the Al concentration have been varied independently. In model 2, the Al concentration increases in the tetragonal phase with respect to the orthorhombic phase (see Table 3.2), reinforcing the idea that Al clustering is the driving force of the phase separation observed in sample B.

From real-space analysis a value of 20 Å is derived for the average width of Al-free domains in sample B [14].

3.2.2 EPR

EPR spectra recorded in the range $105 < T < 380$ K using a Bruker Elexsys spectrometer (modulation amplitude 3 gauss, microwave attenuation 15 dB, gain 60 dB) are reported in Fig.3.3. They are rather similar at T = 280 K, being composed of a Lorentzian-shaped line (L) at g$\sim$ 2, to which a broad, low-intensity Gaussian shaped line (G) adds at lower values of the magnetic field. At lower temperatures, G becomes more intense and broader, and moves towards lower field values. These effects are more accentuated for sample A (Fig. 3.3a), while L increases markedly at lower temperatures (T$\leq$ 200 K) only for sample B (Fig. 3.3b).

The narrowed L Lorentzian shape is due to units like:
$-\ Cu^{2+}\ \downarrow -\ O^{2-}\ \uparrow\downarrow -\ Cu^{2+}\ \uparrow -\ O^{-}\ \uparrow -\ Cu^{2+}\ \uparrow -\ O^{2-}\ \uparrow\downarrow -$ (Scheme I)
In fact, the ferromagnetic (FM) coupling between the three unpaired spins on the right of Scheme I continuously swaps with the anti-FM coupling occurring

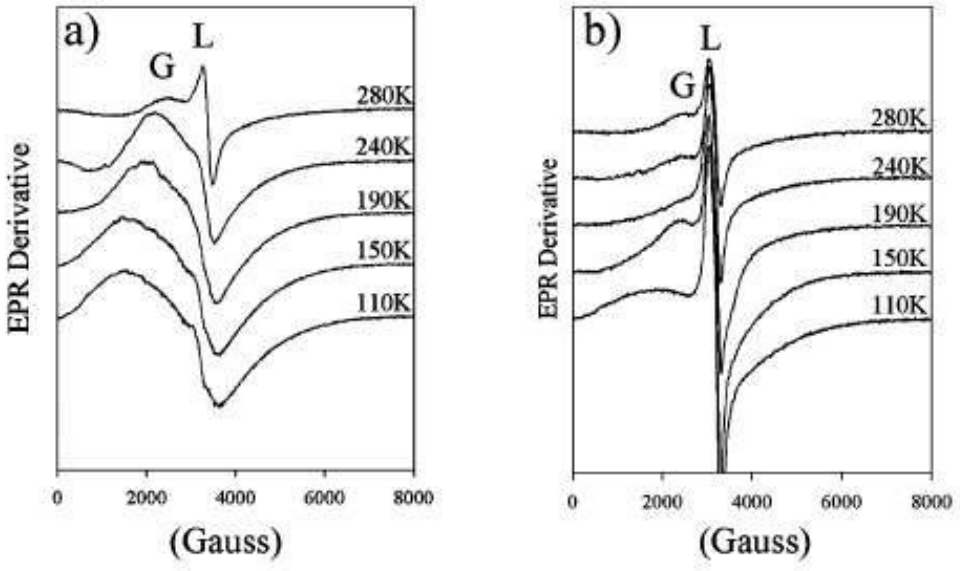

Figure 3.3: EPR spectra corresponding to the A sample (a) and to the B sample (b) at different temperatures. G and L refers to the Gaussian and Lorentzian shaped peaks, respectively, from Ref. [14].

between the central and the left Cu ions in Scheme I.

The G pattern is generated [32] from different spin-polarized clusters of O^- holes with limited mobility [33] packed in spin bags [34] (SBs).

The pronounced increase of the L/G ratio in sample B can be ascribed to Al-clustering which causes the formation of more ordered system, in which SBs almost disappear while longer chain fragments like those of Scheme I build up.

3.3 Effects of thermal treatment on Al-defect clustering in $SmBa_2Cu_{2.85}Al_{0.15}O_{6+\delta}$

The dependence of crystal structure from thermal treatment is determined by the arrangement of Al in the Cu(1) layer Fig. 3.4[16].

As discussed in §1, in the oxidized pure system $SmBa_2Cu_3O_7$ O(4) sites are occupied and O(5) sites are vacant(see Fig. 3.5(a) and Fig. **??**(b)). In the original oxidized Al-doped sample A, Al^{3+} ions (four-fold coordinated) substitutes Cu^{2+} ions in Cu(1) site with random spatial distribution, causing the O(4) neighboring oxygen ion to move to O(5) site and therefore, since the neighboring Cu(1) must be three-fold coordinated, two oxygen will leave the matrix(see Fig.3.5(b)). This process causes a break of the linear O-Cu-O chains or a deflect of them by 90 degrees. The matrix becomes divided into small orthorhombic domains and the the sample appears macroscopically tetragonal (Fig. 3.4 (a)).

Reduction of the sample at low temperature, T$\leq$ 973 K, where Al diffusion coefficient is negligible (Al^{3+} ions are immobile), removes the oxygen between Cu ions, while the oxygen between Al^{3+} ions remains pinned in the layer (Fig. 3.4 (b)).

Instead if the sample is reduced at higher temperatures, T$\geq$ 973 K, where the Al diffusion coefficient is sufficiently great, oxygen content is minimized by the formation Al-O-Al- clusters (Fig.3.6 and Fig. 3.4 (c)).

If this reduced sample is reoxidized at low temperature, such as 673 K (sample B), where clustered Al^{3+} ions are expected to remain immobile, the number of effective domain-wall pinning centers per unit volume is reduced and there is the formation of macroscopically orthorhombic domains (Fig. 3.4 (d)).

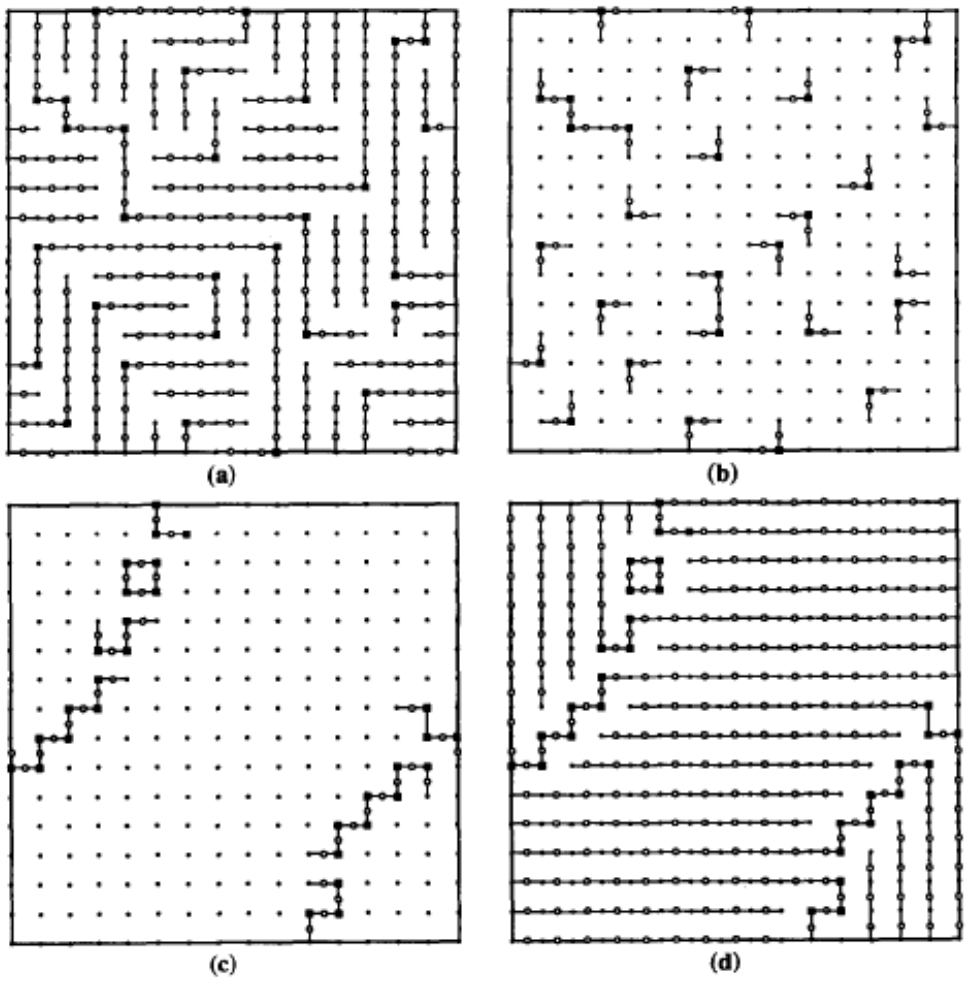

Figure 3.4: Al (■), Cu (•) and O (□) distribution within the Cu (1) layer. For the oxidized (a), the random Al arrangement leads to the formation of small orthorhombic domains. Reduction at low temperature (b) only affects the oxygen between Cu ions, whereas for a reduction at high temperature (c) the Al ions may form [Al-O] clusters. The [Al-O] clusters reduce the defect density in the Cu-O layer, so that larger orthorhombic domains can form in the reoxidized sample (d), from Ref. [16].

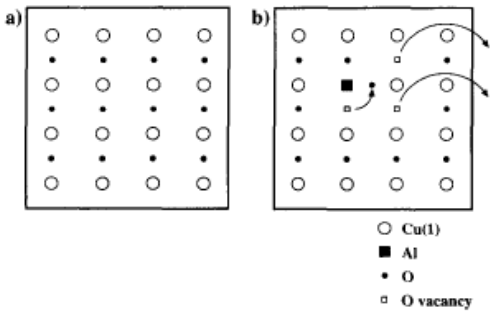

Figure 3.5: In the oxidized pure system $SmBa_2Cu_3O_7$ (a) the oxygen atoms are located at the O(4) sites and form Cu-O chains along the a axis. The O(5) sites remain vacant. Doping by trivalent Al^{3+} leads to a disorder in the oxygen sublattice and thus to a reduction of the total oxygen content (b), from Ref. [16].

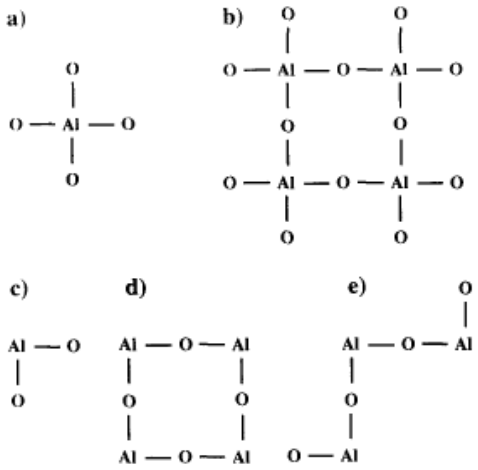

Figure 3.6: Possible Al-O arrangements within the Cu(1) layers for octahedral (a,b) and tetrahedral (c,e) coordination of Al^{3+}. Clustering of Al defects (d,e) minimize oxygen contents by sharing oxygen ions, from Ref. [16].

Chapter 4

Magnetization measurements on $SmBa_2Cu_{2.85}Al_{0.15}O_{6+\delta}$

In this Chapter, high resolution magnetization measurements M(H,T) carried out in the pure sample $SmBa_2Cu_3O_7$ (§1), in the oxidized $SmBa_2Cu_{2.85}Al_{0.15}O_{6+\delta}$, sample A, (§2), and in the reoxidized $SmBa_2Cu_{2.85}Al_{0.15}O_{6+\delta}$, sample B, (§3), are presented.

Measurements have been carried out by means of Quantum Design MPMS-XL7 SQUID Magnetometer.

In general, two different processes can be performed to obtain the magnetization M ay constant field:

- In zero-field-cooling process (ZFC), the system is cooled down in zero field to the temperature T, then the magnetic field H is applied and the measure of M is carried out.
- In field-cooling process (FC), the magnetic field H is applied at high temperature (in our case 300 K), then the system is cooled down to the temperature T and the measure of M is performed.

The value of M at the end of the two processes, can be different if one of the two processes, or both, leads the system to a thermodynamical non-equilibrium state.

4.1 Isothermal and isofield magnetization curves in $SmBa_2Cu_3O_7$

The sample of chemical composition $SmBa_2Cu_3O_7$ was synthesized by solid-state reaction following the procedure described in Ref. [15]. The crystal structure is described in Chapter 3.1 (see Fig.**??** (b)).

In Fig. 4.1 the temperature dependence of magnetic susceptibility in applied field $H = 20$ Oe is reported. The occurrence of two slightly different phases,

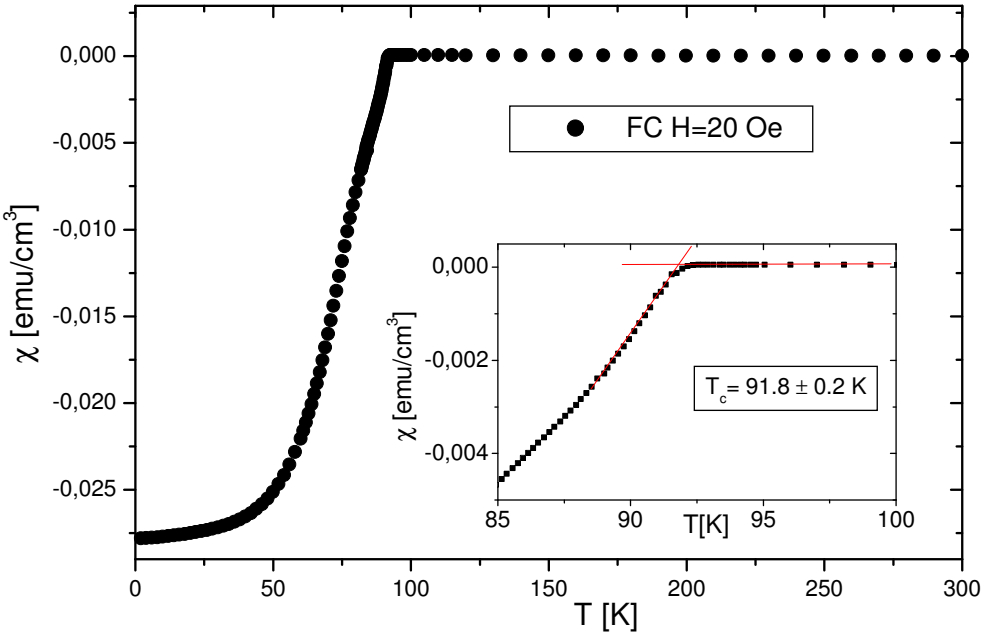

Figure 4.1: Magnetic susceptibility of $SmBa_2Cu_3O_7$ powders as a function of temperature, obtained in a field-cooling process at applied magnetic field $H = 20$ Oe. In the inset, by zooming the experimental data of the main figure, the evaluation of the transition temperature T_c is shown. It should be remarked that in the scale adopted the paramagnetic, Pauli-like, contribution is negligible, as well as other diamagnetic contribution present above T_c

.

undergoing superconducting transition at different temperatures, is evident from the change of the slope of the curve around 90 K. The higher transition temperature was estimated extrapolating to zero the linear behavior of χ in the temperature range 90-92 K, as shown in the inset of Fig. 4.1. One derives $T_c = 91.8 \pm 0.2$K.

Magnetization measurements at a constant field H have been performed as a function of temperature. In general, three contribution to the magnetization M_{tot} were observed: the Pauli-like contribution M_P only slightly T-dependent , a contribution due to impurities M_{imp}, and the contribution related to the superconducting properties M. $M_P + M_{imp}$ is found to be linear in T in the temperature range $\Delta T = 150 - 95$ K, where M is practically zero. So M in the proximity of T_c was extracted by subtracting from M_{tot} the value obtained extrapolating for $T \rightarrow T_c^+$ the curve $M_P + M_{imp}$ vs T in ΔT.

Typical magnetization curves $M(H = const, T)$ for different applied field, in field-cooling condition, are reported in Fig.4.2.

The diamagnetic contribution to magnetization curves due to superconduct-

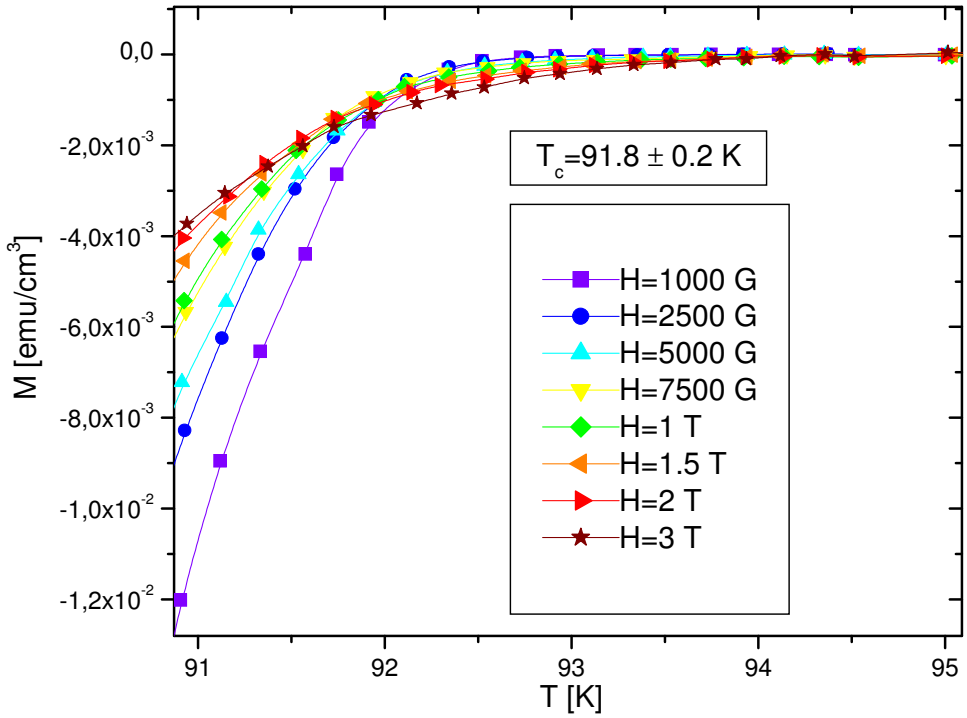

Figure 4.2: Magnetization as a function of temperature, in proximity of the transition, in $SmBa_2Cu_3O_7$, obtained in field-cooling processes. The solid lines are guides to the eye.

ing fluctuations M_{fl} as a function of field for different temperatures is represented in Fig. 4.3. The data in each isothermal curve were extracted from the data in Fig. 4.2, fixing the temperature to a value $T \geq T_c$ and collecting the value of M for different fields. Being $T \geq T_c$ this contribution is not due to the superconducting equilibrium state but to metastable Cooper pairs that arise for $T \rightarrow T_c$, associated to thermal fluctuations of the order parameter (see Chapter 1). Finally, M was multiplied by 3 because, being the sample formed by non-oriented powders, only 1/3 of the sample has on average $\mathbf{c} \parallel \mathbf{H}$ and we consider negligible the contribution to magnetization due to sample regions with $\mathbf{c} \perp \mathbf{H}$. Actually, the dependence of fluctuating magnetization on the angle between $\mathbf{c}$ and $\mathbf{H}$ in an anisotropic superconductor is more complex, a detailed calculation are given in [35] for a randomly oriented powder. However, for anisotropy factor $\gamma \approx 7$ the fraction $\frac{1}{3}$ is close to the result of the detailed analysis [35]. It's worth to stress that there will be no difference between the curves obtained in this way, i.e. in FC processes, an the ones derived in ZFC processes, because no irreversibility effects has been detected in the temperature range $92.5 \leq T \leq 94$ K.

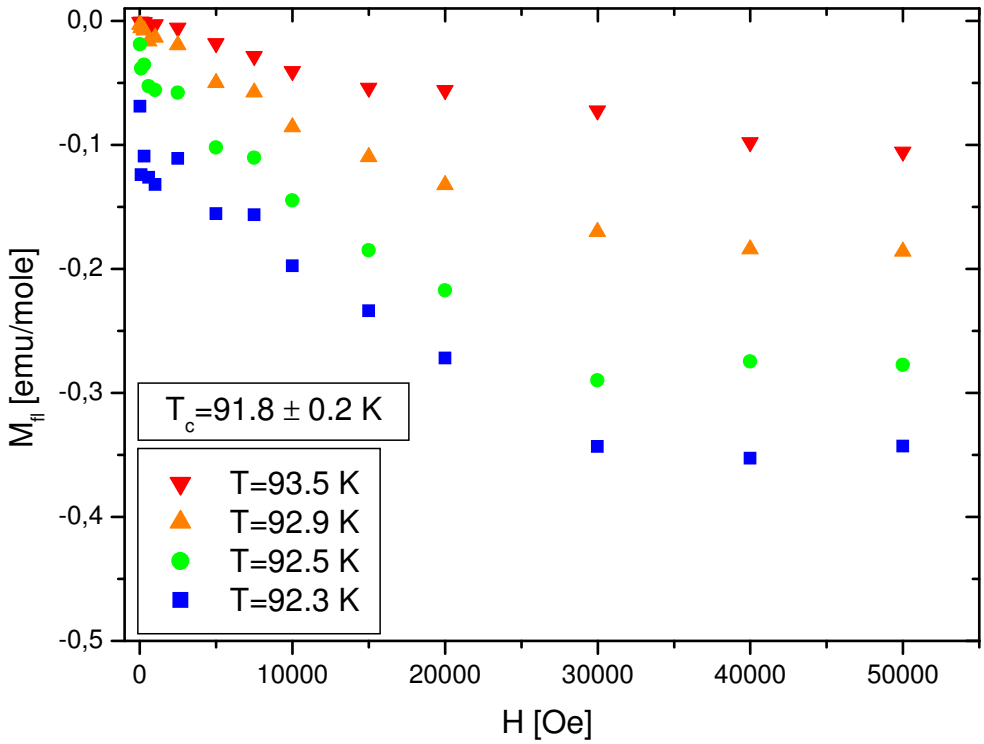

Figure 4.3: Diamagnetic magnetization as a function of field along the c-axis, for different temperatures above T_c, in $SmBa_2Cu_3O_7$, obtained in field-cooling processes. the changeover from the linear field regime ($-M_{fl} \propto H$) to $-M_{fl} \propto \sqrt{H}$ for $T \to T_c$ is manifest.

4.2 Isofield magnetization curves: oxidized $SmBa_2Cu_{2.85}Al_{0.15}O_{6+\delta}$ and reoxidized $SmBa_2Cu_{2.85}Al_{0.15}O_{6+\delta}$

The sample of chemical composition $SmBa_2Cu_{2.85}Al_{0.15}O_{6+\delta}$ (sample A) was synthesized by solid-state reaction following [15] and subsequently was annealed for 96 hours at T = 673 K and $P(O_2) = 1$ atm to induce oxidation (sample (A), oxidized $SmBa_2Cu_{2.85}Al_{0.15}O_{6+\delta}$); an aliquot of sample (A) was further annealed at T = 1073 K and $P(O_2) = 10^{-4}$ atm for 96 hours and then at T = 400 K and $P(O_2) = 1$ atm for the same time (sample (B), reoxidized $SmBa_2Cu_{2.85}Al_{0.15}O_{6+\delta}$), in order to obtain Al clustering [14] . The crystal structure of the two samples is described in Chap. 3.2 of this thesis (see Tab. 3.2), the effects of thermal treatment on Al-defects clustering are described in Chap. 3.3 (see also [16]).

In Fig. 4.4 the temperature dependence of magnetic susceptibility in a applied field $H = 15$ Oe is represented for A sample (Fig. 4.4(a)) and for B sample (Fig. 4.4(b)). The slope of the curve χ vs. T indicates that both

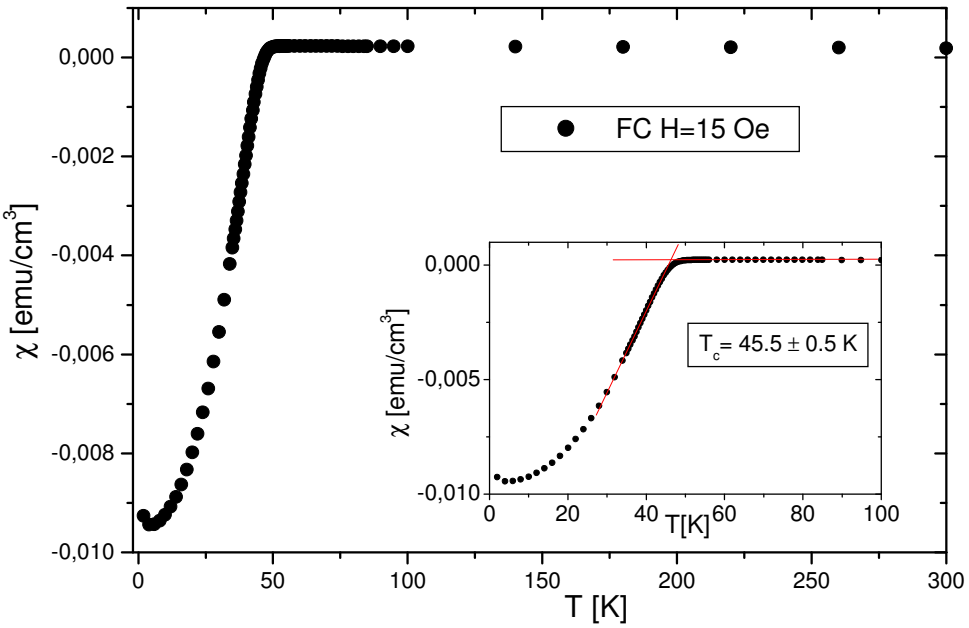

(a)

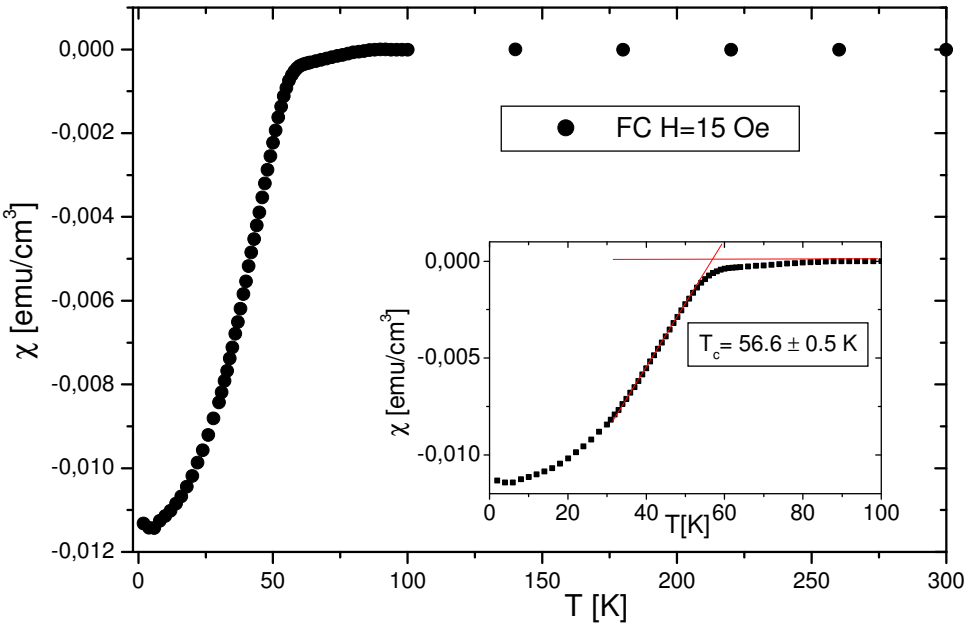

(b)

Figure 4.4: Magnetic susceptibility of the A (a) and B (b) samples obtained in field-cooling-processes at applied magnetic field $H = 15$ Oe. In the insets, by zooming the experimental data of the main figure, the T_c evaluation is shown.

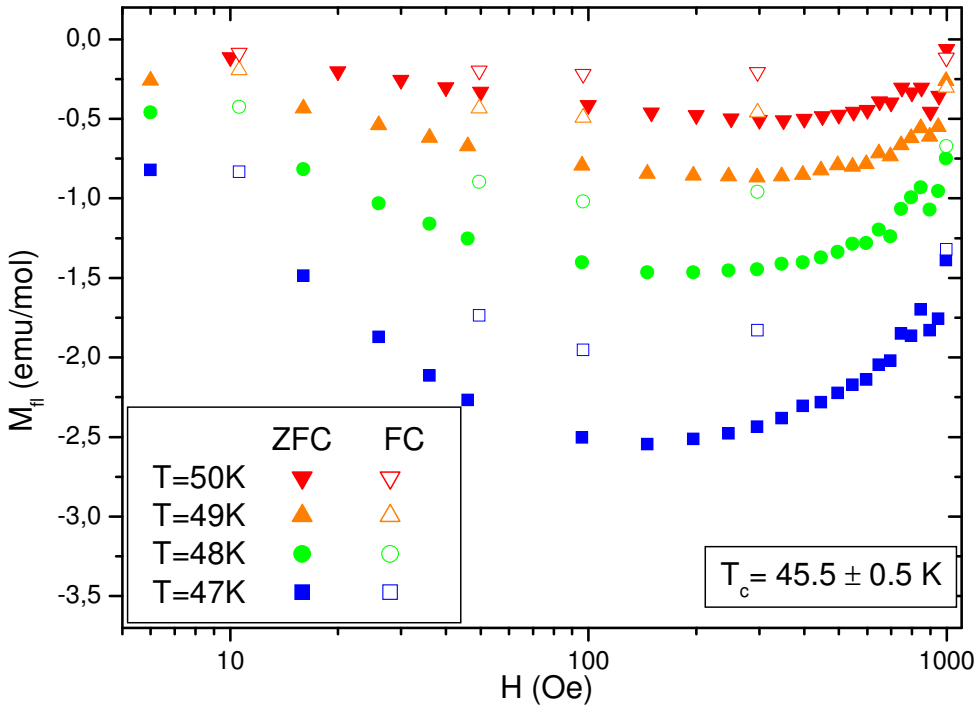

Figure 4.5: Diamagnetic magnetization as a function of field along the c-axis for different temperatures above T_c in oxidized $SmBa_2Cu_{2.85}Al_{0.15}O_{6+\delta}$ (sample A), obtained in field-cooling (empty symbol) and zero-field-cooling (filled symbols) processes.

samples are monophasic. The transitions temperatures T_c were estimated extrapolating at zero the linear behavior of χ occuring below T_c, as shown in the insets in Fig. 4.4. One has $T_c = 45.5 \pm 0.5$ K for A sample and $T_c = 56.6 \pm 0.5$ K for B sample.

4.3 Isothermal magnetization curves: oxidized $SmBa_2Cu_{2.85}Al_{0.15}O_{6+\delta}$ and reoxidized $SmBa_2Cu_{2.85}Al_{0.15}O_{6+\delta}$

The diamagnetic contribution to magnetization due to superconducting fluctuations M_{fl} as a function of field for different temperatures, obtained in zero-field-cooling (ZFC) and field-cooling (FC) processes, is represented in Fig. 4.5 for sample A and in Fig. 4.6 for sample B.

For ZFC processes, $M_{fl}(H)|_T$ has been obtained subtracting to the magnetization at the temperature T of interest the value of magnetization at a temperature (70 K for A sample, 100 K for B sample) where the effect of fluctuations can be neglected. In this way the Pauli contribution to the magnetization,

slightly dependent from T, is eliminated. The residual contribution due to paramagnetic impurities is linear in the field for high fields in both samples and so can easily removed.

For FC processes, to obtain $M_{fl}(H)|_T$ a procedure similar to the one described in §1 for $SmBa_2Cu_3O_7$ was utilized. First iso-field FC curves $M_{tot}(T)|_H$ were measured. Three contribution to the total magnetization M_{tot} were observed: a Pauli like contribution M_P slightly dependent from T, a contribution due to impurities M_{imp}, and the contribution due to the superconducting system M. Then curve $M_P + M_{imp}$ vs T was evaluated in a temperature range ΔT where M is practically zero ($\Delta T = 100-55$ K for sample A and $\Delta T = 200-100$ K for sample B). So M in the proximity of T_c was extracted by subtracting from M_{tot} the value obtained extrapolating for $T \to T_c^+$ the curve $M_P + M_{imp}$ vs T in ΔT. Then $M(H)|_T$ in proximity of T_c was obtained from $M(T)|_H$ data fixing the temperature to a value $T \geq T_c$ and collecting the value of M for different fields. Finally, M_{fl} was derived multiplying M by 3 because, as already explained.

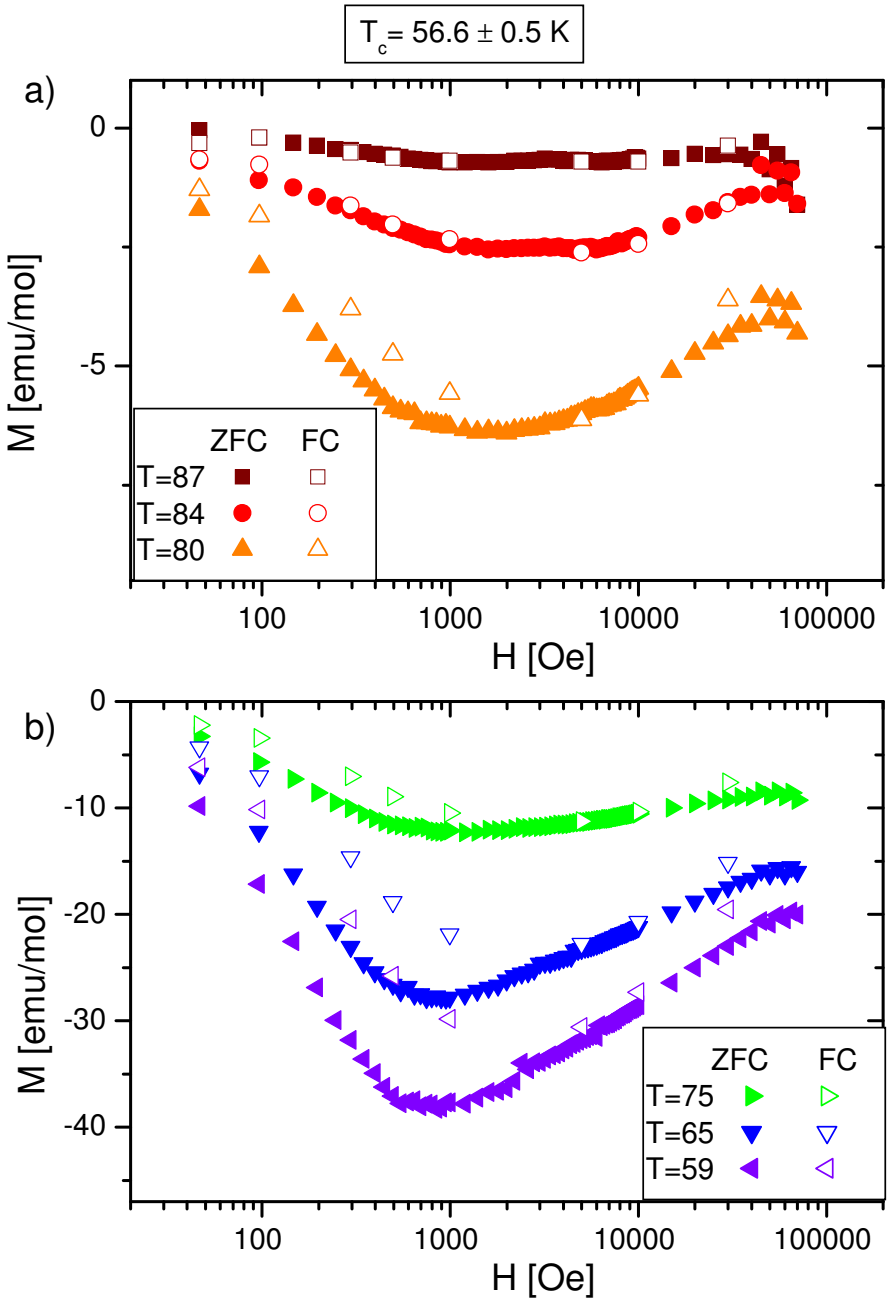

Figure 4.6: Diamagnetic magnetization as a function of field along the c-axis for (a) higher and (b)lower temperatures above T_c in reoxidized $SmBa_2Cu_{2.85}Al_{0.15}O_{6+\delta}$ (sample B), obtained in field-cooling (empty symbol) and zero-field-cooling (filled symbols) processes.

Chapter 5

Results and Discussion

In this Chapter the experimental data reported in Chapter 4 are discussed in the framework of the fluctuations theory based on Ginzburg-Landau functional (GL), briefly recalled at Chapter 2. Isothermal magnetization curves in $SmBa_2Cu_3O_7$ sample are found to be explained with the diamagnetic contribution to the total magnetization due to fluctuations of the order parameter modulus, calculated on the basis of an anisotropic GL functional (§1). On the contrary, it is showed that the diamagnetic response of $SmBa_2Cu_{2.85}Al_{0.15}O_{6+\delta}$ samples cannot be ascribed to a conventional GL-scenario, but has to be discussed in terms of phase fluctuations of the local order parameter in a layered system of vortices, where charge inhomogeneities induce local superconducting regions with local transition temperature T_c^{loc} higher than the bulk transition temperature T_c (§2).

5.1 Fluctuations of the order parameter modulus in $SmBa_2Cu_3O_7$

Ginzburg-Landau description of fluctuating diamagnetism breaks down when a magnetic field comparable to H_{c2} is applied. For example, it was experimentally observed [36] that the scaled magnetization $m = M_{fl}(T_c)/H^{1/2}T_c$ is not independent from the applied magnetic field H but is progressively reduced by H and practically quenched for $H \approx H_{c2}(0) * 10^{-2}$, while, on the basis of the conventional GL theory it would be a universal numerical constant for all materials and for all applied fields, according to the equation

$$M_{fl}(T_c, H \to 0) = -\frac{0.32 k_B T_c}{\Phi_0^{3/2}} \sqrt{H}. \tag{5.1}$$

This break-down is due to the fact that the application of magnetic field favours short-wave-length fluctuation modes, which in the conventional GL theory [37] are neglected.

To determine, in our case, the range of validity of the G-L theory we will limit our consideration first to the zero-dimensional case, i.e $d \ll \xi(T)$,or, as extended approximate case, $d \leq \xi(T)$. In the 0-D case one can derive the Fluctuating Diamagnetism as due to metastable superconducting droplets of dimension d of the order of $\xi(T)$[36], see §2.2.1 and Appendix A.

According to equation 2.26, the smallest droplets contribute most to the fluctuating diamagnetism. At the same time, to such droplets ($d \leq \xi(T)$) is associated a high free-energy cost, caused by the sharp gradients in the order parameter (related to short-wave-length fluctuation modes).

Then, from the zero-dimension expression for the fluctuating magnetization, Eq. 2.25, one can deduce that for low fields $-M_{fl}$ is linear in H, then increasing the field an upturn in the field dependence occurs for the value $H_{up}(\epsilon) \sim \frac{\Phi_0}{d\xi(\epsilon)}$ and $|M_{fl}|$ decreases (see Eq.2.25). The above results reveal the breakdown of the conventional GL theory, evidencing the existence of an " upturn field " H_{up}.

Let's now consider the case of HTSC. If we assume $d = \xi(T)$, $\xi_0 \simeq 10\mathring{A}$ (typical of HTSC) and $\epsilon \simeq 10^{-2}$, H_{up} turns out of the order of $20T$. Therefore, fluctuating diamagnetism in $SmBa_2Cu_{2.85}Al_{0.15}O_{6+\delta}$ compounds could be described on the basis of a GL functional for fields smaller than several Tesla. In particular experimental isothermal magnetization curves in $SmBa_2Cu_3O_7$ sample can be analyzed in the framework of the theory described in §2.2.

In §2.2.3 it is described how starting from the generalization of the GL functional for a layered superconductor (LD functional) in a perpendicular magnetic field (Eq. 2.27) the fluctuation part of the free energy can be obtained, see Eq. 2.34. The diamagnetic contribution to magnetization due to superconducting fluctuations $M_{fl} = -\frac{1}{V}\frac{\partial F}{\partial H}$ can be obtained from Eq. 2.34 by numerical derivation [9]. In the "pure " compound $SmBa_2Cu_3O_7$ a qualitative agreement between M_{fl} obtained in this way and the experimental data is obtained.

On the other hand, handling with Hurwitz zeta function, a general formula for magnetization in 3D case can be carried out [20, 21, 22], see Eq. 2.40. From this equation, it can be seen that, while for weak fields at temperatures relatively far from T_c ($\frac{H}{Hc2(0)} \ll \epsilon$) there is a linear dependence between magnetization and magnetic field, see Eq. 2.41, at T_c M_{fl} results:

$$M_{fl(3)}(0,h) = -\frac{0.32 k_B T}{\Phi_0^{3/2}} \frac{\xi_{0\|}^2}{\xi_{0\perp}^2} \sqrt{H}. \tag{5.2}$$

This crossover from a 3D linear regime to a 3D non linear regime is evident in experimental data presented in Fig.5.1.

The 3D nature of fluctuations in $SmBa_2Cu_3O_7$ samples is confirmed by the comparison of isofield magnetization measurements with the laws derived by scaling arguments.

In this approach, once fixed the dimension of the system, the singular part of free energy depends only on the number of flux quanta per coherence area, see [24], and magnetization follows the behavior described by Eq. 2.50. For

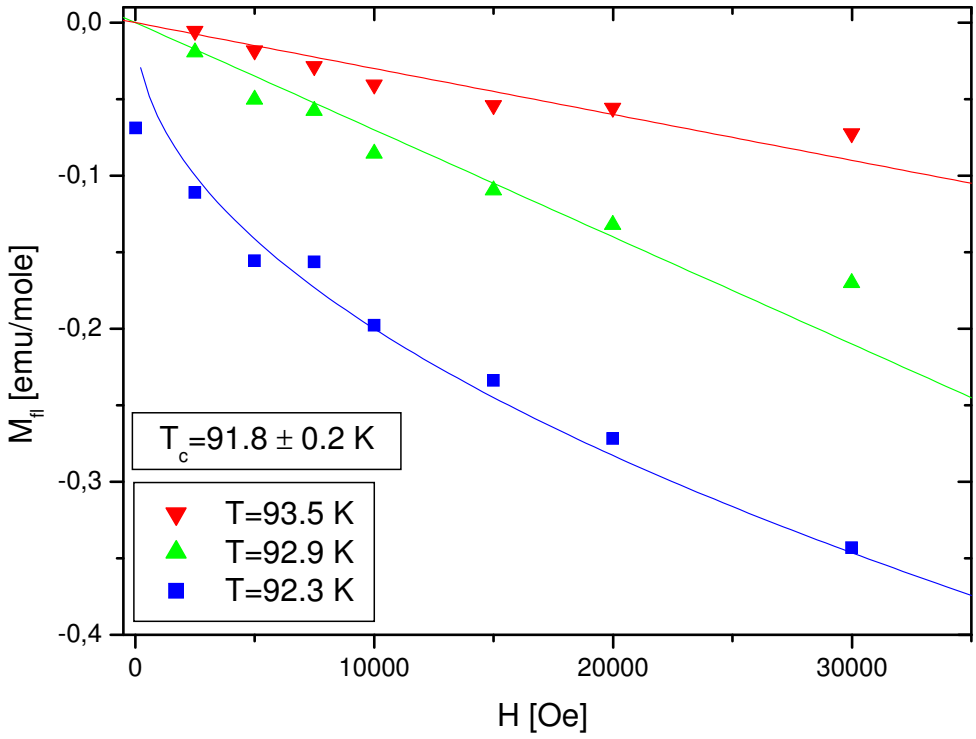

Figure 5.1: Diamagnetic magnetization above T_c as a function of field along the c-axis (calculated as reported in Chapter 4.1), for representatives temperatures, in $SmBa_2Cu_3O_7$, obtained in field-cooling processes, taken from Fig. 4.3. The solid lines describe the field dependence for different temperatures according to the GL theory for optimally doped HT$_c$ cuprates

3D anisotropic systems Eq.2.50 takes the form:

$$\frac{M_{fl}(T_c)}{H_{\perp}^{1/2}} = \gamma \frac{k_B T_c}{\Phi_0^{3/2}} m_3(\infty) \tag{5.3}$$

where $\mathbf{H} \parallel \mathbf{c}$, $\gamma = \frac{\xi_{0\parallel}}{\xi_{0\perp}}$ and $m_3(\infty) = -0.32$ in agreement with GL result of Eq.5.2. So, a crossing of isofield curves for $T = T_c$ when the magnetization is rescaled by $\sqrt{H}$ is expected.

In Fig. 5.2 scaled magnetization m vs H in $SmBa_2Cu_3O_7$ sample is plotted for different fields, around the transition temperature. A good agreement with scaling predictions for 3D anisotropic systems (Eq.5.3) is found. The isofield curves cross each other at a temperature T^* slightly greater than T_c, in agreement with the results obtained in $YBa_2Cu_3O_7$ by I. Zucca. [38]. Little discrepancy between the values of T_c and T^* were found also in other works [39, 40].

In Fig. 5.3 the scaled magnetization in a field of 1000 G, around the superconducting transition, in $SmBa_2Cu_3O_7$ and in optimally $YBa_2Cu_3O_7$ (oriented

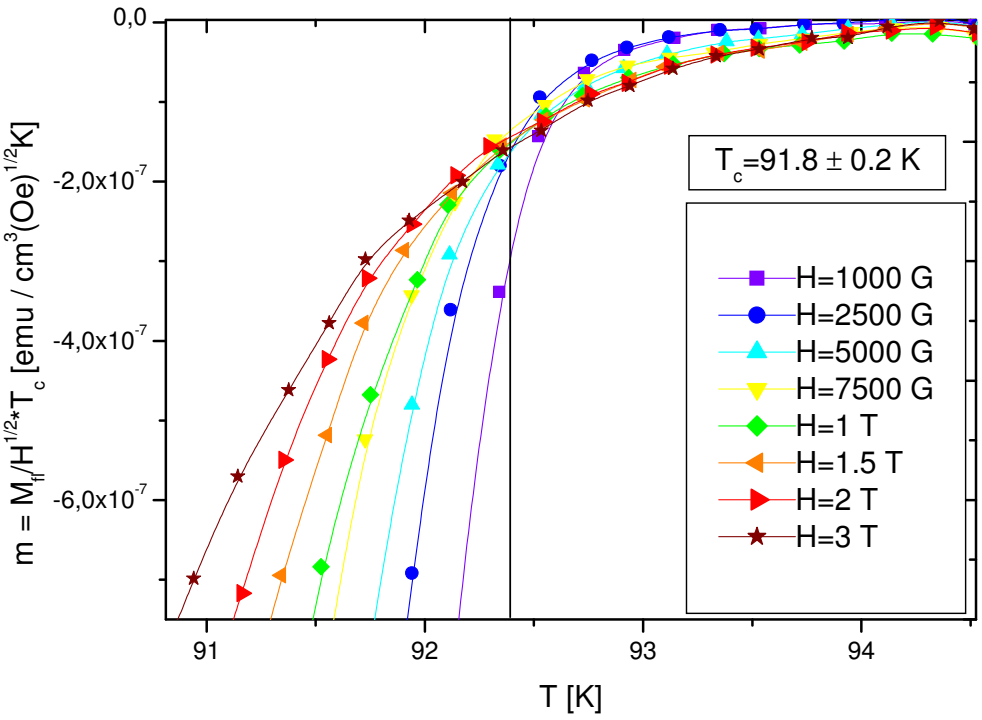

Figure 5.2: Scaled magnetization $m = M_{fl}/H^{1/2}T_c$ as a function of temperature, around the superconducting transition, for different magnetic fields along the c-axis (calculated as reported in Chapter 4.1), in $SmBa_2Cu_3O_7$, obtained in field-cooling processes. The solid lines are guides for eyes.

powder), taken from ref. [35], are compared. It can be noted that the two compounds show a similar behavior. In $YBa_2Cu_3O_7$ the scaled magnetization is about a factor 1.3 greater than in $SmBa_2Cu_3O_7$. This has to be ascribed to the fact that a fraction of the sample, about the 20% if we consider an anisotropy factor $\gamma \approx 7$, undergoes the transition at a temperature lower than 91.8 K.

Summarizing, the observed fluctuating diamagnetism in pure $SmBa_2Cu_3O_7$ (optimally doped) sample can be ascribed to conventional fluctuations of the order parameter, well described on the basis of an anisotropic GL functional.

5.2 Evidence of phase fluctuations in underdoped compounds

First it will be shown that the observed diamagnetism in $SmBa_2Cu_{2.85}Al_{0.15}O_{6+\delta}$ samples for temperature higher than T_c cannot be ascribed to conventional GL fluctuations.

In Fig.5.4 the scaled magnetization $m = M_{fl}/H^{1/2}T_c$ in the two samples is plotted in function of temperature, for different magnetic fields. No crossing

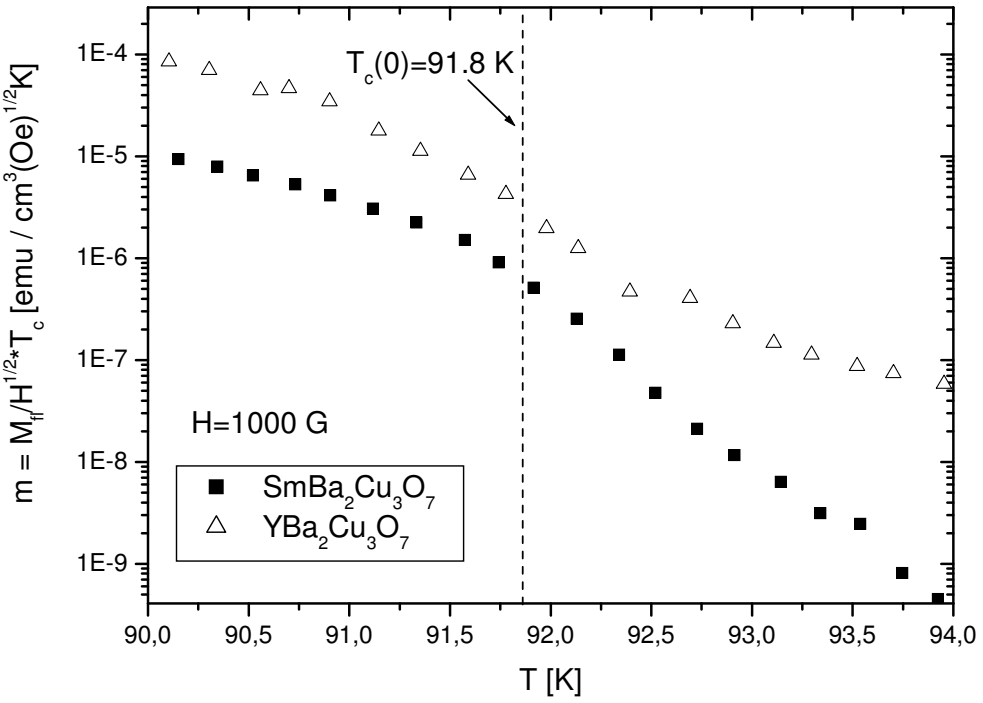

Figure 5.3: Diamagnetic magnetization $m = M_{fl}/H^{1/2}T_c$ as a function of temperature, around the superconducting transition in a field of 1000 G (■) along the c-axis (calculated as reported in Chapter 4.1) in $SmBa_2Cu_3O_7$, obtained in field-cooling processes. For comparison the data in oriented powder of optimally doped YBCO in a field of 1000 G are reported (△).

of m vs. T curves at T_c is observed in both samples, in contrast to scaling predictions for 3D anisotropic system , see Ref. [24] and Eq.5.3. Furtermore the upturn in the field dependence of M_{fl}, Fig. 5.5, cannot be ascribed to the saturation of magnetization expected in GL fluctuation regime. In fact, the fluctuating diamagnetism is primarly related to fluctuation-induced superconducting droplets of dimension $d \simeq \xi(T)$ [36]. By assuming the condition of zero dimension for these droplets an upturn in the field dependence of M_{fl} for $H_{up}(\epsilon) \sim \frac{\Phi_0}{\xi^2}\epsilon$ is predicted for these droplets, see ref.s [20] and [3]. This fact for $\xi_0 \simeq 10\mathring{A}$ and $\epsilon \simeq 10^{-2}$ implies that H_{up} is in the range of $20T$, while in $SmBa_2Cu_{2.85}Al_{0.15}O_{6+\delta}$ the upturn occurs for fields of the order of 10^2 G for oxidized sample and 10^3 G for reoxidized sample. Moreover magnetization curves measurements performed under zero-field-cooling (ZFC) and field cooling (FC) conditions are not superimposed (Fig.5.7); such irreversible effects have been ascribed to the existence of stable superconducting zones [14] for $T \leq T_c$ (local T_c).

Neither the precursor diamagnetism can be ascribed to a diffuse transition characterized by a distribution of local transition temperatures T_c^{local}, typical

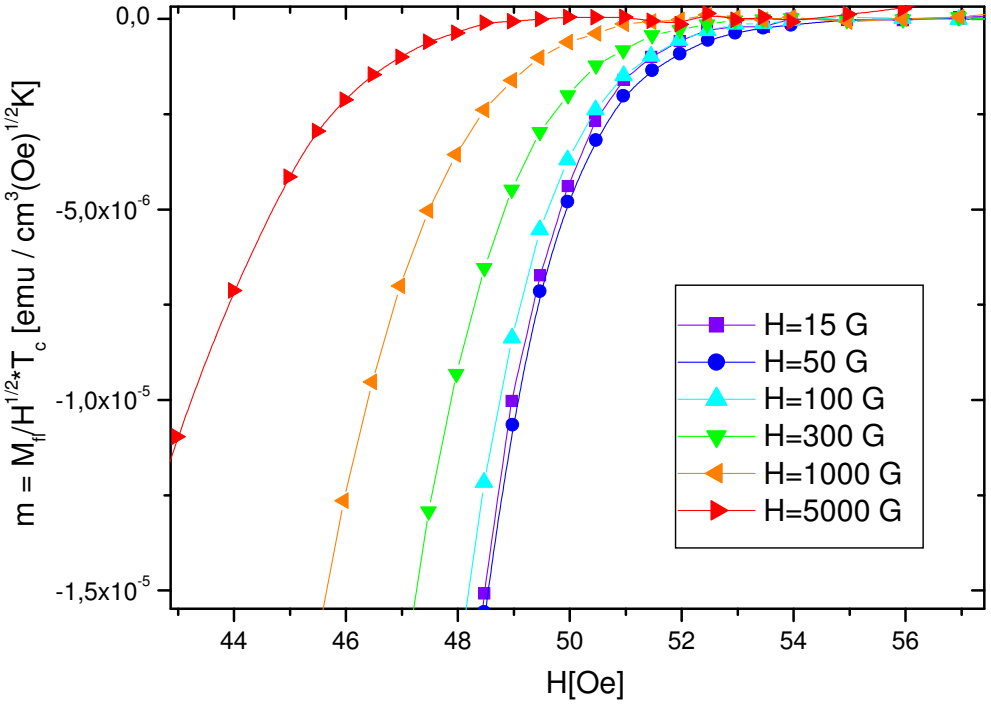

(a)

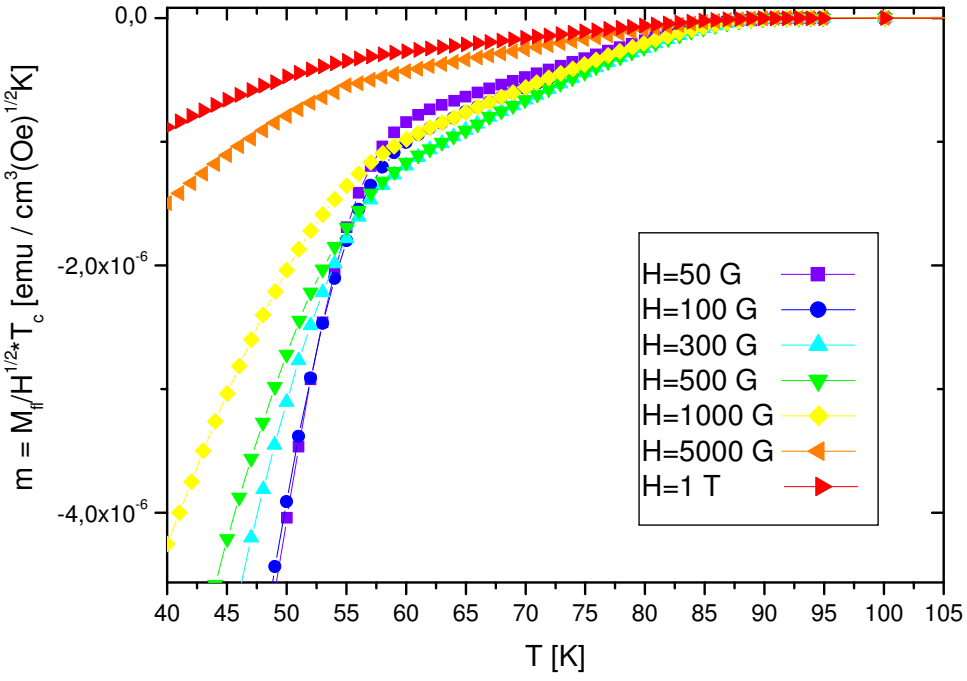

(b)

Figure 5.4: Scaled magnetization $m = M_{fl}/H^{1/2}T_c$ as a function of temperature, around the superconducting transition, for different magnetic fields along the c-axis (calculated as reported in Chapter 4.3), obtained in field-cooling processes, in oxidized $SmBa_2Cu_{2.85}Al_{0.15}O_{6+\delta}$ (sample A)(a), and in reoxidized $SmBa_2Cu_{2.85}Al_{0.15}O_{6+\delta}$ (sample B)(b).

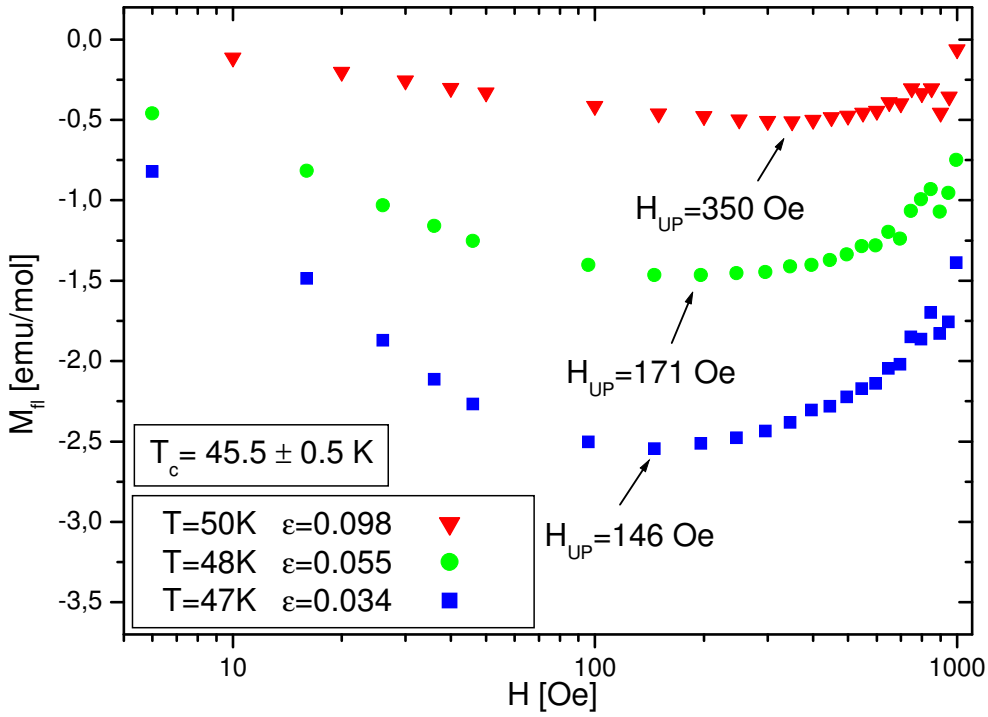

(a)

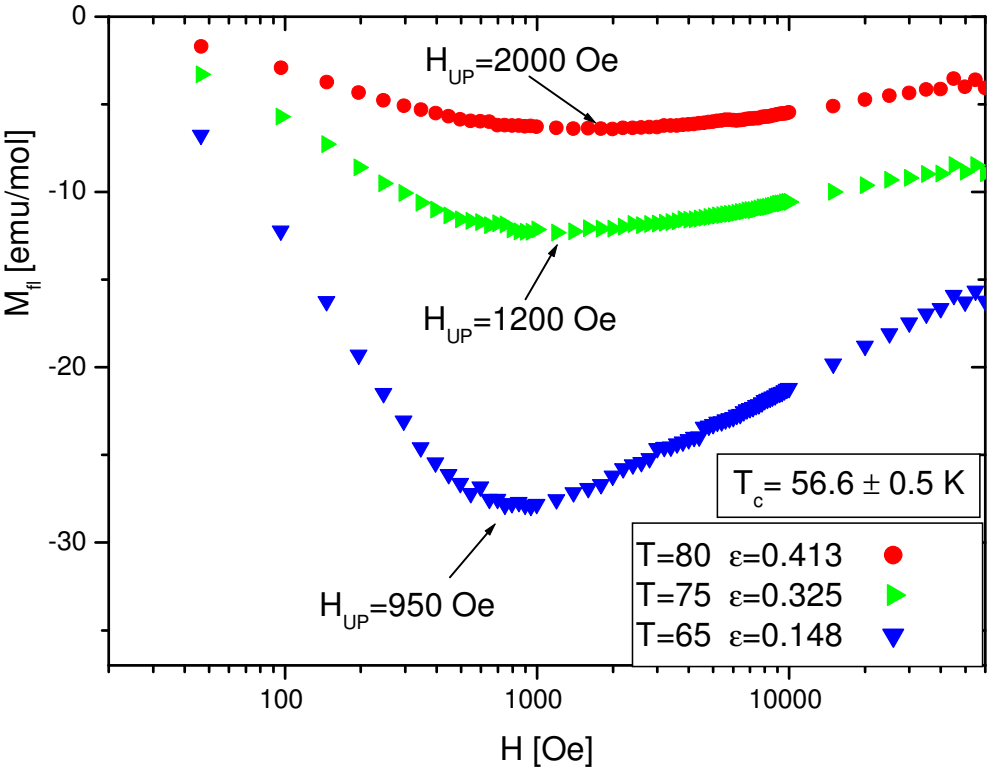

(b)

Figure 5.5: Diamagnetic magnetization as a function of field along the c-axis (calculated as reported in Chapter 4.3), for different temperatures above T_c in oxidized $SmBa_2Cu_{2.85}Al_{0.15}O_{6+\delta}$ (sample A)(a), and in reoxidized $SmBa_2Cu_{2.85}Al_{0.15}O_{6+\delta}$ (sample B)(b). H_{up} denotes the upturn field at which the slope of M_{fl} changes sign.

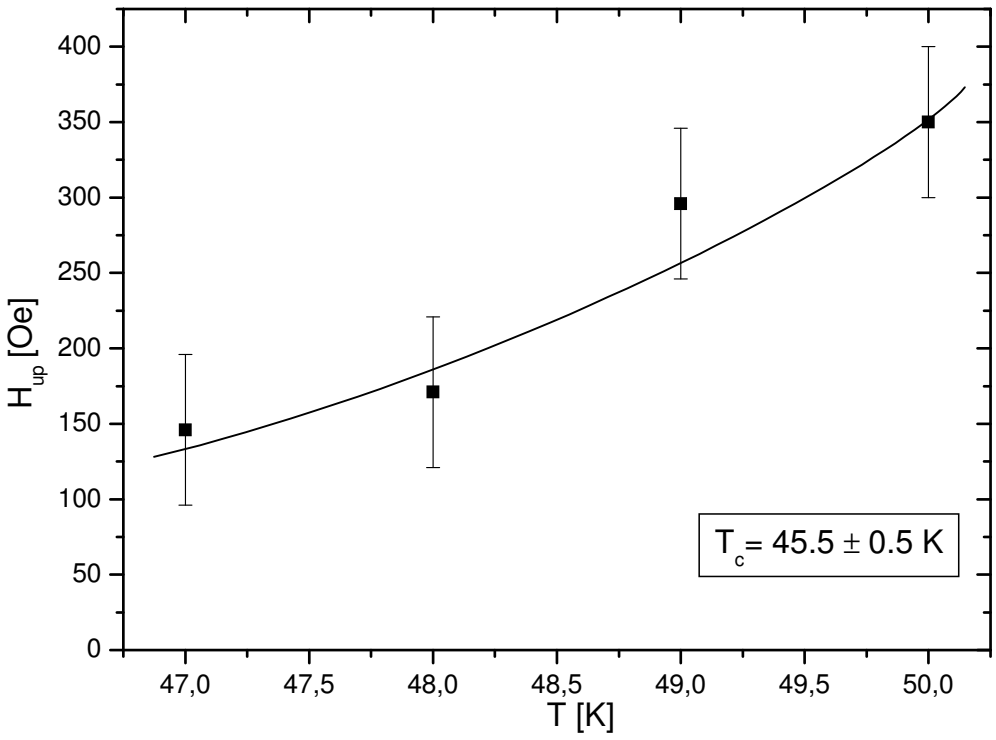

(a)

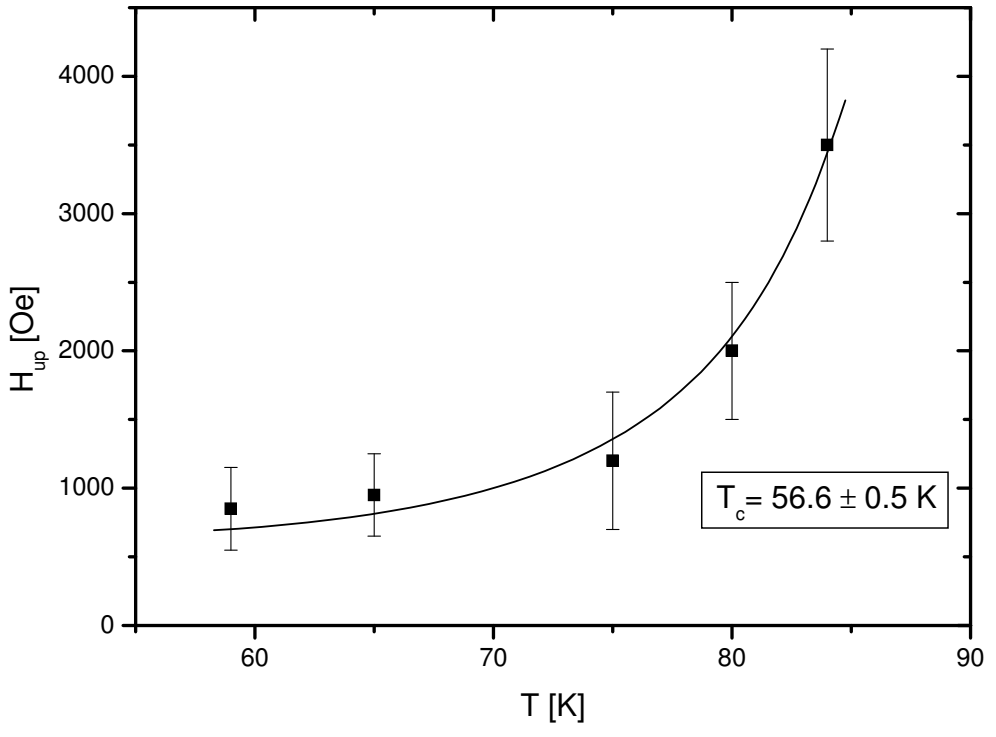

(b)

Figure 5.6: Temperature behavior of the upturn field H_{up} in oxidized $SmBa_2Cu_{2.85}Al_{0.15}O_{6+\delta}$ (sample A)(a), and in reoxidized $SmBa_2Cu_{2.85}Al_{0.15}O_{6+\delta}$ (sample B)(b).

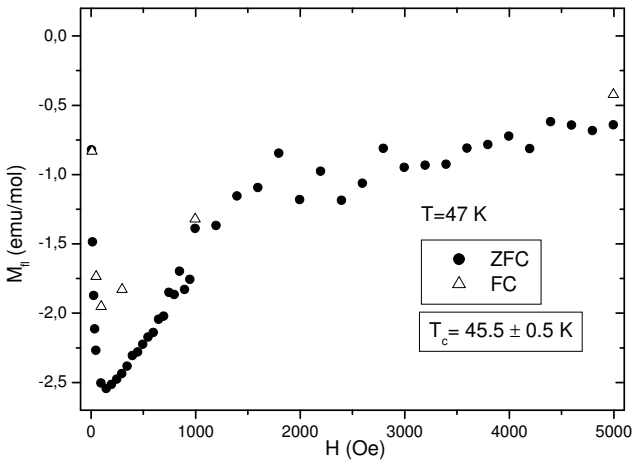

(a)

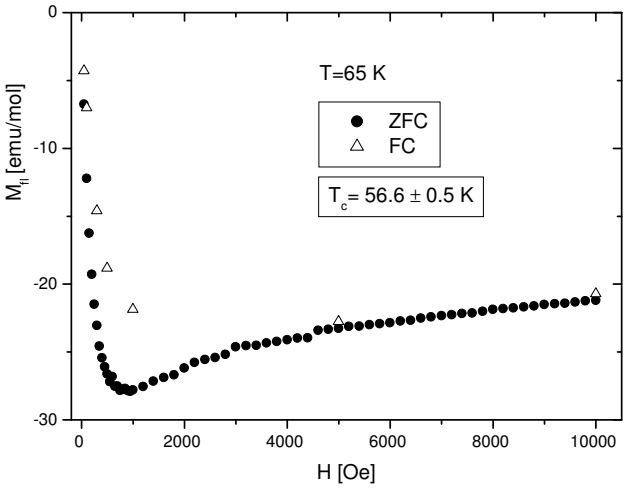

(b)

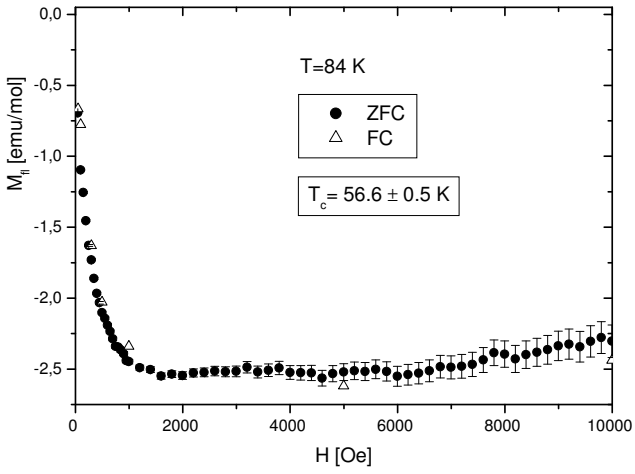

(c)

Figure 5.7: Typical magnetization curves in oxidized $SmBa_2Cu_{2.85}Al_{0.15}O_{6+\delta}$ (sample A)(a), and in reoxidized $SmBa_2Cu_{2.85}Al_{0.15}O_{6+\delta}$ (sample B)(b,c).

of heterogenous systems, as considered in [41] for underdoped $La_{1.9}Sr_{0.1}CuO_4$.

In fact, in such case the observed diamagnetism at $T \geq T_c$ would be the mean-field superconducting diamagnetic response of (mesoscopic) regions of the sample with $T_c^{local} > T_c$: H_{up} practically coincides with H_{c1} and therefore would decrease with temperature; on the contrary in our case H_{up} increases with temperature, see Fig. 5.6.

The presence of stable superconducting droplets, caused by charge inhomogeneity, is so necessary to explain the observed behavior of M_{fl}. For this droplets, the order parameter amplitude is frozen to a non zero value, being the droplets below the local transition temperature T_c^{local}, but the phase of the order parameter is subjected to thermal fluctuations that produce vortex excitations, see 2.3 and [11]. The magnetic susceptibility related to these droplets can be obtained starting from the phase dependent term of the L-D functional (Eq. 2.64), as described in [9, 11, 12] and reported in §2.3 of this thesis. Summarizing, from Eq. 2.64 the phase fluctuations contribution to the free energy is obtained, and from the orbital diamagnetic response, see Eq. 2.68, the susceptibility is derived

$$\begin{aligned}\chi(H) = \frac{\partial^2 F}{\partial H^2} = \lim_{q\to 0}\frac{K(\mathbf{q})}{q^2} = &-\frac{k_B T}{s\Phi_0^2}\frac{1}{1+2n'}\frac{\left[1+\delta\left(\frac{H}{H^*}\right)^2\right]^2}{n_v} \\ &- \frac{s^2\gamma^2(1+n')}{1+2n'}\cdot\left[1+\delta\left(\frac{H}{H^*}\right)^2\right], \\ &+ \frac{47L^2}{540}\frac{J_\parallel}{s}\left(\frac{2\pi}{\phi_0}\right)^2\left(\frac{H}{H^*}\right)^2\end{aligned} \tag{5.4}$$

where $H^* = \frac{\Phi_0}{L^2}$, $\gamma = \frac{\xi_{0\parallel}}{\xi_{0\perp}}$ and

$$n_v = n_{th} + n_F = n_o \exp\left(-\frac{E_0}{k_B T(1+\delta\left(\frac{H}{H^*}\right)^2)}\right) + \frac{H}{\Phi_0} \tag{5.5}$$

is the vortex density. In Eq. 5.5, n_{th} is the contribution due to phase fluctuations and n_F the one due to external field, and it has been considered that vortex pancakes are correlated for a distance $n's$, where s is the interlayer distance. The variable δ will be discussed below in connection with the presence of an upturn field in magnetization curves.

From Eq. 5.4 we see that χ is negative for $H \leq H^*$, being negligible the term in $\delta\left(\frac{H}{H^*}\right)^2$. Increasing the field this therm grows and χ can change the sign causing an upturn in magnetization curves. The other parameter that determines the behavior of the system is δ whose value depends if we are above or below the irreversibility local temperature T_{irr}^{local}:

$$\delta = \begin{cases} \frac{\pi^2 J_\parallel}{3k_B T} & \text{, when } T > T_{irr}^{local}, \\ \frac{\pi^2 J_\parallel}{k_B T} & \text{, when T<T}_{irr}^{local}. \end{cases},$$

For 2D systems $\frac{J_\parallel}{k_B T}$ is zero at $T > T_{irr}^{local}$, and greater than 2 for $T < T_{irr}^{local}$[11]. As a consequence no upturn in the field dependence of the magnetization is expected for a 2D system above irreversibility temperature. In general, for a real system $\frac{J_\parallel}{k_B T}$ is different from 0 also for $T > T_{irr}^{local}$ and can be demonstrated from Eq. 5.4 that the condition $\chi(H) = 0$ requires that $L > L_0$, where L_0 depends on the temperature and from some characteristics of the material. In our case when the ZFC and FC experimental curves are superimposed, i.e. when the droplets are above the local irreversibility temperature, the signal to noise ratio is too poor to allow a firm conclusion on the presence of an upturn in the field dependence of the magnetization.

Summarizing Remarks and Prospective Studies

The diamagnetic contribution M_{fl} to the magnetization above the superconducting transition has been studied in the family of the new high temperature superconductor $SmBa_2Cu_{2.85}Al_{0.15}O_{6+\delta}$ by means of high resolution magnetization measurements. Those compounds are of particular interest since allow the control of the holes by means of Al for the in-chains Cu substitutions.

For the optimally doped compound $SmBa_2Cu_3O_7$ at $T_c = T_c^{max}$ the magnetization curves have been analyzed in the framework of superconducting fluctuations theories based on the generalization of the Ginzburg-Landau functional for layered superconductors. A good agreement among experimental data and the theoretically predicted $M_{fl}(H)$ was found, with a crossover from 3D linear regime to 3D non linear regime approaching the transition temperature. Moreover, in this compound, the laws derived from scaling arguments for 3D anisotropic system are well obeyed. Thus, in $SmBa_2Cu_3O_7$ the diamagnetic contribution to the magnetization has to be ascribed to conventional GL superconducting fluctuations of the order parameter, causing local concentration of fluctuating Cooper pairs.

On the contrary, for the Al-doped compounds $SmBa_2Cu_{2.85}Al_{0.15}O_{6+\delta}$ the study of experimental isothermal magnetization curves M_{fl} vs H led us to the conclusion that in these systems the observed diamagnetic response can not be due to conventional GL superconducting fluctuations. In fact, an upturn in $M_{fl}(H)$ has been observed for fields H_{up} of the order of 10^2 G for oxidized sample and of 10^3 G for reoxidized sample (for reduced temperatures $\epsilon = (T - T_c)/T_c \approx 10^{-1}$). This upturn cannot be related to the quenching of SF by the external field, as in HTSC this is expected to occur at $H \geq 10^6$ G. Moreover the observed diamagnetic contribution can not be due to a diffuse transition, occurring in the presence of chemical inhomogeneities (and related a distribution of T_c). In fact since H_{up} was found to increase with temperature, while the opposite behavior of H_{up} as a function of temperature is expected in that case, as I am going to recall in the following.

Two different mechanisms in principle could explain the observed enhanced

diamagnetic contribution to magnetization above the transition temperature in HT_c cuprates:

i) the existence of metastable superconducting droplets accompanied by phase fluctuations of the order parameter;

ii) the occurence of a diffuse transition typical e.g. of chemically inhomogeneus systems.

In our samples, the behavior of $H_{up}(T)$ rules out the possibility that FD is due to a diffuse transition because in this case $H_{up}(T)$ is expected to decrease with $T(> T_c)$. In fact in this case the magnetization curve above the bulk T_c would mimic the magnetization behavior below T_c and then H_{up} would practically coincide with H_{c1}.

The data of the present thesis allowed us to extend the study of the behavior of $H_{up}(T)$ to a wider range of temperature and to investigate the role of different Cu-O chain lengths on SF.

In $SmBa_2Cu_{2.85}Al_{0.15}O_{6+\delta}$ ($\delta \approx 1$) the underdoped sample with shorter chain length, the upturn field $H_{up}(T)$ increase from $\simeq$ 100 G to 350 G by increasing temperature. The SF occurs in a relatively narrow range above $T_c = 45.5K$, i.e. $47 \leq T \leq 49$ K. When this sample is reoxidized, T_c increases to $56.6K$, the upturn field increases with temperature from $\simeq$ 800 G to 3500 G. This could be due tan increase of the fragment or to a changeover in the interaction between planes. The SF occur in a wide T-range from $56.6 < T < 92$ K and the diamagnetic magnetization is greatly enhanced.

Summarizing, the presented experimental data on $SmBa_2Cu_{2.85}Al_{0.15}O_{6+\delta}$ definitely prove the existence of metastable superconducting droplets with $T_c^{loc} > T_c$, where strong fluctuations of the phase of the order parameter occur. Such fluctuations give a diamagnetic contribution to $M_{fl}(H)$, that is quenched in correspondence of an upturn field H_{up} which increases with temperature, as theoretically predicted.

The length of Cu-O chain was found to influence the transition temperature and the temperature range where SF occur, the value of $H_{up}(T)$ and the magnitude of their diamagnetic contribution to the total magnetization $-M_{fl}$.

Further work related to the present thesis will be the quantitative comparison between the theoretical predictions and the experimental findings in $SmBa_2Cu_{2.85}Al_{0.15}O_{6+\delta}$ samples. The experimental data will give us information about the effective size of superconducting droplets and their temperature dependence, shedding light on the character of the bulk superconductive transition in underdoped superconducting cuprates. The study of the influence of the Cu-O chains on the microscopic superconducting mechanism properties, like e.g. the T_c value and the role of charge reservoir attributed to the chains should be triggered by our present work.

Appendices

Appendix A

Superconducting fluctuations in metallic nanoparticles

Authors

E. Bernardi[1], A. Lascialfari[1], A. Rigamonti[1], L. Romanò[2], V. Iannotti[3], G. Ausanio[3], C. Luponio[4].
[1] Department of Physics "A.Volta", CNR-INFM and Unità CNISM, University of Pavia, Via Bassi 6, I-27100, Pavia, Italy.
[2]Department of Physics and Unità CNISM-CNR, University of Parma, Parco Area delle Scienze 7A, I-43100, Parma, Italy
[3]Coherentia CNR-INFM, Physical Sciences Department, "Federico II" University, Piazzale V. Tecchio 80, I-80125, Napoli, Italy
[4]Department of Materials Engineering and Production, "Federico II" University, Piazzale V. Tecchio 80, I-80125, Napoli, Italy

Abstract

High-resolution superconducting quantum interference device magnetization measurements in lead nanoparticles with particle size d less than the superconducting coherence length are used to study zero-dimensional uctuating diamagnetism. The diamagnetic magnetization $M_{dia}(H, T =\text{const})$ as a function of the applied magnetic field H at constant temperature is reported in the critical region and compared with the observed behavior in the temperature range where the first-order fluctuation corrections are expected to hold. The magnetization curves are analyzed in the framework of exact fluctuation theories based on the Ginzburg-Landau functional for $\xi \gg d$. The role of the upturn field H_{up}, where the slope of $M_{dia}(H)$ changes sign, is discussed. The relevance of the magnetization curves over a wide range of magnetic fields and

(1)	(2a)	(2b)	(3)
$d_{e1} = 160\text{A}^\circ$	$d_{e2} = 250\text{A}^\circ$	$d_{e2} = 400\text{A}^\circ$	$d_{e3} = 750\text{A}^\circ$
$\sigma_{d1} = 40\text{A}^\circ$	$\sigma_{d2} = 60\text{A}^\circ$	—	$\sigma_{d3} = 200\text{A}^\circ$
$d_{m_1} = 170\text{A}^\circ$	—	—	$d_{m_3} = 720\text{A}^\circ$
$T_c = 7.09 \pm 0.005$	$T_c = 7.09 \pm 0.005$	$T_c = 7.1 \pm 0.03$	$T_c = 7.09 \pm 0.005$
$\epsilon_c = 9 \times 10^{-2}$	$\epsilon_c = 2.2 \times 10^{-2}$	—	$\epsilon_c = 1.1 \times 10^{-2}$
$H_c^{grain} \approx 2500 \pm 400$ Oe	—	—	$H_c^{grain} \approx 1150 \pm 100$ Oe

Table A.1: Expected (average) diameters of the particles, standard deviation of the particle diameters, median diameters of the particles, superconducting transition temperatures in the limit $H \to 0$ (in degrees K), limits of the critical region (see text) and critical fields of the grains (as obtained from the extrapolation of $T_c(H)$ for relatively low field according to Eq.A.3 It is noted that by using an effective, properly averaged, diameter of the grains the estimates of ϵ_c do not change much.

the role of H_{up} for the study of fluctuating diamagnetism, in particular, when the first-order fluctuation correction breaks down, is pointed out. The size and temperature dependences of H_{up} in the critical region are obtained from the experimental data and compared to the theoretical derivations for M_{dia}

Introduction

Superconducting fluctuations (SF) and precursor effects occurring above the superconducting transition temperature T_c have attracted great interest over the past few decades and resulted in advanced theoretical descriptions[20]. The effect of an external magnetic field H is especially interesting. While the field is a necessary tool to carry out relevant measurements, a strong field is expected to suppress the fluctuating Cooper pairs. Thus a variety of phenomena are reflected in the dependence of the SF and of the fluctuating diamagnetism (FD) on the external field H. Moreover, experimentally studying the effect of H on SF can be quite challenging, as for the cases of the field dependence of the spin susceptibility controlling the NMR spin-lattice relaxation [42] or the diamagnetic susceptibility χ_{dia} related to FD [17].

A meaningful study of the field-dependence of SF can be carried out in grains of size d smaller than the coherence length ξ, i.e., in the zero-dimensional (0D) limit. In such samples one has an enhancement of the fluctuations relative to those at higher dimensions and and an enlargement of the critical temperature regime. In 0D only spatially uniform fluctuations of the order parameter $\Psi(\mathbf{r})$ need to be considered. Thus the Ginzburg-Landau (GL) free energy functional

$$\begin{aligned}\mathcal{F}[\Psi(\mathbf{r})] = F_{normal} + \int dV \{ a\,|\Psi(\mathbf{r})|^2 + (b/2)\,|\Psi(\mathbf{r})|^4 \\ + (1/4m)|[-i(\hbar/2\pi)\nabla - (2e/c)\mathbf{A}]\Psi(\mathbf{r})|^2\}\end{aligned} \tag{A.1}$$

.

where [20] $a = \alpha_0[T - T_c(0)] = \alpha_0 T_c \epsilon$,**A** is the vector potential of the field and = $\epsilon = [T - T_c(0)]/T_c(0)$, no longer requires a Fourier series expansion of $\Psi(\mathbf{r})$ and so exact solutions for fields $H \ll H_c$ become possible. An understanding of the field dependence of SF in 0D is important for the FD in bulk superconductors also, as the dominant contribution to the diamagnetic susceptibility χ_{dia} for T_c^+ is due to metastable superconducting "droplets" of diameter of the order of $\xi(T)$. Then the isothermal magnetization curves $M_{dia}(H, T$ =const) can be qualitatively understood by assuming these fluctuating droplets are zero-dimensional [35, 9].

Attempts to study the magnetic aspects of the SF in metallic nanoparticles were carried out long ago, particularly through the electronic spin susceptibility via NMR T_1 relaxation measurements [43, 44] and measurements of the diamagnetic susceptibility χ_{dia}[45]. In T_1 measurements conclusive evidence for effects related to SF proved to be elusive, as the expected increase of the relaxation rate for T_c^+ was smeared out in 0D particles by a rounding of the transition and renormalization due to non linear fluctuations[44]. For the Knight shift measurements it was difficult to isolate the contributions of SF, and again a reduction in $\chi"_{spin}(\mathbf{k}, \omega)$ in grains was observed near T_c[43, 46].

Fluctuation diamagnetism in Aluminium nanoparticles was successfully studied in a pioneering experiment by Buhrman and Halperin [45] by measuring the magnetization as a function of temperature, in constant magnetic fields. The data were analysed in terms of χ_{dia} for $H \to 0$, as derived in exact theories [47, 48] for the GL free energy functional in 0D limit. The behaviour of $M_{dia}(T \approx T_c)$ in non-zero magnetic fields was discussed by extending the zero-field equations with the replacement of the reduced temperature ϵ by $(\epsilon + H^2/H_c^2)$, where H_c is the size-dependent critical field. The tendency towards the expected limiting slope $\chi_{dia} \propto H^{-2}$ was emphasized[45].

More recently Li *et al.*[49] have carried out conductivity, specific heat and susceptibility measurements in Pb nanoparticles that have highlighted quantum size effects on superconducting (SC) properties. Electron tunnelling in nanometer-scale Al particles has been used [50] to study the structure of the electronic energy levels. Size effects on T_c of lead nanoparticles embedded in an amorphous matrix have been studied by Tsai *et al.*[51]. Gladilin *et al.*[52] have developed an exhaustive theory on the magnetic response and the SC properties of ultrasmall grains. For a description of the properties of ultrasmall particles, see the reviews in Ref.[53].

In this paper we report the results of a study of the superconducting fluctuations and of the related fluctuating diamagnetism in Lead nanoparticles with diameters ranging from 150 to 750 A°, sizes for which effects of finite-level spacing should be negligible (see the Section Experimental). By means of high-field resolution SQUID measurements, isothermal magnetization curves $M_{dia}(H, T_c^+)$ were obtained and used to study the effect of magnetic field on the fluctuating pairs, particularly in the temperature range very near T_c where the first-order fluctuation correction breaks down and the role of the $|\Psi(\mathbf{r})|^4$

term in Eq. A.1 becomes crucial (the critical region). The importance of studying the magnetization curves on approaching T_c rather than the more common susceptibility measurements as a function of temperature at constant field has been noted for 3D and 2D superconductors [21]. For metallic nanoparticles we will show that isothermal magnetization curves provide novel insights regarding critical fluctuations in the case of 0D as well.

Experimental results

The Pb nanoparticles were produced by a modification of the Polyol Process technique [54]. All chemical reagents and solvents (Sigma-Aldrich products) had purity higher than 99%. The reaction was performed in a sealed glass vessel surmounted by a cooling column in order to obtain polyol reflux. To produce a relatively narrow distribution of the nanoparticle dimensions, a high homogeneity of solution was obtained during the reaction process by vigorous mechanical stirring. 50 ml of tetraethylene glycol (TEG: $C_8H_{18}O_5$) were introduced in the sealed vessel and heated by a thermostatic bath at 320 °C to reach the TEG boiling. At this time a solution of PbO in TEG was introduced in the vessel. In order to produce grains of different sizes, the concentration of PbO in TEG and the reaction time were adjusted between 0.02 - 0.4 mol and 15 - 50 minutes, respectively.

The powder was washed several times with ethanol at the beginning of the process and with acetone at the end. At the end of the reaction process the fine-powder fraction of Pd particles was separated from the coarse powder using a centrifuge. The particles were electrically isolated from one another by natural thin layers of oxide which were produced by ageing the particles in atmosphere for about 30 days.

A variety of techniques were used to characterize the Pb powders. A Philips PW 1710 diffractometer utilizing Cu K radiation ($\lambda = 1.5418$ A°) was used to carry out powder X-Ray Diffraction (XRD) measurements. XRD patterns between $25° < 2\theta < 65°$ were collected. A Philips EM 208S Transmission Electron Microscope with a copper (Cu) grid coated with a formvar membrane was utilized at 100 keV for imaging the nanoparticles. Lead (Pb) nanoparticles were suspended in ethanol by sonicating, then the Cu grid was dipped in the solution. Finally, by means of an EDWARDS E306 metallizer, the grids containing the Pb nanoparticles were coated by a very thin carbon layer in order to avoid breaking the membrane. The nanoparticles have also been analyzed through Atomic Force Microscopy (AFM). The AFM (Digital Instruments Nanoscope IIIa) was equipped with a sharpened silicon tip with a radius less than 5 nm. Images of the surface profiles were obtained by operating the AFM in the tapping mode, with a scan size and rate of 2 μm and 2 Hz, respectively.

The X-Ray diffraction peaks in Fig. A.1(a) are those expected for fcc Pb, with an additional smaller peak produced by the thin layer of superficial oxide, which is estimated to be approximately 5% of the total grain weight. In the

same Figure (part b and part c) TEM images are shown. From these the oxide thickness can be estimated to be about 10% of the nanoparticle diameter. The particles size distribution, based on the TEM images and fitted to a log-normal distribution of the particle diameters, is shown in Fig. A.1(d), for sample 1. In Fig.FigAppB2 the AFM image for sample 3 and the related particle size distribution, fitted to a log-normal distribution of the particle diameters, are given.

In Table A.1 we report the expected diameter $d_e = \exp(\mu + \sigma^2/2)$, the standard deviation of the particle diameters $\sigma_d = \exp(\mu + \sigma^2/2)[\exp(\sigma^2) - 1]^{1/2}$, where μ and σ are the mean and standard deviation of $\ln d$, respectively, treated as fitting variables, and the median diameter d_m, obtained by finding the value at which the integral of the distribution given by a log-normal function is equal on each side of d_m.

The effects of finite-level spacing (see Ref. [53]) are negligible for particle size $d \geq 100\text{A}^\circ$, for the temperature range we are going to consider. The level spacing δ can be estimated from the inverse of the density of states at the Fermi level $\delta \approx 1/N(0)v$, where v is the nanoparticle volume. From $N(0) = (2m)^{3/2}8\pi E_F^{1/2}/h^3$ and for lead, with $E_F = 1.1 \times 10^5(K)k_B$ and bulk value of the zero-temperature BCS gap $\Delta(0) = 1.35$ meV, one can write $(k_B T_c/\delta) \approx 3.4 \times 10^{-6} d^3$ (with d in A°). Thus $(k_B T_c/\delta) \approx 1$ for $d \approx 70$ A° and only for particles of smaller size will the level spacing become comparable to $\Delta(0)$ and therefore invalidate the GL approach (See Ref.s [53], [48] and [49]).

From the thickness of the oxide layers, by assuming the condition of random loose packing the density of nanoparticles with respect to bulk Pb could be roughly estimated. Any uncertainty in the absolute value of the susceptibility per unit volume of Lead does not affect the major conclusions to be derived in the next Section.

The zero-field transition temperatures (see Table A.1) have been obtained by linearly extrapolating to zero the susceptibility in a field of 1 Oe plotted vs T^4 for $T \to T_c^-$ (inset in Fig.A.3(a)). Also in Figs. A.3 a close-up of the data for χ_{dia}, for a field of 2 Oersted and near T_c, are shown as a function of the reduced temperature ϵ, for samples 1 and 3.

The field dependence of the transition temperature $T_c(H)$ has been estimated by extrapolating to zero the data for (M_{dia}/H) obtained in the temperature range where this quantity varies linearly with T^4 (Fig.A.4).

In Figs.A.5 representative isothermal magnetization curves are reported in the temperature range around $T_c(0)$. The extraction of the diamagnetic contribution from the magnetization requires a detailed subtraction procedure when the magnetic field is increased to relatively strong values. In fact, in the range $H > H_{up}$, $|M_{dia}|$ decreases on increasing the field (see Figs.A.5), while the paramagnetic contributions due to the Pauli paramagnetism and to a small amount of paramagnetic impurities continue to increase on increasing H. Thus from the computer-stored raw magnetization data around $T_c(0)$ the magnetization values measured at a higher temperature (around 8°K) where the SF

are negligible have been subtracted. The slight variation of the paramagnetic contribution with temperature did not prevent reliable estimates of M_{dia} for magnetic field up to about 600 Oe, as indicated by the error bars in Fig.A.5(b).

Analysis of data

The temperature range $\epsilon < \epsilon_c$, where critical fluctuations are expected to occur and so the term in $|\Psi(\mathbf{r})|^4$ in Eq.A.1 becomes important, can be estimated according to slightly different criteria. The Ginzburg-Levanyuk criterion in 0D, under the assumption of the BCS condition for ξ_0, yields [20] $\epsilon_c \approx 13.3(T_c/T_F)(\xi_0^3/v)^{1/2}$, where T_F is the Fermi temperature. Alternatively, the critical reduced temperature may be defined as the one below which the first-order fluctuation correction to the mean field behaviour of $< |\Psi(\mathbf{r})|^2 >$ is no longer sufficient [48], in which case one obtains $\epsilon_c \approx 0.95[N(0)vk_BT_c]^{-1/2}$, where $N(0)$ is the single-spin density of states per unit volume. Assuming that the electron mean free path is limited by surface scattering one then finds[45] $\epsilon_c \approx (6k_BT_c)^{1/2}/(d/2)^{3/2}|T_cdH_c/dT|_{T_c}$. In Lead the electron density is $n = 1.32 \times 10^{23}\mathrm{cm}^{-3}$ and $\xi_0 = 900$ Å. The experimental result for the thermodynamic bulk critical field yields $dH_c/dT\ |_{T_c}= 81$ Oe /°K. In Table A.1 the average values of the critical temperature estimated according to the criteria described above are listed.

In the framework of the first-order fluctuation correction theory, which is valid for $\epsilon > \epsilon_c$ and H_c, the single particle magnetization is given by [20]

$$\begin{aligned} M_{dia} &= -k_BTH(4\pi^2\xi_0^2d^2/5\Phi_0^2)/[\epsilon + 2\pi^2\xi_0^2d^2H^2/5\Phi_0^2] \\ &= -2k_BTH(H_c^{grain})^{-2}/[\epsilon + H^2/(H_c^{grain})^2]. \end{aligned} \tag{A.2}$$

$H_c^{grain} = (2.5)^{1/2}\Phi_0/\pi\xi_0d$ is defined as the zero-temperature critical field of the grain. In fact in the same theoretical scenario the field dependence of the superconducting transition temperature is given by

$$\begin{aligned} T_c(H) &= T_c(0)[1 - 4(\pi^2\xi_0^2H^2d^2/10\Phi_0^2)] \\ &\equiv T_c(0)[1 - H^2/(H_c^{grain})^2] \end{aligned} \tag{A.3}$$

Note that Eq. A.2 implies an upturn in the field dependence of M_{dia} around the magnetic field value

$$H_{up} = \epsilon^{1/2}(2.5)^{1/2}/\pi\xi_0d \equiv \epsilon^{1/2}H_c^{grain}. \tag{A.4}$$

The solid lines in Fig.A.5(a) correspond to Eq.A.2, with no free parameters, using $H_c^{grain} = 1150$ Oe , as extracted from the field dependence of the transition temperatures on the basis Eq.A.3. The experimental values for H_{up} and for H_c^{grain} are close to those obtained from the above Equations by assuming $\xi_0 = 900$ Å, particularly if we use an effective grain size larger than the nominal one due to the size distribution. For instance, for the sample at $d = 750$ Å

Eqs.A.3 and A.3 yield $H_{up} \approx 1.2 \times 10^3\, \epsilon^{1/2}$Oe and $H_c^{grain} \approx 1400$ Oe. The distribution of particle diameters is particularly detrimental because of the small size of the grains and introduces large errors into the estimate of the field dependence of T_c for strong magnetic fields (See Fig.A.4). The zero-temperature critical field for grains where $H_c^{grain}(T \to 0)$ is much larger than for bulk Lead, and it is difficult to extrapolate the data for $T_c(H)$ according to Eq.A.3.

For sample (3) (average diameter $d = 750$ Å) the comparison of the field dependence of T_c (Fig.A.4) with the curve derived on the basis of the temperature dependence of H_c [49] (for the sample at $d = 860$ Å) indicates that Eq.A.2 is valid, but only for $H \leq H_c^{grain}/2$. This limit of validity could be expected as H_c^{grain} is intrinsically related to the first-order fluctuation correction.

From Fig.A.5 (a) it appears that the experimental data at $T = 7.16$ K are very well fitted by Eq.A.2. However, for temperatures closer to T_c, and particularly for $T = 7.095$ K, inside the critical region, the departure of M_{dia} from the behaviour expected on the basis of Eq.A.2 is noticeable. We shall see that the magnetization curves derived from the full form of the GL functional and of the exact partition function will account for this departure. Based on the results presented in Fig.A.5) we believe that the isothermal magnetization curves convey information on the FD which is much more reliable than the more commonly studied isofield data as a function of temperature (open circles).

Therefore the conclusion is that above the critical region our data are well described by the theoretical predictions for fluctuating diamagnetism as outlined above. The departures of the experimental results for M_{dia} with respect to the magnetization given in Eq.A.2 appearing in Fig.A.5(a) occur when entering the critical region, and the susceptibility is smaller than the one derived from the first order fluctuation approximation (See Eq.A.2 and the solid lines in Fig.A.3).

Now we turn to the discussion of the magnetization curves in the critical region. For sample 1 the majority of the measurements were made in the temperature range where $\epsilon \leq \epsilon_c$. In the limit $H \to 0$ the magnetization is linear in the field and the susceptibility can be written

$$\begin{aligned} \chi_{dia} &\approx d^{3/2}(12 k_B T_c)^{1/2}/33.9\lambda_L(0)\Phi_0 \\ &\approx d^{3/2} 0.6 (k_B T_c)^{1/2}/\Phi_0^2 H_c^{bulk}, \end{aligned} \tag{A.5}$$

which is characterized by a weak temperature dependence (see plots in Ref.[48]). With the value $H_c^{bulk} = 800$ Oe for the bulk critical field, Eq.A.5 yields $\chi_{dia}(T \to T_c) = -1.5 \times 10^{-5}$ for the sample with $d = 750$ Å, in good agreement with the data in Figs.A.3. Although the observed scaling factor of $\chi_{dia}(T \approx T_c)$ with the grain size does not follow the expected $d^{3/2}$ dependence, this departure is likely to be a trivial consequence of errors in our estimate for the filling factor due to the presence of the insulating oxide.

From the comparison of the solid lines with the experimental data in Fig.A.5 and from the temperature dependence of the upturn field (Fig.A.6) it is evident that the mean field correction breaks down below about 7.13 °K in sample 3

and in almost the whole temperature range that has been explored in sample 1.

In the critical region the role of the magnetic field should be discussed starting from the complete expression of the GL functional (Eq.A.1) and by using a partition function of the form [20]

$$Z_{(0)} = [\pi^3 v k_B T/2b]^{1/2} \exp(x^2)(1-(x)) \tag{A.6}$$

with $x = a(H)(v/2bk_BT)^{1/2}$ while $a(H)$, is the coefficient of the $|\Psi|^2$ term including the factor $H^2d^2/10$. Note that the first-order fluctuation correction derived for $\epsilon > \epsilon_c$ corresponds to the approximate form of the free energy $F_(0) = -k_BT\ln(\pi/\alpha\epsilon)$.

From Eq.A.6 the magnetic field dependence of M_{dia} can now be derived. The parameter $a(H)$ becomes $\alpha_0 T_c[\epsilon+(H/H_c^{grain})^2]$, while the factor $(v/2bk_BT)^{1/2}\alpha_0 T_c$ has to be estimated using the relation $(\alpha_0^2/b) = 8\pi^2 N(0)/7\zeta(3)$. The resulting expression for the magnetization (per unit volume) becomes

$$\begin{aligned} M_{dia} = (2\alpha\sqrt{b}\sqrt{v})k_B^{3/2}T_cT^{1/2}[H/(H_c^{grain})^2] \\ \times [x - e^{x^2}/\sqrt{\pi}(1-(x))] \end{aligned} \tag{A.7}$$

and H_{up} can be estimated by numerical procedure. Eq.A.7, in the limit $H \to 0$ yields the susceptibility including the quartic term in the GL functional.

In Fig.s A.7 the curves $M_{dia}vsH$ resulting from Eq.A.7 are compared with the experimental data for several temperatures. Note that for sample 3 at $T = 7.16$ K the theoretical curve coincides with the one shown in Fig.A.5(a), as expected since at this temperature $\epsilon > \epsilon_c$. However, for the other two temperatures significant differences appear with respect to the theoretical calculations shown in Fig.A.5. Using the complete form of the partition function, the resulting magnetization curves are in very good agreement with the experimental findings, particularly for $M_{dia}(H \approx H_{up})$, having kept all the parameters unchanged. Thus the role of the term $|\Psi|^4$ in the GL functional is crucial in the critical region and must be included to quantitatively describe the data.

The theoretical curves derived for the sample at $d = 160$ A° are reported in Fig.A.7. From the comparison with the magnetization data one can observe that the trend of $M_{dia}vsH$ is rather well reproduced up to a field strength of the order of H_{up} , where we have used the value $H_c^{grain} = 2500$ Oe for the critical field (Table A.1). For small grain size the theoretical curves are very sensitive to the value of H_c^{grain} through the coefficient $a(H)$ in Eq.A.6, which is difficult to determine precisely by means of Eq.A.3 on the basis of the field dependence of T_c. Nonetheless, the value of the upturn field and the magnetization for $H = H_{up}$ is rather well accounted for by our calculations. Upon increasing the field above H_{up} the experimental data appear to decrease towards zero faster than the theoretical predictions. An attempt to take into account the size distribution of the grains reported in Fig.A.1(d) does not lead to any significant improvement of the theoretically predicted behaviour

at strong fields. On the other hand one should note that at strong fields the experimental error increases rapidly as a consequence of the subtraction procedure explained in the Experimental section. Furthermore the smallest grains in the distribution of the diameters quantum size effects could drastically modify the superconducting properties [53, 20], which in turn could produce the discrepancy between theory and experiment for $H > H_{up}$. Attempts are now under way to obtain powders with a narrower distribution in diameters of the grains.

From the behaviour of M_{dia} in the critical region as shown in Fig.A.7(b) one can see that the upturn field increases with increasing temperature while the diamagnetic magnetization $M_{dia}(H = H_{up})$ increases when H_{up} decreases. This implies that the qualititave behaviour predicted for the magnetization curves by the first order correction theory is still valid even in the critical region, although the temperature dependence of the susceptibility and of the upturn field are strongly modified. This is reflected in Fig.A.6, since by scaling the reduced temperature in term of c for each size, the quantity $(H_{up}d)$ approximately keeps a size-independent value, in spite of the breakdown of the mean field result $H_{up} \propto /\epsilon^{1/2}d$. The inset in Fig.A.6 shows the temperature dependence of H_{up} (normalized to the value slightly above ϵ_c) expected in the critical region according to our derivation based on the exact GL functional and the full form of the partition function. The experimental findings for $(H_{up}d)\, vs\, \epsilon/\epsilon_c$ are well described by our calculations.

Summarizing Remarks

By means of magnetization measurements we have studied the superconducting fluctuations and the related fluctuation diamagnetism above the superconducting transition temperature in Pb nanoparticles of size smaller than the coherence length. The isothermal field dependence of the diamagnetic magnetization M_{dia} above T_c has been discussed in the framework of exact theories based on the Ginzburg-Landau functional in the zero-dimensional condition.

The first-order fluctuation correction is found to be valid only outside the critical region $\epsilon > \epsilon_c$ where it accurately describes the behaviour M_{dia} for magnetic fields H not too close to the critical field. Also, the scaling properties of $dT_c(H)/dH$ for small fields and of the upturn field H_{up} in the magnetization curves are well described within that approximation.

In the critical region, however, the role of the field and the limits of validity of the first-order fluctuation correction have been analysed by comparing the experimental findings to the derivation of M_{dia} as a function of the magnetic field starting from the complete form of the GL functional and with the exact expression of the zero-dimensional partition function. We find that the role of the $|\Psi|^4$ term in the GL functional is crucial in describing the data in the critical region. For the sample with average grain diameter of 750 Å the fluctuating diamagnetism can be well described by our extended model even

in the critical region, without introducing any adjustable parameters. For the sample with the smallest average diameter of 160A°, the agreement of the numerically derived M_{dia} with the experimental findings is again good for fields of the order of H_{up}. Poor agreement between the theoretically predicted $M_{dia}vsH$ and our data is observed for fields above H_{up}, when the fluctuating diamagnetic contribution is approaching zero and the subtraction procedure of the paramagnetic term introduces large errors.

The temperature dependence of the upturn field and the scaling properties with the grain size are also well described by our calculations both outside and inside the critical region, with the product $(H_{up}d)$ vs reduced temperature being approximately size-independent and following the predicted temperature dependence, even though the mean field result $H_{up} \propto (\epsilon^{1/2}/d)$ evidently breaks down. The relevance of the magnetization curves $M_{dia}vsH$ and of the upturn field H_{up} for the study of the fluctuating diamagnetism above the superconducting transition temperature has been emphasized.

Acknowledgments

Preliminary measurements carried out by I. Zucca are acknowledged. Prof. W.-H. Li , (National Central University of Chung-Li) is thanked for the loan of a batch of Pb nanoparticles, particularly sample (2b) (see Table A.1), used for comparison. A.A. Varlamov is gratefully thanked for stimulating discussions and for having introduced the authors to the study of the superconducting fluctuations. The authors also thank the Centre CISME (Centro Interdipartimentale di Servizio per la Microscopia Elettronica) of the "Federico II" University for access to their TEM. Useful discussions with P. Carretta are acknowledged. Mike Graf (Boston College) is gratefully thanked for critical reading of the manuscript. The work has been carried out in the framework of a FIRB-MIUR project "microsistemi basati su materiali magnetici innovativi strutturati su scala nanoscopica." (Pnr 2001-2003).

Phys. Rev. B, **74**, 134509 (2006).

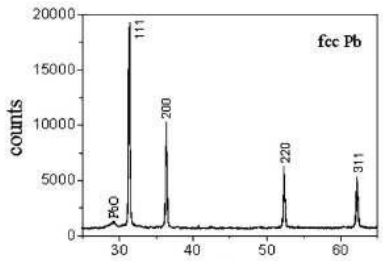

(a)

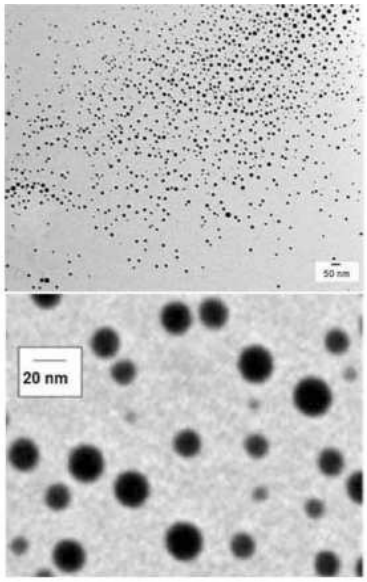

(b)

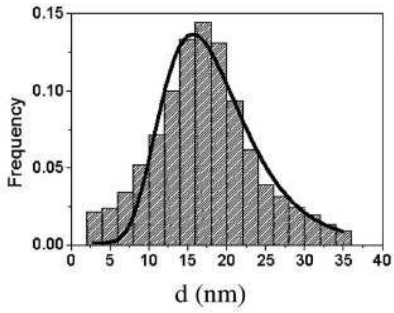

(c)

Figure A.1: (a) XRD of Pb nano-powder. (b) TEM images of Pb nanoparticles (Mag. 40000 X). (c) TEM images of Pb nanoparticles (Mag. 350000 X). (d) Size histogram of Pb nanoparticles produced under experimental conditions shown in (b). The curve in the part d represents a log-normal distribution, which has a median diameter $d_{m1} = 170$ Å (sample (1)) and a standard deviation of the particle diameters $\sigma_{d1} = 40$ Å.

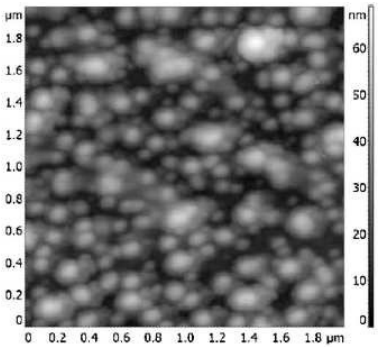

(a)

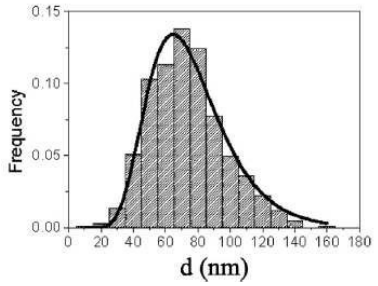

(b)

Figure A.2: (a) AFM image of Pb powder onto mica substrate obtained by increasing the concentration of PbO in TEG and the reaction time up to threefold. (b) Size histogram of Pb particles produced under experimental conditions shown in (a). The curve in the part (b) represents a log-normal distribution, which has a median diameter $d_{m3} = 720$ Å (sample (3)) and a standard deviation of the particle diameters σ_{d3} =200 Å.

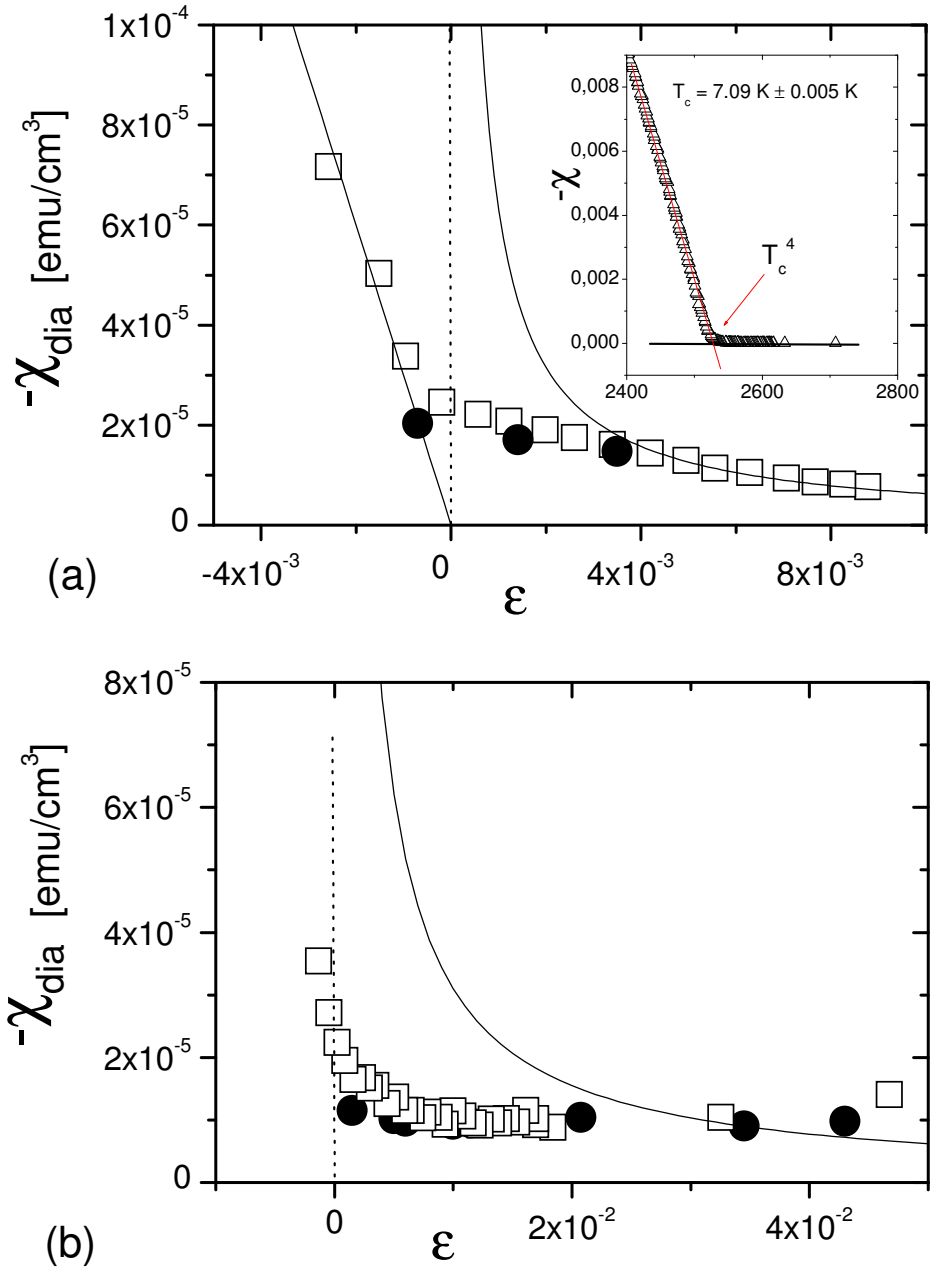

Figure A.3: Blow-up of the temperature dependence of the susceptibility, in magnetic field $H = 2$ Oe, around T_c in sample (3) (a) and in sample (1) (b). The solid circles are the data from the isothermal magnetization curves while the empty squares are from the isofield measurements as a function of temperature. The solid lines track the behaviour of χ_{dia} in the assumption that the non-linear fluctuations can be neglected, namely the behaviour of (M_{dia}/H) for $H \to 0$, according to Eq.2 in the text. The inset in Fig.3 (a) shows how the transition temperature has been determined. ϵ is the reduced temperature.

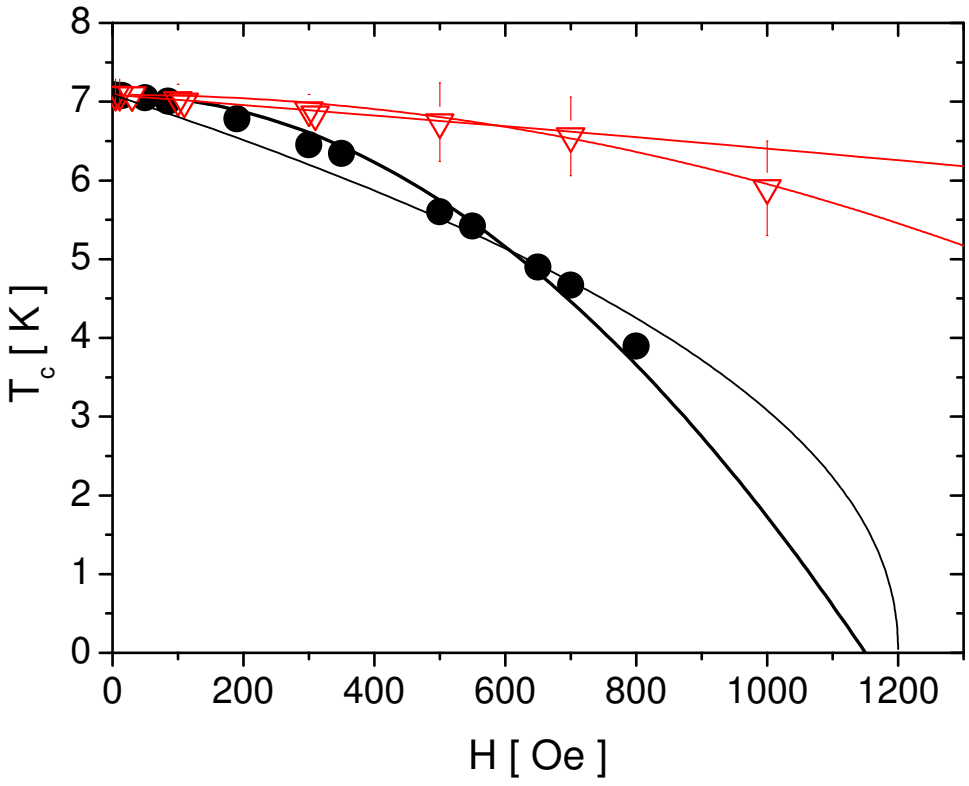

Figure A.4: Field dependence of the superconducting transition temperatures for sample (3) (•) and for sample (1) ($\bigtriangledown$). The dotted lines are the behaviours according to $H_c(T) = H_c(0)[1 - (T/T_c)^{\alpha}]$, with $\alpha = 2.15$ and 2.2, in correspondence to the critical field 1200 Oe (for a sample at $d = 860$ Å) and for the indicative value $H_c^{grain}(0) = 5000$ Oe for d =160 Å (see Ref.12). The solid lines corresponds to Eq.2 in the text and it appears to hold for $H \leq H_c^{grain}(0)/2$. For sample (1) the extrapolation yields H_c^{grain} around 2500 Oe (see Table I).

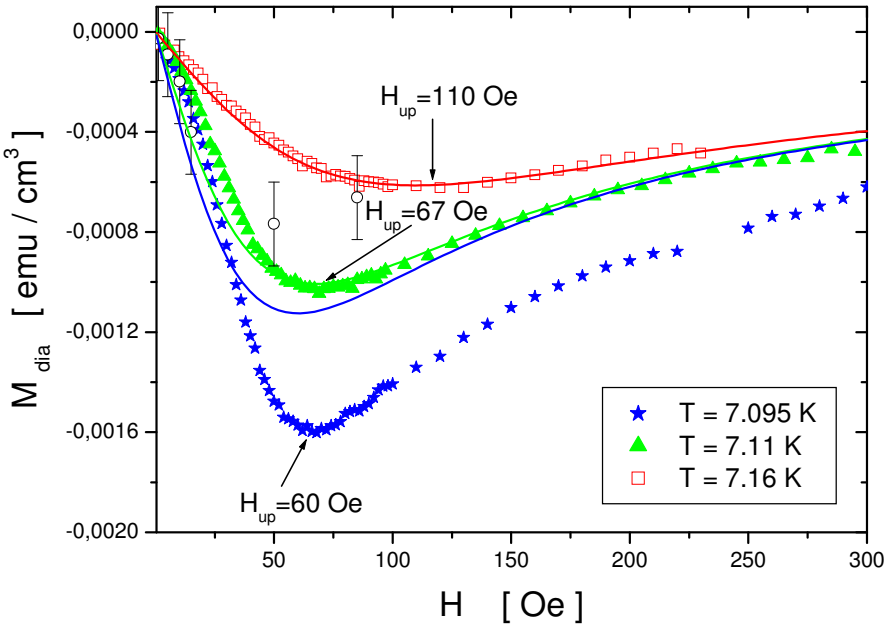

(a)

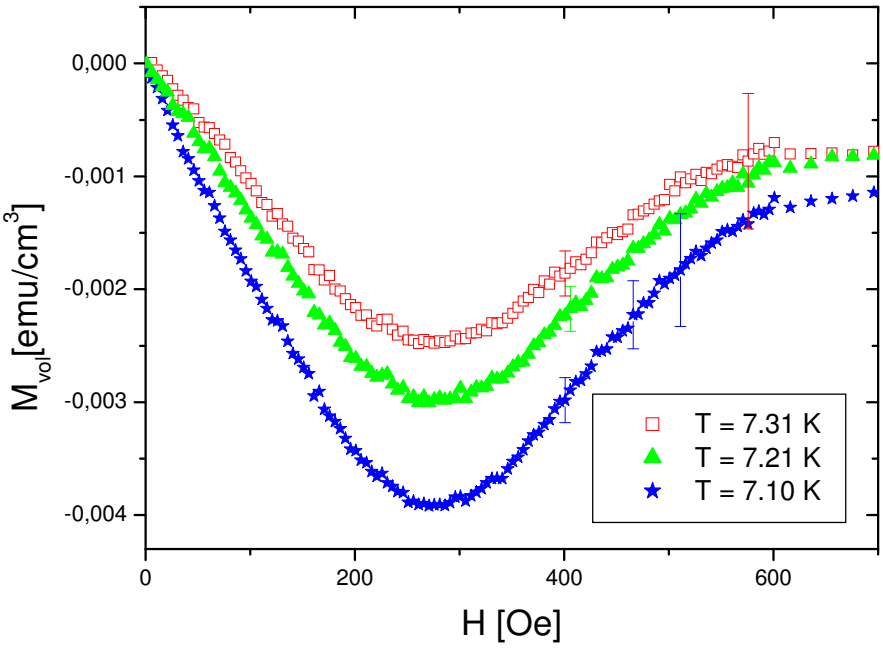

(b)

Figure A.5: (a) Magnetization $M_{dia} vs. H$ in sample (3) at representative temperatures above T_c. The solid lines correspond to Eq.2 in the text for critical field of the grain 1150 Oe . Similar curves have been obtained for samples (2). For $\epsilon \leq \epsilon_c$ the curves depart from the behaviour described by Eq.2. (b) Magnetization curves for sample (1), all corresponding to temperature range where $\epsilon < \epsilon_c$, namely within the critical region. The open circles in part (a) correspond to the data obtained from the isofield measurements as a function of temperature, with large experimental errors.

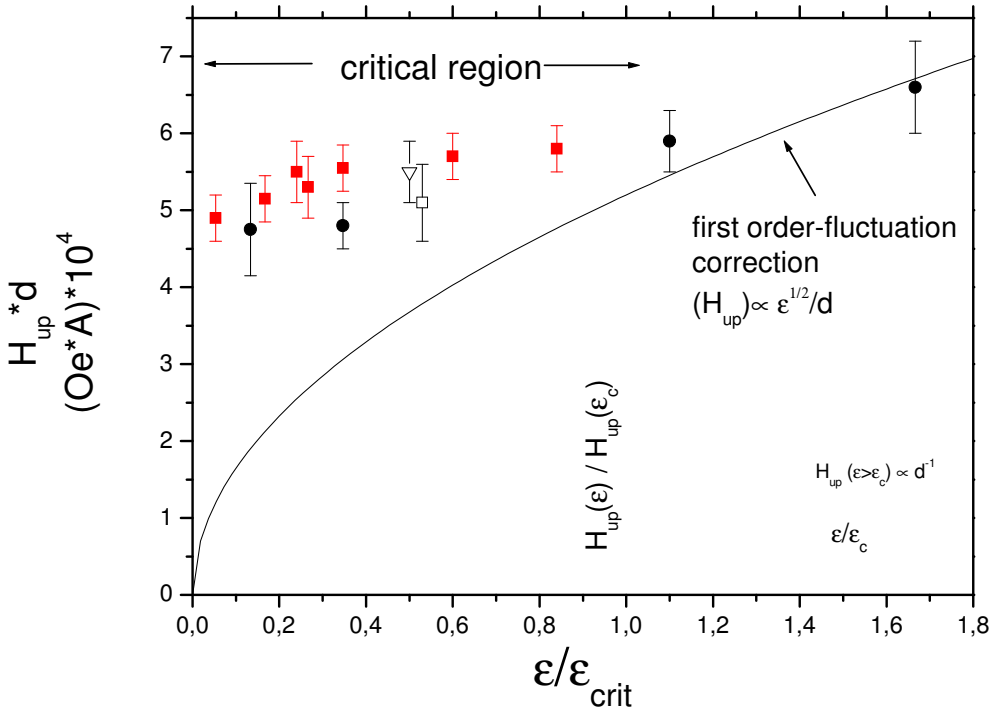

Figure A.6: Temperature behaviour of the upturn field H_{up}, normalized to the grain size, as a function of the reduced temperature (•,sample 3; ▲ sample 1; □ and ▽ samples 2) . The upturn field appears to scale rather well with the grain size on the whole temperature range, while the break down of the first order fluctuation correction occurs for $\epsilon \leq \epsilon_c$. The inset shows the temperature behaviour of H_{up} (normalized to the value slightly above the critical temperature) as obtained from the exact expression of the GL functional and the full form of the partition function (see text).

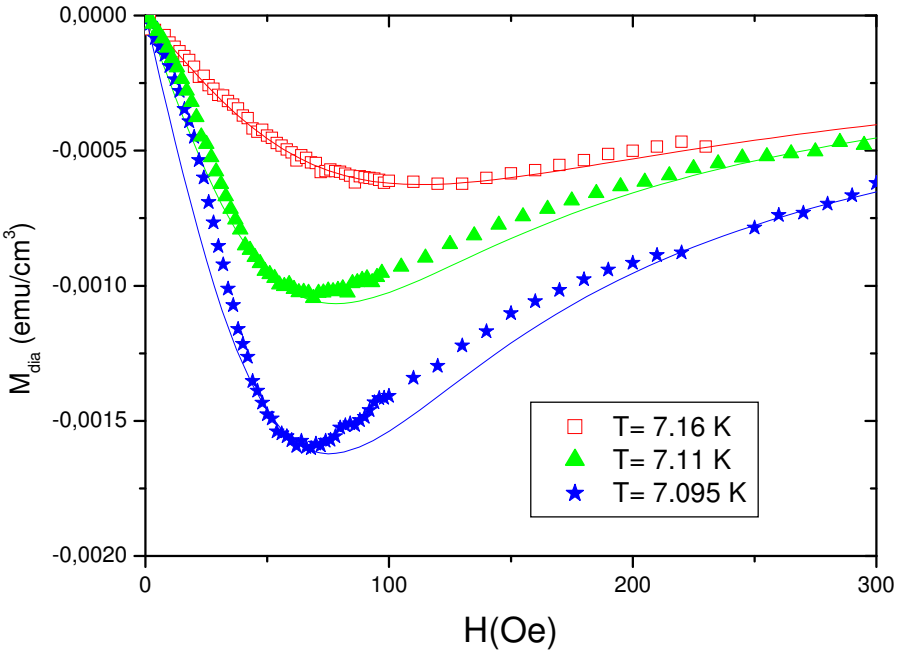

(a)

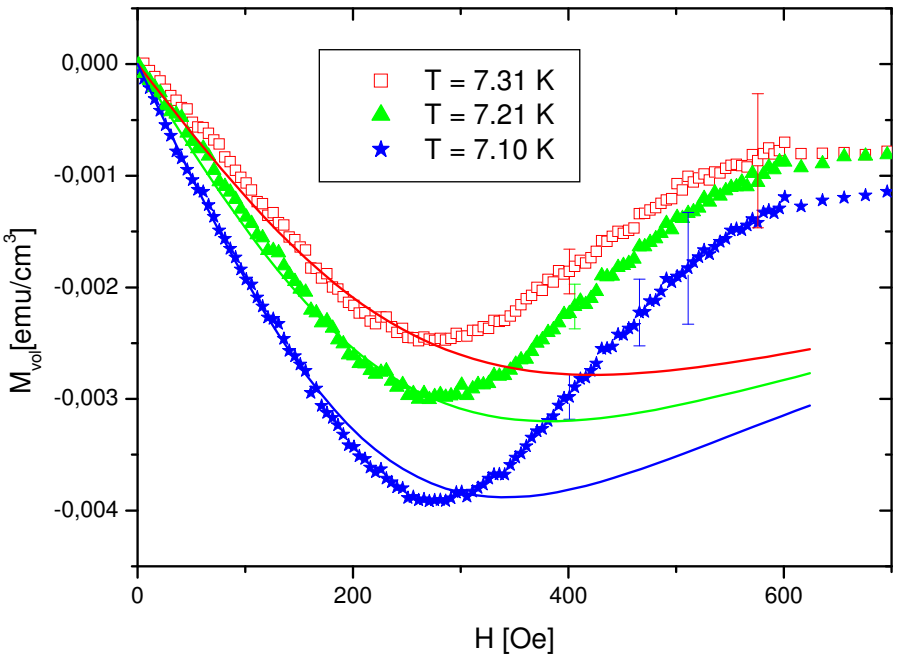

(b)

Figure A.7: Magnetization curves at representative temperatures derived from the exact GL functional and the complete form of the zero-dimensional partition function. Part (a) of the figure refers to the sample at average diameter of the grains 750 Å, with the experimental data taken from Fig.A.5 (a). Part (b) reports the theoretical curves expected at representative temperatures for sample (1), at average diameter size of 160 Å, compared with some experimental data.

Appendix B

Role of defects on superconducting properties

Authors

E. Bernardi[1], A. Lascialfari [1,2], A. Rigamonti[1] and L. Romanò[3]
[1]Department of Physics "A.Volta", CNR-INFM and Unità CNISM, University of Pavia, Via Bassi 6, I-27100, Pavia, Italy.
[2]Institute of General Physiology and Biological Chemistry, University of Milano, Via Trentacoste 2, I-20134 Milano, Italy and S3-CNR-INFM, Modena, Italy.
[3]Department of Physics and Unità CNISM, University of Parma, I-43100 Parma, Italy.

Abstract

The fluctuation-related diamagnetism above the superconducting transition temperature T_c in neutron irradiated and in Al-doped MgB_2 is studied by means of high-resolution isothermal measurements of the diamagnetic contribution to the magnetization, $M_{dia} = M_{dia}(H, T{=}\text{const})$. In both the neutron irradiated and the Al-doped compounds, T_c decreases on increasing the fluence and the Al amount, respectively. The magnetic field dependence of M_{dia} is apparently similar in both types of compounds: in the limit $H \to 0$, $-M_{dia}$ goes as H^n (with n in between $\frac{1}{2}$ and 1), while by increasing the field above a given value H_{up} an upturn in the field dependence occurs and M_{dia} decreases. From the temperature behaviours of H_{up} it is proved that the origin of the precursor diamagnetism is quite different in neutron irradiated and in Al-doped MgB_2. In the latter the magnetization curves reflect the precursor diamagnetism typical of heterogeneous systems and unrelated to superconducting

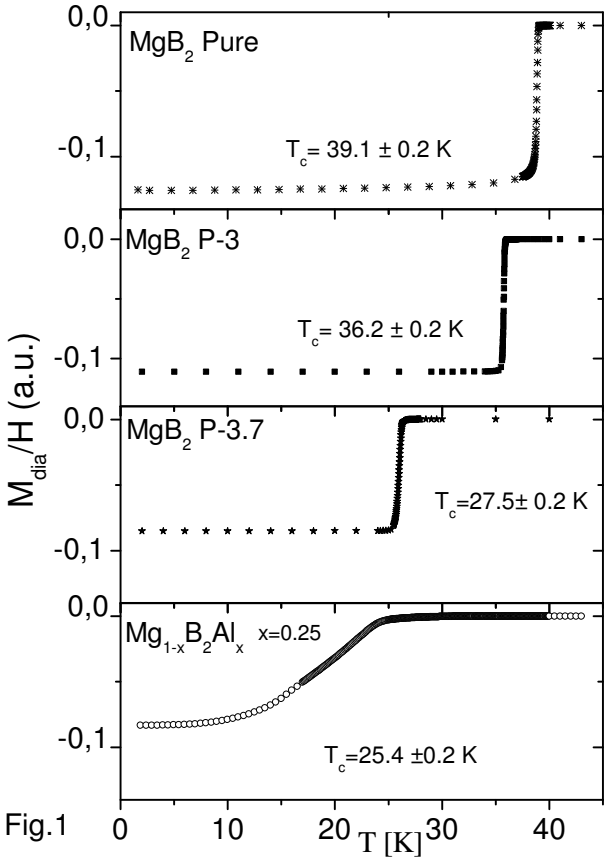

Figure B.1: Temperature dependences of the volume diamagnetic magnetization (measured in the limit of magnetic field $H \rightarrow 0$) in the two samples of neutron irradiated and in $Mg_{0.75}B_2Al_{0.25}$. For comparison the data in pure MgB_2 (Ref.12) are also reported.

fluctuations, being due to site-dependence of the transition temperature. At variance, neutron-irradiated MgB_2 displays different and novel properties. The fluence-dependent transition temperature is practically site-independent, the superconducting fluctuations and the related diamagnetism basically retaining the features of the pure (unirradiated) MgB_2. Upon irradiation, the anisotropy parameter involved in the fluctuations spectrum decreases. Correspondingly also the upturn field H_{up} decreases, consistently with a less anisotropic coherence length in strongly irradiated compounds. The implications of these experimental findings on the disorders induced by heterovalent substitutions and by neutron irradiation in MgB_2 are discussed.

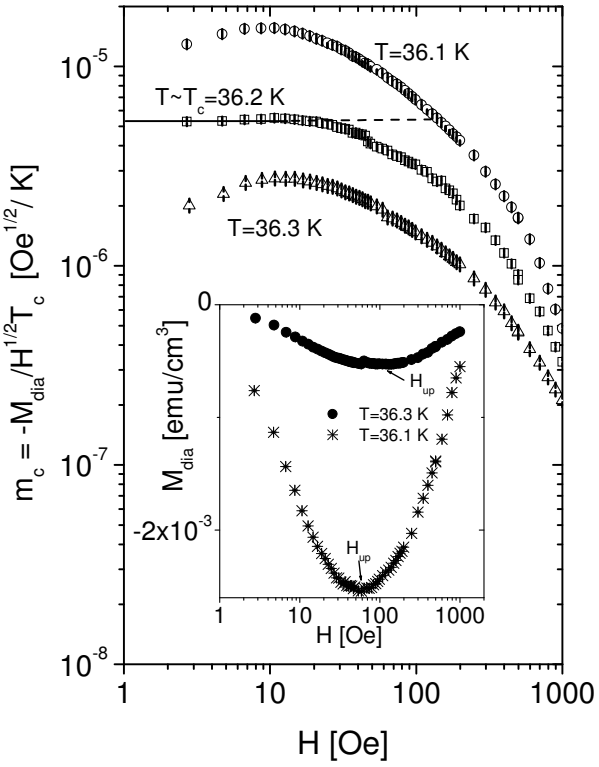

Figure B.2: Field dependence of the scaled magnetization in MgB_2 neutron irradiated P-3 sample, at typical temperatures around T_c . For $H = 50 - 60$ Oe and $T = T_c$ the Prange law (see Refs.10,11) is verified, while for $T > T_c$ the tendency towards $-M_{dia}$ linear in the field is noticed. The solid line tracks the field dependence that would occur if no field induced quenching of the fluctuating pairs should occur. In the inset some representative magnetization curves are shown, with the arrows indicating the upturn fields.

Introduction

The superconducting properties of MgB_2 are presently of strong interest, both in view of the perspective technological applications as well as in regards of the mechanism underlying the occurrence of the superconductivity. On the other hand, these properties of MgB_2 are known to be heavily modified when some kind of disorder is introduced. The effects of heterovalent (Al for Mg) substitutions and of neutron irradiation on the transition temperature, the critical current and the critical fields, on the two-superconducting bands and the crossover from clean to dirty regimes, have been subjects of extensive studies (see Refs. [55]-[60] and references therein). The character of the disorder, related to grain boundaries, to point-like pinning centres and/or Al ions, is worthy of particular attention. From specific heat measurements and from the sharpness of the transition in neutron irradiated (nir) compounds an homo-

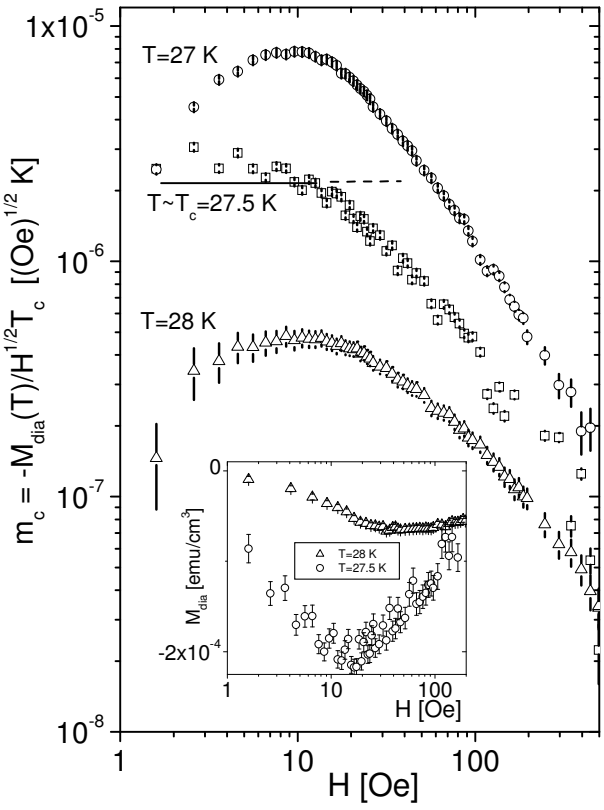

Figure B.3: Scaled magnetization around T_c in the P-3.7 sample. In the inset two representative magnetization curves are shown (solid line according to the Prange law, see Caption to Fig.B.2).

geneous defect structure has been claimed with little, if any, change in the band structure [61, 62]. In Raman spectra [63] disorder-induced violations of the selection rules have been discussed, as related to disorder of similar nature both in nir and in Al- doped (ald) MgB_2 compounds.

In recent years the fluctuating diamagnetism (FD) in superconductors and, in particular, the isothermal magnetization curves slightly above the transition, have been proved to be useful tools in order to get insights on the disorder effects in terms of site-dependence of T_c and/or of the occurrence of phase-fluctuating, non-percolating superconducting mesoscopic regions. On approaching the transition temperature from above, the superconducting fluctuations (SF) imply the arise of metastable Cooper pairs, leading to a diamagnetic contribution to the magnetization (See Refs [61, 62]). It has to be remarked that recent experimental findings in high-T_c cuprate superconductors and in MgB_2 also increased the interest toward SF, since small coherence length, reduced carrier density, high transition temperature and anisotropy cause strong enhancement of the fluctuations [17, 20, 35, 9, 10, 64]. On the

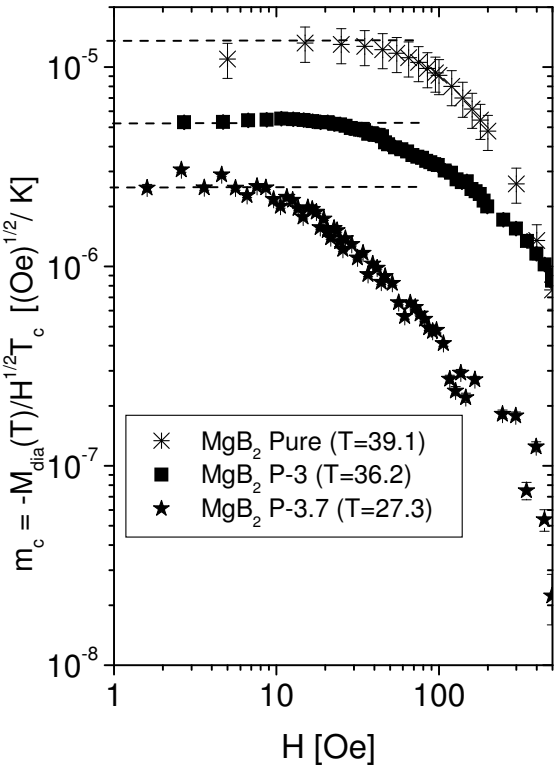

Figure B.4: Comparison of the scaled magnetization at T_c in the two nir samples with the correspondent data in pure MgB_2. The dotted lines are guide to the eye according to a scaled field-independent scaled magnetization.

other hand, it was also suggested that the SF can reflect the electronic properties of the superconducting state. As additional remarkable feature, in underdoped and overdoped YBCO dramatic deviations from the conventional GL behavior are observed, leading to an anomalous diamagnetism justified on the basis of the existence of superconducting regions at non-zero order parameter strongly fluctuating in the phase [9, 10].

In pure, undoped and unirradiated MgB2 the following features on FD have been evidenced [12]:

i) for T_c^+ and in the limit of magnetic field $H \to 0$ the diamagnetic contribution to the magnetization goes as $-M_{dia} \propto H^{1/2}$;

ii) in the magnetization curves $M_{dia} = M_{dia}\ (H, T{=}\text{const})$, at a temperature-dependent magnetic field H_{up} the magnetization $|M_{dia}|$ begins to decrease on increasing field, due to field-induced quenching of the fluctuating pairs;

iii) H_{up} increases with increasing the measuring temperature (above T_c);

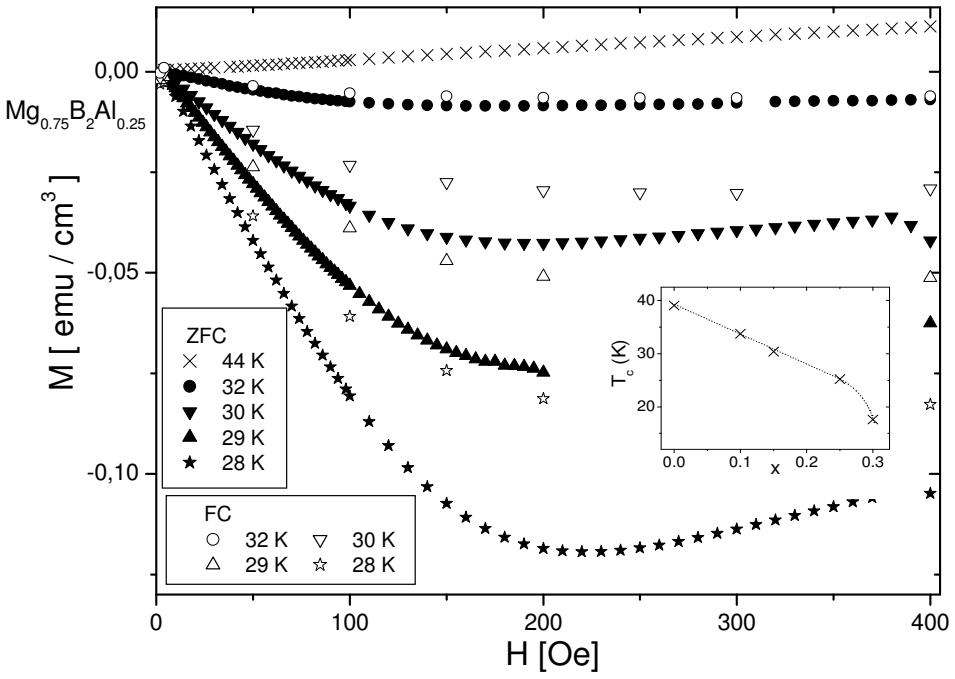

Figure B.5: Representative isothermal magnetization curves in Al-doped MgB_2. The inset shows the doping dependence of the transition temperature.

iv) the scaled magnetization at T_c, for $H \to 0$, namely $m_c = |M_{dia}|/H^{1/2}T_c$, that according to general Ginzburg-Landau theories for Gaussian fluctuations [10,11] and scaling arguments for isotropic 3D superconductors should take the universal value $0.324\, k_B/\Phi_0^{3/2}$, is enhanced because of the anisotropy in the coherence length;

v) two-bands evidence in the superconducting fluctuating diamagnetism was detected for temperature slightly above T_c[13].

On the other hand an enhancement of the diamagnetism above T_c has to be expected in heterogeneous superconductors. In fact, as a consequence of the disorder, non-percolating regions become superconducting at a local temperature $T_c^{local}(\mathbf{r})$ above the bulk T_c^{bulk}. In this case the magnetization curves for $T > T_c^{bulk}$ might mimic the ones expected below T_c, for a given volume fraction of the compound. Theoretical descriptions of this anomalous diamagnetism have been given [65, 66]. An experimental example, for instance, has been found in YNi_2B_2C [22]. A way to discriminate between precursor diamagnetism associated to diffuse transitions and fluctuation related diamagnetism (possibly enhanced by phase fluctuations of non-zero order parameter as in underdoped superconducting cuprates) is to look at the temperature behaviour of H_{up} in the isothermal magnetization curves [13, 41].

In this paper we report the results of a study of the fluctuating diamag-

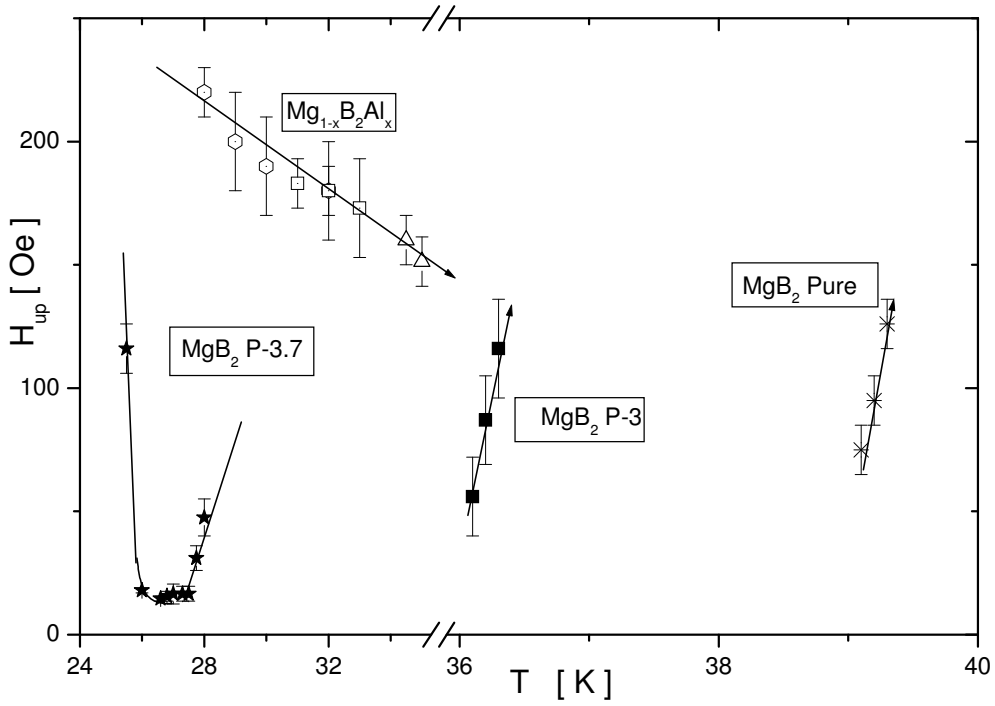

Figure B.6: Upturn field in the isothermal magnetization curves as a function of the measuring temperature in ald (,x=0.25,□, x=0.15, △, x=0.1), in nir MgB_2 and in the pure un-irradiated compound. The solid arrows are guide for the eyes. The dotted line for the P-3.7 sample tracks the temperature behaviour of Hup above and below the transition temperature in the strongly irradiated samples.

netism in neutron irradiated and in Al-doped MgB_2. From the comparison of the experimental findings it will turn out that the disorder in neutron irradiated MgB_2 does not cause diffuse transition. Although the transition temperature decreases on increasing the neutron fluence, a kind of "homogeneous defect structure" or disorder occurs: the transition remains sharp, the FD is fluctuations-related and H_{up} increases with increasing temperature. Furthermore the anisotropy parameter decreases with respect to the unirradiated MgB_2. At variance, the Al for Mg substitution induces a diffuse transition, with an anomalous enhancement of the precursor diamagnetism of quite a different nature.

Experimental results

The samples used in the present work have been prepared and characterized according to the procedures explained elsewhere [56, 62]. For $Mg_{1-x}B_2Al_x$ the doping amount varied from $x = 0.1$ to $x = 0.3$. The two nir samples we are going to deal with in this report belong to the P-batch [62]: P-3, exposed to

thermal neutron fluence of 7.6x1017 cm^{-2} and P-3.7 exposed to the fluence of 5.5x1018 $^{-2}$. The main properties of the compounds are reported in Refs. [56] and [62].

The diamagnetic magnetization above T_c has been measured by means of the Quantum Design MPMS-XL7 SQUID magnetometer, separating the paramagnetic Pauli-like contribution from the diamagnetic one, according to the experimental procedure detailed in Refs. [35] and [64].

The volume susceptibilities measured in magnetic field of a few Oersted in pure MgB_2, in the two samples of irradiated MgB_2 and in a typical ($x = 0.25$) Al-doped compound are reported in Fig. B.1.

In Fig. B.2 isothermal magnetization data at typical temperatures around the transition temperature in the P-3 sample are shown. In the plots the scaled magnetization $m_c = |M_{dia}|/H^{1/2}T_c$ is reported as a function of the magnetic field. It is reminded that in the absence of any field-induced quenching of the fluctuating pairs for T_c one should have field-independent m_c (Prange law. see Refs [17, 20]), while for T_c the magnetization is linear in the field. In the inset of Fig. B.2 typical magnetization curves are shown. It is noted that for H_{up} the magnetization $|M_{dia}|$ decreases on increasing the field.

In Fig.B.3 the results for the scaled magnetization m_c obtained in the P-3.7 compound are reported. The noticeable increase in the experimental error with respect to the P-3 sample is due to the decrease of the anisotropy (see the subsequent discussion) and of the transition temperature, both factors implying the decrease of the absolute value of the magnetic moment. Furthermore it was noticed that the large neutron fluence for the P-3.7 sample induced an increase of the paramagnetic background, thus causing a larger error in the subtraction procedure. The paramagnetic contribution for strong neutron fluence suggests that paramagnetic centers are produced by radiation damage. The lowering of T_c is possibly due to pair-breaking mechanism. EPR measurements are urged at the aim of obtaining insights on the nature of those centers, information that cannot be derived from bulk magnetic measurements as from the SQUID magnetization.

Figure Fig.B.4 shows the comparison of the scaled magnetization m_c between pure MgB_2 and the nir samples. As already mentioned, for Gaussian flucutations and according to scaling arguments [20, 35] the scaled magnetization at T_c has to be written

$$m_c = -M_{dia}/\sqrt{H}T_c = -0.324[k_B\Phi_0^{3/2}] \tag{B.1}$$

This equation follows from differentiation with respect to the field of the free energy for anisotropic superconductor (Ref. [35] and references therein), for randomly oriented powder.γ in Eq. B.1 is the anisotropy parameter,$\gamma = \xi_{ab}(0)/\xi_c(0)$, ξ_{ab} and ξ_c being the in-plane and the out of plane components of the zero-temperature coherence length. In anisotropic superconductors the factor γ enhances the universal value [17] $m_c = 0.324\, k_B/\Phi_0^{3/2}$. In pure MgB_2 the anisotropy parameter γ is $\gamma \approx 7$ and the upturn field H_{up}, for temperature close to T_c, is around 80 Oe [35]. From Figure B.4 it appears that in

the irradiated samples the upturn field decreases (see also the inset in Fig.3). Furthermore the anisotropy factor has to be decreased by a factor about 2 for the P-3 sample. Even more marked appears the reduction of the anisotropy in the P-3.7 sample. The comparison with the data in pure MgB_2 would lead to the conclusion that the P-3.7 sample is almost an isotropic 3D superconductor (see subsequent discussion).

In Fig. B.5 representative results (raw magnetization data) obtained in Al-doped MgB_2 are reported for the sample at $T_c = 25.4$ °K. At a first glance the magnetization curves could be considered similar to the ones measured in nir samples. A strong enhancement of the FD with respect to the pure compound is noticeable, the volume susceptibility reaching a value around 10^{-3} for T close to T_c. For T_c no anomalous diamagnetic contribution is present and the paramagnetic magnetization follows the Pauli-like field and it is practically temperature independent. On approaching the bulk T_c, M_{dia} is linear in the field and the upturn field is well above 200 Oe. It should be remarked that the difference between field-cooled and zero-field cooled data (difference not present in nir samples) in itself is a first indication that the diamagnetic contribution comes from region of the sample that are below the local irreversibility temperature (see the subsequent discussion).

Discussion and conclusions

We first briefly discuss the experimental findings in the Al-doped compound. The Al for Mg substitution acts on the superconducting properties most as an electron doping. Other effects are the change of the phonon spectrum (related to the different atomic size) and disorder-induced modification of the coupling between the bands [57, 55, 59, 56]. The transition temperature upon substitution decreases almost linearly down to about $T_c = 24$ K for Al amount $x = 0.25$ and then drops to about 15 K for $x = 0.3$ (see inset in Fig. B.5). Correspondently the transition loses the sharpness characteristic of the pure MgB_2. The diamagnetic susceptibility at T_c, in the low field limit, increases from $\chi_{dia} \approx 8.10 - 5$ emu/cm^3 in pure MgB_2 to about $\chi_{dia} \approx 10^{-3}$ emu/cm^3, in the sample at Al amount 0.25 while M_{dia} is practically linear in the field up to almost 100 Oe. The magnetization curves above the transition to the bulk superconducting state show an upturn field that decreases on increasing temperature. As already mentioned, irreversibility effects are detected. All these features are the signature of the anomalous diamagnetism expected in heterogeneous, disordered systems underlying a diffuse transition. In other words, the diamagnetism is not related to superconducting fluctuations and the magnetization curves mimic the ones expected below the transition to the superconducting state in any II-type superconductors, with a certain smoothing of the upturn field, likely due to the distribution of the local critical fields H_{c1}. Evidently, on approaching the bulk T_c from above, non-percolating mesoscopic superconducting regions are characterized by non zero order parameter,

thus causing a dramatic increase in the diamagnetism. Besides the early theoretical descriptions [65, 66] the problem of this anomalous diamagnetism has been recently considered by Cabo *et al.* [41], in the light of the detection of non conventional Ginzburg-Landau fluctuating diamagnetism in underdoped cuprates [10].

The shape of the magnetization curves for T_c^{bulk} results from a Gaussian distribution of transition temperatures, with H_{c1} playing a role similar to the one of the upturn field [67, 68]. Further work is in progress in regards of this aspect [68].

A quite different situation is induced upon neutron irradiation. The transition remains sharp (see Figure B.1) and the isothermal magnetization curves above T_c (Fig.s B.2 and B.3) basically show the field and temperature behaviours evidenced in the un-irradiated compound, in spite of the marked decrease of the transition temperatures. Furthermore the values of the scaled magnetization at T_c (see Eq. B.1 evidences the tendency towards isotropic superconductivity, with $\gamma \approx 1$.

In Fig.B.6 the temperature behaviour of the upturn field H_{up} detected in three Al-doped compounds, for the nir samples and in pure, untreated MgB_2, are collected. In pure MgB_2 and in the slightly irradiated compound, H_{up} increases on measuring the magnetization at constant temperatures, all above T_c. On the contrary in Al doped compounds the upturn field decreases on increasing the measuring temperature above bulk T_c. Finally in the strongly irradiated compound P-37 the upturn fields are sketched in Fig.6 for temperature above and below the transition temperature. The flattening of the data around T_c indicates the changeover from the fluctuation induced diamagnetism (for $T \geq T_c$) to the incipient magnetization curves occurring below T_c.

From the experimental data it seems possible to conclude that the irradiation induces a kind of homogeneously defected structure, which is reflected in the spectrum of the superconducting fluctuations and the related diamagnetism above the transition. The reduction in the anisotropy factor γ implies that the coherence length along the c axis and in the plane are forced by the irradiation towards a common value, at least for the sample exposed to the fluence of 5.5x1018 neutrons/cm^2.

The decrease in the upturn field upon irradiation is more difficult to handle, the role of the magnetic field in suppressing the superconducting fluctuations in a two-bands superconductors being hard to treat in the framework of the microscopic Gor'kov theory accounting for non-locality and shortwavelength fluctuations [20]. In the crude assumption of the so-called "zero dimensional model" for the superconducting droplets responsible of the FD (see Ref.s [35] and [64]), one approximately writes for the single particle magnetization

$$M^0_{dia}(\epsilon, T) = -k_B T H[4\pi^2\xi^2 d^2/5\Phi_0^2]/[\epsilon + (2\pi^2\xi^2 H^2 d^2/5\Phi_0^2)] \qquad \text{(B.2)}$$

where $\xi = (\xi_{ab}^2 \xi_c)^{1/3}$ is an effective coherence length, ϵ the reduced temperature and d an average size of the fluctuating SC droplets responsible of the FD, that

can be assumed of the order of ξ . Under these simplifying assumptions the upturn field in the isothermal magnetization curves is given by

$$H_up \approx \sqrt{2}.5\sqrt{\epsilon}\Phi_0/\pi\xi_0 d \tag{B.3}$$

According to this equation the reduction of Hup upon neutron irradiation would mean that the effective, almost-isotropic coherence length is increased. This is somewhat surprising, in view of the remark that the π band, at larger value of the coherence length, should be brought by the irradiation to the dirty regime more easily than the σ band. On the other hand, one should remark that also the upper critical field H_{c2}, that in the clean limit is inversely proportional to ξ^2, was found to decrease for the sample P-37 [62]. An effective, common coherence length shorter than ξ_π can be assumed to occur in the dirty regime for both the two bands [55].

As regards the possible persistence of two-band effects [64] in the spectrum of the superconducting fluctuations, first we remark the following. The two-band spectrum is observable in the magnetization curves only for magnetic field perpendicular to the c axis and for temperature rather far from T_c. On approaching the transition, the two bands merge and the magnetization curve is no longer structured [64]. A careful experimental attempt has been performed on the P-3.7 sample to look for the evidence of a double structure in the magnetization curves. However the signal to noise ratio for temperatures rather far from T_c is too poor to allow a firm conclusion. Furthermore the tendency upon neutron irradiation towards the isotropy condition can be expected to wipe out any double-structured magnetization curve.

Summarizing, from the isothermal magnetization curves above the superconducting transition temperature the different nature of the diamagnetism occurring in Al doped MgB_2 with respect to the one in neutron irradiated MgB_2 has been evidenced, thus emphasizing the quite different character of the related disorders. Upon Al doping a diffuse transition occurs, with site dependent transition temperatures which imply a strong anomalous diamagnetism above the bulk T_c^{bulk}, originated from the region of the sample having $T_c^{local} > T_c^{bulk}$. At variance, the neutron irradiation, although decreasing the transition temperature, introduces a kind of "homogeneous disorder": the transitions remain sharp and the spectrum of the superconducting fluctuations revealed by the fluctuating diamagnetism retains most of the features typical of unirradiated MgB_2. The effect of the magnetic field in suppressing the superconducting fluctuations above a certain H_{up} is confirmed, with two significant modification with respect to untreated MgB_2. The upturn field H_{up} as well as the anisotropy factor decrease on increasing the neutron fluence. The implications of these novel findings have been discussed, suggesting a crossover to a dirty regime for both the two-bands, with a common almost isotropic spectrum for the superconducting fluctuation corresponding to an increased effective coherence length.

Acknowledgments

Marina Putti (Dipartimento di Fisica, Università degli Studi di Genova, Italy) is gratefully acknowledged for lenting the samples used in the present work and for stimulating comments. Ileana Zucca is gratefully acknowledged for preliminary measurements on Al-doped MgB_2 samples.

Phys. Rev. B, **77**, 064502 (2008)

,

Bibliography

[1] J.P. Gollup, M.R. Beasley, R. Callarotti and M. Tinkam, *Phys. Rev. B*, **7**, 3039, (1973).

[2] J. Kurkijarvi, V. Ambegaokar e G. Eilenberger, *Phys. Rev. B*, **5**, 868, (1972).

[3] E. Bernardi, A.Lascialfari, A. Rigamonti, L. Romanò, V. Iannotti, G. Ausanio, and C. Luponio, *Phys. Rev. B*, **74**, 134509 (2006).

[4] W.G. Kogan, M. Ledvij, A. Yu Simonov, J.H. Cho and D.C. Johnston, *Rep. Rev. Lett.*, **70**, 1870 (1993).

[5] M.A. Hubbard, M.B. Salamon and B.W. Veal, *Physica C*, **248**, 138 (1995).

[6] A.E. Koshelev,*Phys. Rev.*, **50**, 506 (1994).

[7] A. Budzin and V. Dorin, in *Fluctuation Phenomena in High Temperature Superconductor*, **50**, 506 (1994).

[8] W.E. Lawrence and S. Doniach, in E. Kanda (ed,)*Proc. 12th Int. Conf. Low Temp. Phys.* p.361 (1970).

[9] A. Lascialfari, A. Rigamonti, L.Romanò, P.Tedesco, A. Varlamov and D.Embriaco *Phys. Rev. B* , **65**, 144523 (2002).

[10] A. Lascialfari, A. Rigamonti, L.Romanò, A. Varlamov and I.Zucca, *Phys. Rev. B* , **68**, 100505 (2003).

[11] L. Romanò, *Int. Journ. of Mod. Phys. B*, **17**, 423 (2003).

[12] A.Sewer, H. Beck, *Phys. Rev. B* , **64**, 014510 (2001).

[13] A.Rigamonti, A.Lascialfari, L. Romanò, A.Varlamov and I. Zucca, *J. of Superconductivity*, 0896-1107 (2005).

[14] M. Scavini, M. Daldosso, S. Cappelli, M. Brunelli, C. Ferrero and A.Lascialfari, *Europhys. Lett.* , **76**, 443-449 (2006).

[15] M. Scavini, L. Mollica and L. Malavasi, *Solid State Sci.*, **6**, 1187 (2004).

[16] E. Brecht, W. W. Schmahl, G. Miehe, M. Rodewald, H. Fuess, N.H. Andersen, J. Hanßmann, Th. Wolf, *Physica C*, **265**, 53-66 (1996).

[17] M. Tinkam in *"Introduction to superconductivity"*, McGaw-Hill (1996).

[18] H.B. Callen in *Thermodynamics and an Introduction to Thermostatistics* 2. ed, John Wiley & sons (1985).

[19] W.J. Skocpol and M. Tinkham, *Rep. Prog. Phys.*, **38**, 1049 (1975).

[20] A.I. Larkin, A.A. Varlamov, in *"Theory of Fluctuations in Superconductors"*, Oxford University Press (2005).

[21] T. Mishonov and E. Penev, *Int. Journ. of Mod. Phys. B*, **14**, 3831 (2000).

[22] A.Lascialfari, T. Mishonov, A. Rigamonti, I. Zucca, G. Behr, W. Loser, S.L. Drechsler, *Eur. Phys. J. B*, **35**, 325 (2003).

[23] R.E. Prange, *Phys. Rev. B*, **1**, 2349 (1978).

[24] A.Junod, J.Y. Genoud, G. Triscone, T. Schneider, *Physica C*, **294**, 115 (1998).

[25] C.Paracchini and L.Romanò, *Physica C*, **191**, 76 (1992).

[26] Francis S.Galasso in *Perovskites and High Tc Superconductors* Chap. 12, (1990).

[27] A. N. Fitch, *J. Res. Natl. Inst. Stand. Technol.*, **109**, 133 (2004).

[28] Larson A. C. and von Dreele R. B., GSAS, General Structure Analysis System (Los Alamos) (2001).

[29] B. H. Toby, *J. Appl. Cryst.*, **34** , 210 (2001).

[30] Jeong I. K. et al., *J. Appl. Cryst.*, **34**, 536 (2001).

[31] Proffen TH. and Billinge S. J. L. ,*J. Appl. Cryst.*, **32** , 572 (1999).

[32] Bonneviot L. and Olivier D., in Catalyst Characterization, edited by Imelik B. and Vdrine J. C. (Plenum Press, New York) 1994, pp. 181-214.

[33] Eremin M. V. and Sigmund E., *Solid State Commun.*, **90** , 795 (1994).

[34] Thomann H. et al., *Phys. Rev. B*, **38** , 6552 (1988).

[35] A. Lascialfari, T. Mishonov, A. Rigamonti, P. Tedesco and A. Varlamov, *Phys. Rev. B*, **65** , 180501 (2002).

[36] J.P. Gollup, M.R. Beasley, R. Callarotti and M. Tinkam, *Phys. Rev. B*, **7**, 3039 (1973).

[37] L.P. Gor'kov, *Zh. Eksperim. i. Teor. Fiz.*, **36**, 1918 (1959)[*Soviet Phys.–JETP***9**, 1364 (1959)].

[38] I. Zucca in Ph. D. thesis *Superconducting Diamagnetic Fluctuations and Precursor diamagnetism: From BCS to High T_c Superconductors*, **248**, 138 (1995).

[39] C. Baraduc, A.Budzin, J.Y. Henry, J.P. Brison and L. Puech, *Physica C*, **248**, 138 (1995).

[40] A. Lascialfari, P.Tedesco, I. Zucca, *Int. Journ. of Mod. Phys. B*, **17**, 805 (2003).

[41] L. Cabo, F. Soto, M. Ruibal, J. Mosqueira and F. Vidal, *Phys. Rev. B*, **73**, 184520 (2006).

[42] P. Mosconi, A.Rigamonti and A.A. Varlamov, *Appl. Magnetic Resonance* **19** , 345 (2000).

[43] For an exhaustive review on the NMR studies in BCS superconductors, see D.E. MacLaughlin in *Solid State Physics*, **31** , p.1-69 (1976) at the pages 63-67.

[44] For a mise a point of the theory and a critical review of the experiments, see E. Simanek in *Local Properties at Phase Transitions*, Ed.s K.A. Muller and A. Rigamonti, North Holland (1976), p. 838-855.

[45] R.A. Buhrman and W.P. Halperin, *Phys. Rev. Lett.* **30**, 692 (1973).

[46] S. Kobayashi, T. Takahashi and W. Sasaki, *J.Phys. Soc. Japan* **36**, 714 (1974).

[47] V.V. Shmidt in *Proceedings of IXX International Conference on Low Temperature Physics*Edited By M.P. Malkov, L.P.Pitaesvski and A. Shalnikov, (Viniti Pub. House, Moscow 1967) Vol. II B , p.205.

[48] B. Muhlschegel, D.J. Scalapino and R.Denton, *Phys. Rev. B* **6** , 1767 (1972).

[49] W-H. Li, C.C. Yang, F.C. Tsao and K.S. Lee, *Phys. Rev. B* **68**, 184507 (2003).

[50] C.T. Black, D.C. Ralph and M.Tinkham, *Phys. Rev. Lett.* **76**, 688 (1996)

[51] A.P. Tsai, N.Chandrasekhar and K. Chattopadhyay, *App. Phys. Lett.* **75** , 1527(1999).

[52] V.N. Gladilin, V.M. Fomin and J.T. Devruse, *Phys. Rev. B* **70** , 144506 (2004).

[53] J.von Delft, Ann. Phys. (Leipzig) **10**,1 (2001); J. von Delft and D.C. Ralph, Phys. Reports **345**, 61 (2001)

[54] Figlarz et al., United States Patent No. 4,539,041 (3 September 1985).

[55] M. Putti, V. Braccini, C. Ferdeghini, I. Pallecchi, A. S. Siri, F. Gatti, P. Manfrinetti, and A. Palenzona. *Phys. Rev. B*, **70** , 052509 (2004),

[56] M. Putti, C. Ferdeghini, M. Monni, I. Pallecchi, C. Tarantini, P. Manfrinetti, A. Palenzona, D. Daghero, R. S. Gonnelli, and V. A. Stepanov, *Phys. Rev. B*, **71** , 144505 (2005).

[57] M. Putti, M. Affronte, P. Manfrinetti, and A. Palenzona, *Phys. Rev. B*, **68**, 094514 (2003).

[58] I. Pallecchi, C. Tarantini, H. U. Aebersold, V. Braccini, C. Fanciulli, C. Ferdeghini, F. Gatti, E. Lehmann, P. Manfrinetti, D. Marré, A. Palenzona, A. S. Siri, M. Vignolo, and M. Putti, *Phys. Rev. B*, **71**, 212507 (2005)0.

[59] M. Ortolani, D. Di Castro, P. Postorino, I. Pallecchi, M. Monni, M. Putti, and P. Dore, *Phys. Rev. B*, **71**, 172508(2005).

[60] M. Iavarone, R. Di Capua, A. E. Koshelev, W. K. Kwok, F. Chiarella R. Vaglio, W. N. Kang, E. M. Choi, H. J. Kim, S. I. Lee, A. V. Pogrebnyakov, J. M. Redwing, and X. X. Xi, *Phys. Rev. B*, **71**, 214502(2005).

[61] M. Putti, M. Affronte, C. Ferdeghini, P. Manfrinetti, C. Tarantini, and E. Lehmann, *Phys.Rev. Lett.*, **96**, 077003(2006).

[62] C. Tarantini, H. U. Aebersold, V. Braccini, G. Celentano, C. Ferdeghini, V. Ferrando, U. Gambardella, F. Gatti, E. Lehmann, P. Manfrinetti, D. Marré, A. Palenzona, I. Pallecchi, I. Sheikin, A. S. Siri, and M. Putti, *Phys. Rev. B* , **73**, 134518 (2006).

[63] D. Di Castro, E. Cappelluti, M. Lavagnini, A. Sacchetti, A. Palenzona, M. Putti, and P. Postorino, *Phys. Rev. B*, **74** , 100505 (2006).

[64] L. Romanò, A. Lascialfari, A. Rigamonti, and I. Zucca, *Phys. Rev. Lett.*, **94**, 247001 (2005).

[65] Yu. N. Ovchinnikov, S. A. Wolf, and V. Z. Kresin, *Phys. Rev. B* , 4329 **60**, 4329 (1999).

[66] E. V. de Mello, E. S. Caixeiro, and J. L. González, *Phys. Rev. B* **67** 024502 (2003).

[67] E. S. Caixeiro, J. L. Gonzalez, and E. V. L. de Mello, *Phys. Rev. B*, **69**, 024521 (2004).

[68] L. Romanò, unpublished.

List of Pubblications

1. Zero-dimensional superconducting fluctuations and fluctuating diamagnetism in lead nanoparticles, E. Bernardi, A. Lascialfari, A. Rigamonti, L. Romanò, V. Iannotti, G. Ausanio, and C. Luponio, *Phys. Rev. B* **74**, 134509 (2006)

2. Fluctuating diamagnetism in the Critical Region of the Superconducting Transition in Lead Nanoparticles, E. Bernardi, A. Lascialfari, A. Rigamonti, L. Romanò, V. Iannotti, G. Ausanio, and C. Luponio, *Advances in Science and Technology* **47**, 98-103 (2006)

3. Superconducting fluctuating diamagnetism in neutron irradiated MgB2 in relation to precursor diamagnetism in Al-doped MgB2, E. Bernardi, A. Lascialfari, A. Rigamonti, and L. Romanó, *Phys. Rev. B* **77**, 064502 (2008)

4. Towards the understanding of the early growth conditions for superconducting (Y,Ca)BCO whiskers M.M. Rahman Khan, A. Agostino, S. Cagliero, M. Truccato, L. Pastero, E. Bernardi, *Appl. Phys. Lett.*, submitted

5. Superconducting Properties of Textured NbN Film from ^{93}Nb NMR Relaxation and Magnetization Measurements, E. Bernardi, A. Lascialfari, A. Rigamonti, M. Corti, A. Gauzzi and J.C. Villegier, *Phys. Rev. B* , submitted

Acknowledgements

I'm grateful to Prof. Alessandro Lascialfari for the supervision of my scientific activity, and for the firm guidance.
Prof. A. Rigamonti is gratefully acknowledged for the essential help and for the enlightening discussions.
I also acknowledge the fundamental collaboration with M. Scavini of the Department of Physical Chemistry and Electrochemistry of University of Milan, who worked on the synthesis and preparation of $SmBa_2Cu_3O_7$ and $SmBa_2Cu_{2.85}Al_{0.15}O_{6+\delta}$ powders.
A special thanks to Prof. M. Corti to Prof. P.Carretta and to S. Aldovrandi for the precious help in the experimental activity.
I thank all the NMR group of Pavia for the support.
Thanks to Dr. M.C. Mozzati for the precious help she gave to me in my experimental activity with SQUID.
I thank Laura Romanò for his encouraging comments about this work.
I thank my father and my brother, because without them I never succeeded in finishing this work.

Ringraziamenti

A mio padre e a mio fratello.

Ad Alessandro Lascialfari, perche è una persona fuori dal comune.
Al Prof. A. Rigamonti per tutti i consigli e per l'esempio che mi ha dato in questi anni.

A S. Aldovrandi, a P. Carretta e a M. Corti per l'aiuto in laboratorio.
A M.C. Mozzati e a P. Gallinetto, per tante cose e perchè mi sono stati vicino.
Ai miei compagni di ufficio: Nico Dario, Edo, Manuel.
Ai miei compagni di corso Silvia, Valentina e Manuel.
Un bacio a Marta.

Alla mia famiglia, al Renzo e allo zio Fede.

Ai miei amici, per quanto ci siamo divertiti.